

---

# The Effects of Aerosol-Cloud Interactions on Warm Cloud Properties

---

Alyson R. DOUGLAS

A dissertation submitted in partial fulfillment of

the requirements for the degree of

Doctor of Philosophy

(Atmospheric and Oceanic Sciences)

at the

UNIVERSITY OF WISCONSIN-MADISON

2020

Date of final oral examination: May 4th, 2020

The dissertation is approved by the following members of the Final Oral Committee:

Tristan L'Ecuyer, Professor in Atmospheric and Oceanic Sciences

Ankur Desai, Professor in Atmospheric and Oceanic Sciences

Tracey Holloway, in Atmospheric and Oceanic Sciences

Samuel Stechmann, Professor in Math

Dr. Tim Wagner, Researcher SSEC

# Abstract

## The Effects of Aerosol-Cloud Interactions on Warm Cloud Properties

by Alyson R. DOUGLAS

When aerosols enter the atmosphere through anthropogenic and natural activities, they interact with clouds in the atmosphere in what is termed aerosol-cloud interactions (ACI). ACI alter the cloud's radiative properties by acting as cloud condensation nuclei within the cloud, thereby reducing the mean drop size and increasing the cloud's albedo and cooling the earth by reflecting incoming shortwave radiation in what is termed the first indirect effect. By reducing the mean drop size throughout the cloud, aerosol also act to delay precipitation formation, leading to larger, longer lived clouds and further cooling the earth in a process known as the second indirect effect.

Using four years of satellite observations, the overall impact of aerosols on warm cloud radiative effect is evaluated. Warm clouds are defined as clouds with cloud top temperatures below freezing level. The estimates are constrained within regimes of stability, relative humidity of the free atmosphere, and by the scene liquid water path to control for how meteorology modulates the strength and sign of ACI. The sum of the first and second indirect effect, estimates of how aerosols alter the warm cloud shortwave effect and cloud fraction, are compared to an estimate of the full indirect effect, which includes all changes to the warm cloud shortwave radiative

effect. The decomposed, or summative, indirect effect ( $-0.26 \pm .15 \text{ Wm}^{-2}$ ) is less than the full indirect effect ( $-0.32 \pm .16 \text{ Wm}^{-2}$ ), though they lie within each other's uncertainty estimates. When the decomposed indirect effect is further constrained by precipitation, the estimate decreases to  $.21 \pm .15 \text{ Wm}^{-2}$ . The difference between the full indirect effect forcing and the decomposed forcings may be secondary indirect effects not included in our decomposition.

The second indirect effect includes not only the cloud extent broadening, but the cloud depth increasing. This deepening response may increase warming due to a larger longwave cloud radiative effect. The longwave indirect effect susceptibility is decomposed to determine how large it may potentially be and whether it could offset any cooling due to the shortwave indirect effect. We find the longwave indirect effect does have the potential to offset cooling through cloud deepening in regions where the shortwave indirect effect is extremely small, however the magnitude of the longwave component is sensitive to the diurnal cycle.

Cloud deepening signals clouds may be invigorated, or experiencing a state where precipitation formation and turbulence increase due to ACI. The effects of aerosol on precipitation formation and vertical motion are investigated using WALRUS, an algorithm of latent heating within the cloud determined using CloudSat radar returns. The LWP is constrained to thicker clouds ( $150 \text{ gm}^2 < \text{LWP} < 200 \text{ gm}^2$ ) and within regimes of stability. We find there are signs of invigoration in unstable, polluted clouds

compared to their clean and/or stable counterparts. The rate of precipitation formation throughout the cloud, and specifically in the center of the rain system, increases in unstable, polluted conditions. This effect may be heightened by a potential invigoration feedback, whereby precipitation formation stimulates vertical motion which then speeds up precipitation formation.

# Acknowledgements

Thank you to Tristan L'Ecuyer for advising me through my senior thesis, master's thesis, and dissertation.

Thank you to Alex Sherman for helping me with Python more than any other sane person would.

Thank you to Indie Coffee, Union South, and Aldo's Cafe for their coffee, baked goods, and ability to caffeinate me at all hours, no questions asked.

This work was funded by the the NASA CloudSat/CALIPSO Science Team.

All data was provided by NASA satellites including CALIPSO, CloudSat, and Aqua along with NASA's MERRA-2 reanalysis product.

# Contents

<b>Abstract</b>	<b>i</b>
<b>Acknowledgements</b>	<b>iv</b>
<b>Contents</b>	<b>v</b>
<b>List of Figures</b>	<b>viii</b>
<b>Abbreviations</b>	<b>xii</b>
<b>1 Introduction</b>	<b>1</b>
1.1 Motivation . . . . .	1
1.2 Background . . . . .	4
1.2.1 Forcing due to aerosol-cloud interactions . . . . .	4
1.2.2 Components of the ERFaci . . . . .	5
1.2.3 Global climate models and aerosol-cloud interactions . . . . .	7
1.2.4 Satellite observations of aerosol-cloud interactions . . . . .	8
1.2.5 Constraining aerosol-cloud interactions . . . . .	12
1.2.6 LWP: a confounding relationship . . . . .	14
1.2.7 Inclusion of regimes within my work . . . . .	15
<b>2 Data</b>	<b>17</b>
2.1 Satellites used in analysis . . . . .	18
2.1.1 CloudSat . . . . .	18
2.1.2 Aqua . . . . .	20
2.1.3 CERES . . . . .	21
2.2 Reanalysis products used . . . . .	22
<b>3 Decomposing the Shortwave Indirect Effect</b>	<b>23</b>
3.1 Foreword . . . . .	23
3.2 Abstract . . . . .	24
3.3 Introducton . . . . .	25
3.4 Methodology and Observations . . . . .	30

3.4.1	Data . . . . .	30
3.4.2	Methodology . . . . .	35
3.4.3	Regimes . . . . .	36
3.4.4	Decomposing the ERFaci . . . . .	38
3.5	Results and Discussion . . . . .	46
3.5.1	Estimate of the ERFaci . . . . .	46
3.5.2	Impact of LWP . . . . .	50
3.5.3	Constrained by local meteorology . . . . .	52
3.5.4	Constraints on cloud state and local meteorology . . . . .	56
3.5.5	Impact of precipitation and environment on susceptibility . . . . .	58
3.5.6	Contribution of RFaci and cloud adjustments to global ERFaci . . . . .	59
3.5.7	Regional variation due to precipitation . . . . .	62
3.6	Conclusions . . . . .	64
<b>4</b>	<b>Exploring the Longwave Indirect Effect</b>	<b>67</b>
4.1	Introduction . . . . .	67
4.1.1	Background . . . . .	67
4.1.2	Motivation . . . . .	69
4.2	Data & Methods . . . . .	70
4.2.1	Data . . . . .	70
4.2.2	Decomposing the longwave susceptibility . . . . .	71
4.2.3	Establishing constraints with regimes . . . . .	73
4.3	Results and Discussion . . . . .	74
4.3.1	The longwave susceptibility to aerosol . . . . .	74
4.3.2	The cloud deepening susceptibility . . . . .	75
4.3.3	The cloud extent susceptibility . . . . .	78
4.3.4	Diurnal influence on susceptibilities . . . . .	79
4.3.5	Inducing cloud feedbacks . . . . .	82
4.4	Conclusions . . . . .	83
<b>5</b>	<b>Invigoration of Warm Rain due to Aerosol-Cloud Interactions</b>	<b>86</b>
5.1	Foreword . . . . .	86
5.2	Significance Statement . . . . .	87
5.3	Abstract . . . . .	87
5.4	Introduction . . . . .	88
5.5	Results and Discussion . . . . .	92
5.5.1	Aerosol Effects on Rain Formation . . . . .	92
5.5.2	Aerosol Effects on Evaporative Processes . . . . .	95
5.5.3	Aerosol Effects on Vertical Motion . . . . .	98
5.6	Conclusions . . . . .	101
5.7	Data and Methods . . . . .	103

<b>6</b>	<b>Synthesis</b>	<b>107</b>
6.1	Motivation . . . . .	107
6.2	Investigating the effects of aerosol-cloud interactions on warm cloud properties . . . . .	108
6.3	Future work . . . . .	112
<b>A</b>	<b>Appendix of Information</b>	<b>115</b>
A.1	Abstract . . . . .	115
A.2	Introduction . . . . .	116
A.3	Methods . . . . .	124
A.3.1	Data . . . . .	124
A.3.2	Cloud . . . . .	124
A.3.3	Aerosol . . . . .	127
A.3.4	Regimes . . . . .	128
A.3.4.1	Environmental Regimes . . . . .	128
A.3.4.2	Cloud States . . . . .	130
A.3.5	Sensitivity . . . . .	132
A.4	Results . . . . .	136
A.4.1	Unconstrained Sensitivity . . . . .	136
A.4.2	Sensitivity to Cloud State . . . . .	137
A.4.3	Sensitivity within Environmental Regimes . . . . .	138
A.4.4	Accounting for Cloud and Environmental States . . . . .	141
A.4.5	Sensitivity on Regional Scales . . . . .	143
A.5	Discussion . . . . .	146
A.6	Conclusions . . . . .	150
	<b>Bibliography</b>	<b>161</b>

# List of Figures

- 2.1 An example of the size of the footprints of the various sensors used along the CloudSat/CALIPSO track (green). The cloud fraction is at a 12 km, along track scale (distance between orange lines). The AMSR-E footprint for the 36.5 GHz channel is  $\sim 14$  km (blue circle). The CERES footprint is 12 km (red circle). MODIS aerosol information is provided at a 1 km x 1 km resolution. Within the purple square, there would be 25 observations of MODIS aerosol properties. MERRA-2 reanalysis is at  $.5^\circ \times .5^\circ$  resolution on the grid with the closest profile to each CloudSat pixel being chosen as the environmental state for that time. . . . . 18
- 3.1 The change in aerosol index from SPRINTARS from the pre-industrial to present day (a),  $\frac{\partial \text{CRE}}{\partial \ln(\text{AI})}$  adapted from DL19 (b), and the associated  $\text{ERF}_{\text{Faci}_{\text{warm}}}$  found using Equation 3.2 found with constraints on LWP, EIS, and  $\text{RH}_{700}$  (c,  $-0.32 \pm .16 \text{ Wm}^{-2}$ ) using susceptibilities from DL19 (b) without areal weighting. . . . . 47
- 3.2 The  $\text{RFaci}_{\text{warm}}$ , cloud adjustment, and sum of the two susceptibilities, decomposition susceptibility, found within regimes of cloud state defined by LWP. The total decomposition susceptibility is  $-7.04 \text{ Wm}^{-2} \ln(\text{AI})^{-1}$ . 49
- 3.3 Variations in the a)  $\text{RFaci}_{\text{warm}}$  susceptibility ( $-5.26 \text{ Wm}^{-2} \ln(\text{AI})^{-1}$ ), b) cloud adjustment susceptibility ( $-2.88 \text{ Wm}^{-2} \ln(\text{AI})^{-1}$ ), and c) the sum of the two susceptibilities, the decomposed  $\text{ERF}_{\text{Faci}_{\text{warm}}}$  susceptibility ( $-8.22 \text{ Wm}^{-2} \ln(\text{AI})^{-1}$ ) with meteorological regimes defined by EIS and  $\text{RH}_{700}$ . . . . . 53
- 3.4 10 to 90% range of the decomposition for 11 cloud states when found within 100 environmental regimes of EIS and  $\text{RH}_{700}$ . The  $\text{RFaci}_{\text{warm}}$  (orange fill,  $\lambda_{\text{RFaci}}$ ) and cloud adjustment susceptibilities (green fill,  $\lambda_{\text{CA}}$ ) total  $-4.18 \text{ Wm}^{-2} \ln(\text{AI})^{-1}$  and  $-1.26 \text{ Wm}^{-2} \ln(\text{AI})^{-1}$ , respectively. The sum of the two from 10 to 90 percentiles, the decomposed susceptibility (blue line), totals  $-5.45 \text{ Wm}^{-2} \ln(\text{AI})^{-1}$ . . . . . 55
- 3.5 Globally summed and relatively weighted susceptibilities for different conditions when found within regimes of EIS, RH, and LWP on a regional basis. . . . . 57

3.6	The radiative forcing due to aerosol-cloud interactions (RFaci) (top, $-0.21 \pm .12 \text{ Wm}^{-2}$ ) and cloud adjustments (bottom, $-0.05 \pm .03 \text{ Wm}^{-2}$ ) found on a regional basis with constraints on LWP, EIS, and $\text{RH}_{700}$ without weighting by area. Note the colorbar for $\text{CA}_{\text{warm}}$ (bottom) is 1/3 of the magnitude of $\text{RFaci}_{\text{warm}}$ (top). . . . .	59
3.7	The $\text{ERFaci}_{\text{warm}}$ found as a sum of the $\text{RFaci}_{\text{warm}}$ and cloud adjustments (Figure 3.6) with constraints on the LWP, EIS, and $\text{RH}_{700}$ on a regional basis ( $-0.26 \text{ Wm}^{-2}$ ) without areal weighting. . . . .	61
3.8	The decomposed effective radiative forcing due to aerosol-cloud interactions found as a sum of its components on a regional scale within regimes of EIS, RH, and LWP for a) non-raining clouds ( $-.147 \text{ Wm}^{-2}$ ) and b) raining clouds ( $-.06 \text{ Wm}^{-2}$ ). . . . .	63
4.1	The susceptibility of decomposed longwave indirect effect to aerosol when found with constraints on LWP, EIS, and $\text{RH}_{700}$ during the daytime. . . . .	75
4.2	The susceptibility of cloud top height to aerosol when found with constraints on LWP, EIS, and $\text{RH}_{700}$ during the daytime. . . . .	77
4.3	The daytime susceptibility of cloud top height to aerosol for LWPs between 20 to 60 $\text{gm}^{-2}$ and 60 to 100 $\text{gm}^{-2}$ evaluated on a regional basis and averaged into global bins. (Note the adjusted colorbars) . . .	77
4.4	The susceptibility of cloud fraction to aerosol when found with constraints on LWP, EIS, and $\text{RH}_{700}$ during the daytime. . . . .	79
4.5	The susceptibility of cloud top height to aerosol at night when found with constraints on LWP, EIS, and $\text{RH}_{700}$ . . . . .	81
4.6	The susceptibility of cloud fraction to aerosol at night when found with constraints on LWP, EIS, and $\text{RH}_{700}$ . . . . .	82
4.7	The nighttime susceptibility of cloud top height to aerosol for LWPs between 20 to 60 $\text{gm}^{-2}$ and 60 to 100 $\text{gm}^{-2}$ evaluated on a regional basis and averaged into global bins. . . . .	82
5.1	The maximum rate latent heat release due to precipitation within the cloud against the size of the rain system for all (top) and dry (bottom) warm clouds with an extent of 15 km. Black is for all stabilities, blue is for unstable environments, red is for stable environments; dashed represents pristine and solid represents polluted surroundings. . . . .	91
5.2	The mean amount of latent heating released due to precipitation formation rate in the geometrical center of the rain system against size of the rain system for all (top) and dry (bottom) warm clouds with an extent of 15 km. Black is for all stabilities, blue is for unstable environments, red is for stable environments; dashed represents pristine and solid represents polluted surroundings. . . . .	94

5.3	The maximum rate latent heating released due to evaporation above the cloud against size of the rain system for all (top) and dry (bottom) warm clouds with an extent of 15 km. Black is for all stabilities, blue is for unstable environments, red is for stable environments; dashed represents pristine and solid represents polluted surroundings. . . . .	97
5.4	The mean rate of latent heating due to evaporation below the cloud vs size of the rain system for all (top) and dry (bottom) warm clouds with an extent of 15 km. Black is for all stabilities, blue is for unstable environments, red is for stable environments; dashed represents pristine and solid represents polluted surroundings. . . . .	97
5.5	The difference (polluted - pristine) in vertical motion in unstable environments in unstable (top) and stable (bottom) environments for clouds of rain size 4 km (left), 5 km (middle), and 6 km (right). . . . .	100
6.1	The change in cloud fraction (all - pristine) using modeled pristine cloud fraction at 12 km estimates. . . . .	113
A.1	The sensitivity of CRE to aerosol ( $\lambda_0$ from equation (A.4)) found globally from the mean SW CRE for each $\ln(\text{AI})$ bin (blue dots) without constraints on the environment, cloud state, or region. The red lines represent the standard deviation within each bin of $\ln(\text{AI})$ . . . . .	137
A.2	. . . . .	153
A.3	. . . . .	153
A.4	. . . . .	153
A.5	Values of the sensitivity of CRE to aerosol ( $\lambda_{LWP}$ from equation (A.5)) for different resolutions of cloud state regimes. The weighted, summed $\lambda_{LWP}$ is $-13.12 \frac{\text{Wm}^{-2}}{\ln(\text{AI})}$ with 8 partitions. Plots of warm cloud shortwave CRE against $\ln(\text{AI})$ are shown below for (b) thin (.04 to .06 $\frac{\text{kg}}{\text{m}^2}$ ) and (c) thick (.1 to .15 $\frac{\text{kg}}{\text{m}^2}$ ) cloud states. The red lines represent the standard deviation within each $\ln(\text{AI})$ bin and the blue dots represent the mean SW CRE for each $\ln(\text{AI})$ bin in plots (b) and (c). . . . .	153
A.6	. . . . .	154
A.7	. . . . .	154
A.8	. . . . .	154
A.9	The sensitivity of CRE to aerosol ( $\lambda_{ENV}$ ) from equation (A.7) evaluated with constraints on the environment. When weighted and summed following equation (A.7), $\lambda_{ENV}$ is $-11.0 \frac{\text{Wm}^{-2}}{\ln(\text{AI})}$ . Plots of the individual regimes from an unstable ( $\sim 1\text{K}$ ), dry environment ( $i$ 10% $\text{RH}_{700}$ ) (b) and stable ( $\sim 6\text{K}$ ), moist environment ( $i$ 30% $\text{RH}_{700}$ ) (c) where the red lines represent the standard deviation of the SW CRE within each $\ln(\text{AI})$ bin and the blue dots represent the mean SW CRE for each $\ln(\text{AI})$ bin. . . . .	154
A.10	. . . . .	155

A.11	.....	155
A.12	.....	155
A.13	The sensitivity of the warm cloud CRE to aerosol ( $\lambda_{ENV}$ ) found using equation A.7 for environmental frameworks of a) 25 ( $-11.29 \frac{Wm^{-2}}{\ln(AI)}$ ), b) 100 ( $-11. \frac{Wm^{-2}}{\ln(AI)}$ ) and c) 225 ( $-10.99 \frac{Wm^{-2}}{\ln(AI)}$ ) regimes of EIS and RH <sub>700</sub> .	155
A.14	.....	156
A.15	.....	156
A.16	.....	156
A.17	Frequency of clouds partitioned into of a) 25, b) 100, and c) 225 environmental regimes of EIS and RH <sub>700</sub> .	156
A.18	The sensitivity of CRE to aerosol ( $\lambda_{BOTH}$ ) found with constraints on stability, RH <sub>700</sub> and cloud state limits of ??) .02 to .04 $\frac{kg}{m^2}$ ( $-3.7 \frac{Wm^{-2}}{\ln(AI)}$ ), ??) .04 to .06 $\frac{kg}{m^2}$ ( $-2.2 \frac{Wm^{-2}}{\ln(AI)}$ ), ??) .06 to .08 $\frac{kg}{m^2}$ ( $-1.4 \frac{Wm^{-2}}{\ln(AI)}$ ), ??) .08 to .1 $\frac{kg}{m^2}$ ( $-1. \frac{Wm^{-2}}{\ln(AI)}$ ), ??) .1 to .15 $\frac{kg}{m^2}$ ( $-1.5 \frac{Wm^{-2}}{\ln(AI)}$ ), ??) .15 to .2 $\frac{kg}{m^2}$ ( $-.5 \frac{Wm^{-2}}{\ln(AI)}$ ), and ??) .2 to .4 $\frac{kg}{m^2}$ ( $-.4 \frac{Wm^{-2}}{\ln(AI)}$ ). Panel (h) is the summed, weighted sensitivity $\lambda_{BOTH}$ within each environmental regime. The weighted, summed sensitivity is $-10.6 \frac{Wm^{-2}}{\ln(AI)}$ (sum of panel (h)). Note the colorbar for panel (h) is adjusted due to weighting.	157
A.19	.....	158
A.20	.....	158
A.21	.....	158
A.22	The sensitivities of CRE to aerosol from equation (A.9) within environmental regime resolutions of a) 5 by 5 ( $-10.8 \frac{Wm^{-2}}{\ln(AI)}$ ), b) 10 by 10 ( $-10.6 \frac{Wm^{-2}}{\ln(AI)}$ ), and c) 15 by 15 ( $-10.6 \frac{Wm^{-2}}{\ln(AI)}$ ) summed over all cloud states. Unlike all previous sensitivity estimates, these are weighted by occurrence.	158
A.23	.....	159
A.24	.....	159
A.25	.....	159
A.26	The sensitivity of CRE to aerosol evaluated regionally with (a) no regimes constraints, (b) only cloud state constraints, and (c) only environmental constraints for each 15° by 15° region. Total sensitivities are (a) -11.8, (b) -28.5, and (c) -13.8 when weighted by occurrence. $\frac{Wm^{-2}}{\ln(AI)}$ .	159
A.27	The sensitivity of CRE to aerosol ( $\lambda_{ALL}$ ) found on a regional basis with cloud state and environmental regime constraints. The total regime weighted, global warm cloud sensitivity to aerosol perturbations is $-10.13 \frac{Wm^{-2}}{\ln(AI)}$ .	160

# Abbreviations

<b>CCN</b>	Cloud Condensation Nuclei
<b>ACI</b>	Aerosol Cloud Interactions
<b>N</b>	number of cloud droplets
<b>GCM</b>	Global Climate Model
<b>ERFaci</b>	Effective Radiative Forcing due to aerosol cloud interactions
<b>IPCC</b>	Intergovernmental Panel on Climate Change
<b>CRE</b>	Cloud Radiative Effect
<b>RFaci</b>	Radiative Forcing due to aerosol cloud interactions
<b>CA</b>	Cloud Adjustment
<b>LWP</b>	Liquid Water Path
<b>CMIP</b>	Coupled Model Intercomparison Project
<b>MODIS</b>	Moderate Resolution Imaging Spectroradiometer
<b>CPR</b>	Cloud Profiling Radar
<b>CERES</b>	Clouds and the Earth's Radiant Energy System
<b>AOD</b>	Aerosol Optical Depth
<b>AI</b>	Aerosol Index
<b>AMSR-E</b>	Advanced Microwave Scanning Radiometer for EOS
<b>ECMWF</b>	European Centre for Medium-Range Weather Forecasts
<b>EIS</b>	Estimated Inversion Strength
<b>LW</b>	Longwave

# Chapter 1

## Introduction

### 1.1 Motivation

Aerosol-cloud interactions (ACI) and its influence on the radiative balance remains the largest source of uncertainty in quantifying a climate sensitivity using either observations or climate modeling (Boucher et al., 2013). When aerosols, or suspended droplets released from anthropogenic activities like biomass burning or natural phenomenon like sea spray, interact with clouds in the atmosphere, they act as cloud condensation nuclei (CCN) within the cloud. This increases the number of cloud droplets ( $N$ ), which for a fixed amount of liquid within the cloud, decreases the mean drop size. The albedo of the cloud increases as  $N$  increases and the mean drop size decreases in what is termed the first indirect effect (Twomey, 1977a). While this is a

microphysical interaction, changes to the mean drop size result in macrophysical consequences. Collision-coalescence, or the onset of rain production within warm clouds, is delayed as the drops shrink. In a series of events known collectively as the second indirect effect, as precipitation is suppressed, the cloud grows more expansive, thicker, and lives longer in the atmosphere (Albrecht, 1989). ACI therefore lead to brighter, longer lived clouds and have a cooling effect on the atmosphere. This myriad of effects not only impacts the global radiative balance through reflecting incoming shortwave forcing, but influences the hydrological cycle and numerous climate-cloud feedbacks.

Clouds exist within the interconnected Earth system; any changes to their properties induces a causal sequence of effects throughout Earth's system (Stephens, 2005). Warm cloud's role as "Earth's Sunblock" due to their longevity and large spatial coverage ( $\sim 35\%$  of the Earth's surface) may be threatened in the future due to a changing environment and their connection to the climate system (Hahn and Warren, 2007a, Ramanathan et al., 2001, Rockström et al., 2009). Warm clouds are defined as clouds with cloud top temperatures below freezing. Rapid cloud breakup of mSc due to rising sea surface temperatures not only decreases warm cloud's ability to cool the Earth, but adds covariability with the environment when quantifying ACI (Schneider et al., 2019). This covariability with the environment, and potential for cloud-environment feedbacks, complicates quantifying how ACI cool the Earth.

Any impact on warm clouds' radiative properties, due to either aci, climate change, or a combination of the two, impacts climate feedbacks dependent on the cooling these

clouds provide. Low cloud cover and its effects on the radiative balance may drive tropical cloud feedbacks, including the formation of deep convective systems (Bony and Dufresne, 2005). Deepening of low clouds in the tropics due to precipitation suppression, or the second indirect effect, has been shown to directly control the amplitude of the climate sensitivity within global climate models (GCM) (Brient et al., 2016). Further, changes to warm cloud radiative properties may instigate an internal warm cloud feedback that can either heighten or decrease their ability to cool the Earth (Brient and Bony, 2012). Cloud-climate feedbacks directly control the climate sensitivity beyond aci. Reducing a cloud's ability to precipitate, while increasing the longevity and cooling ability of the cloud, directly connects a change in the radiative balance with a change in the hydrological cycle, meaning ACI act as the link between the radiative balance and hydrological cycle (Watanabe et al., 2018).

Overall, warm clouds drive multiple climate feedbacks (Bony et al., 2015). Any changes to warm cloud radiative properties will not only affect the climate sensitivity, but multiple climate feedbacks and the hydrological cycle. Therefore it remains imperative to quantify how ACI and the first and second indirect effects alter warm cloud properties. Why haven't we already then if it's so important? Our GCMs lack the ability to properly simulate aci. Many GCMs overcompensate the albedo of warm clouds while reducing their extents. This produces a realistic global radiative balance with large regional biases in what is known as the "too few, too bright" problem (Nam et al., 2012).

During my doctoral studies, I aimed to use satellite observations to produce a range of expected relationships within an environmental framework. I quantified the first and second indirect effects on global and regional scales with sets of environmental conditions, referred to herein as regimes. This provides sensitivity benchmarks for global climate models that can be tested to evaluate how well the model captures global and regional regime specific behavior. I begin with quantifying how aerosol-cloud interactions alter the warm cloud albedo and extent (Chapter 3). After determining that the environment plays a role in modulating the magnitude of the change, I extrapolated the environmental regime framework to investigate how ACI affect cloud deepening and the longwave cloud radiative effect (Chapter 4). Finally, I explored how cloud deepening and increased lifetimes may further alter warm cloud precipitation by increasing the rain formation rates and instigating turbulence within the cloud (Chapter 3).

## **1.2 Background**

### **1.2.1 Forcing due to aerosol-cloud interactions**

The cooling due to ACI from pre-industrial to present day times, or the effective radiative forcing due to aerosol-cloud interactions (ERF<sub>aci</sub>), is the change in the top-of-atmosphere radiative balance due to clouds reflecting more sunlight, decreasing the amount of incoming solar radiation. The value depends largely on how it is quantified.

Some estimates of ERF<sub>aci</sub> depend on differencing GCMs with and without anthropogenic emissions ( $-1.4 \text{ Wm}^{-2}$ ) (Penner et al., 2011). Other model derived estimates difference the value of the effective radiative forcing due to aerosol cloud interaction and aerosol radiation interactions (ERF<sub>aci+ari</sub>) from only the effective radiative forcing due to aerosol radiation interactions (ERF<sub>ari</sub>), which often leads to a diminished ERF<sub>aci</sub> value ( $-0.45 \text{ Wm}^{-2}$ ).

Satellite based studies rely on deriving the susceptibility of the cloud radiative effect (CRE) to rising aerosol concentrations and show a similarly damped value ( $-0.78 \text{ Wm}^{-2}$ ) (Boucher et al., 2013). Quantifying the ERF<sub>aci</sub> remains a challenge to observationalists and modelers as covariability and non-linearities obscure the exact figure. The IPCC estimates using all definitions ERF<sub>aci</sub> that its true value lies between  $-1.2$  and  $0 \text{ Wm}^{-2}$  at a 90% uncertainty interval. The range of the ERF<sub>aci</sub> is so large it could offset most of the radiative forcing due to a doubling of CO<sub>2</sub> ( $1.5 \text{ Wm}^{-2}$ ) or have no global effect on the radiative balance (Myhre et al., 2014). Warm clouds alone could offset the warming due to rising CO<sub>2</sub> emissions completely. It has been theorized a modest 15% increase in their cover, from  $\sim 35\%$  to  $40\%$ , would offset the warming due to CO<sub>2</sub> completely (Slingo, 1990).

### 1.2.2 Components of the ERF<sub>aci</sub>

The ERF<sub>aci</sub> is composed of two components, the radiative forcing due to aerosol-cloud interactions (RF<sub>aci</sub>) and cloud adjustments (CA). The RF<sub>aci</sub> summarizes the first indirect effect, whereby clouds become brighter due to aci. Cloud adjustments

include all other changes to the cloud that affect its radiative properties including how the liquid water path (LWP) increases as precipitation is suppressed and how cloud extent increases as the cloud is longer lived. Separating these terms is difficult, as a change in the LWP (a cloud adjustment) results in a higher albedo (an increased RFaci) (Quaas et al., 2009).

Separating these terms leads to large margins of uncertainty, especially in cloud adjustments as the liquid water path adjustment is highly non-linear (Takemura et al., 2007). GCMs can be used to rudimentarily separate the RFaci from CA and decompose the CA into the cloud fraction and LWP responses. Mülmenstädt et al. (2019) attempted to use ECHAM6, a GCM developed by the Max Planck Institute for Meteorology. Their total ERFaci lies above the range instituted by the IPCC at  $-1.35 \pm 0.3 \text{ Wm}^{-2}$ . However, the correlation between the LWP response and RFaci lead to high levels of uncertainty in the results.

The ERFaci and its components, the RFaci and CAs, are dependent on the environment, which can dampen or intensify the reaction of a cloud to aerosol loading (Stevens and Feingold, 2009a). The RFaci is a relatively slow response to both aerosol and any environmental modulation, while some CAs are considered a fast, instantaneous response. This only adds to the connectedness of the system, as the RFaci takes additional time to respond to the environment, aerosol, and any changes to the LWP due to a CA. The inherent covariability between the terms of the ERFaci only amplifies our inability to accurately model ACI within GCMs (Mülmenstädt and Feingold,

2018).

### 1.2.3 Global climate models and aerosol-cloud interactions

GCMs are limited by their dependence on parameterizations in order to simulate clouds and their interactions with the environment and aerosols (Randall et al., 2003). The scale of ACI range from  $10^{-9}$  to  $10^3$  meters (12 orders of magnitude), as the aerosols themselves are only nanometers wide while their effects on the cloud can result in a change of kilometers depth and width. This scale gap leads to a dependence on parameterizations. Modeling each aerosol droplet and its eventual impact on a single cloud droplet for an entire atmosphere filled with clouds and aerosols is beyond our current computing power.

The newest Coupled Model Intercomparison Project version 6 (CMIP6, released in 2019) estimates the ERF<sub>aci</sub> to be  $-0.84 \pm 0.3 \text{ Wm}^{-2}$  (Smith et al., 2020). Unlike previous estimates included in the IPCC 5 report, this CMIP6 ERF<sub>aci</sub> estimate separates the cooling due to changes in cloud extent ( $-0.15 \text{ Wm}^{-2}$ ) vs. due to changes in cloud liquid water amounts ( $-0.04 \text{ Wm}^{-2}$ ). Additionally, the newest estimates of the ERF<sub>aci</sub> include a longwave cloud extent term ( $-0.02 \text{ Wm}^{-2}$ ). Aggregation, or the clumping together, of clouds in the tropics may lead to a net cooling effect through venting longwave radiation back to space (Coppin and Bony, 2015). While many GCMs and other models, both cloud resolving and cloud parameterized, display signals of aggregation, observing signs of aggregation has proven challenging (Holloway et al., 2017). However, if aerosols impact aggregation through promoting further clumping

or initializing the conditions that favor it, longwave cooling due to aggregation may be an additional cloud adjustment term within the ERFaci (Beydoun and Hoose, 2019).

While the latest generation of GCMs have more advanced parameterizations of clouds, they still habitually underestimate the amount of warm clouds (Neubauer et al., 2019). Updated parameterizations have fixed known problems with cirrus and mixed phase, however liquid clouds remain "too few, too bright" (Williams and Bodas-Salcedo, 2017). If the amounts and initial albedos of clouds are incorrect, it is impossible to estimate the ERFaci, RFaci, or CA from GCMs. Moreover, the connections between aci, cloud feedbacks, and the hydrological cycle are sensitive to correctly tuning the cloud sensitivity to aerosol. Even estimating how cloud feedbacks may affect the climate sensitivity, assuming that there is no relationship between ACI and cloud feedbacks, leads to large uncertainty owing to our incorrect modeling of clouds within GCMs (Zelinka et al., 2020a). With our current GCMs, we are unable to predict how aerosols affect clouds and how these effects can instigate cloud feedbacks or the hydrological cycle.

#### **1.2.4 Satellite observations of aerosol-cloud interactions**

Satellite observation studies exploit the synergy between collocated observations in order to maximize the amount of information of any given scene. Many observation based studies of ACI utilize the NASA A-Train satellite constellation, which contains a mix of environmental, aerosol, and cloud sensors in a collocated orbit (L'Ecuyer and Jiang, 2011). By combining active and passive satellite sensors, such the Moderate

Resolution Imaging Spectroradiometer (MODIS) aboard Aqua and the cloud profiling radar (CPR) aboard CloudSat, the aerosol amounts and cloud characteristics of the scene can be determined. Clouds and the Earth's Radiant Energy System (CERES) detects the outgoing and incoming shortwave radiation of every scene at a 12 km scale, making it possible to calculate a CRE and directly observe a radiative susceptibility to aerosol. The IPCC uses these susceptibilities and associated changes in aerosol between pre-industrial and present-day in order to restrict their GCM derived estimates of the ERF<sub>aci</sub> within observationally derived magnitudes.

A study which combined multiple sensors aboard A-Train satellites estimated the marine ERF<sub>aci</sub> to be  $-.20 \pm .31 \text{ Wm}^{-2}$  (Christensen et al., 2016). Warm clouds dominate the ERF<sub>aci</sub> due to their global coverage and high susceptibilities ( $-.36 \pm .21 \text{ Wm}^{-2}$ ), while mixed phased and convective clouds led to a warming effect ( $.01 \pm .06 \text{ Wm}^{-2}$  and  $.15 \pm .23 \text{ Wm}^{-2}$ , respectively). Unlike the CMIP6 GCM based study, which found clouds likely to undergo aggregation such as tropical convective types cool the Earth, Christensen et al. (2016) found these clouds lead to a slight warming due to the deepened convection which increases the amount of longwave radiation emitted back to Earth.

A benefit of using satellite observations to distinguish signals of ACI is that they observe rare phenomena, such as cloud dimming or breakup, that may not be possible to represent within GCMs due to the limitations of cloud parameterizations. Shiptracks provide a unique set of conditions: the shiptrack is a contained region of aerosol

loading while the clouds around the shiptrack remain unperturbed and suitable as a control comparison. Christensen et al. (2014) found in some mixed phase cloud, or those containing both liquid and ice, that shiptracks can lead to varying degrees of brightening and extended lifetimes depending on the phase of the cloud. Mixed phased clouds were sometimes eventually desiccated by induced flow from aci, leading to their lifetimes being only extended by  $\sim 1$  hour compared to  $\sim 3$  hours in their warm counterparts. Shiptrack emissions eventually induce a divergent flow at the top of the cloud, promoting cloud breakup under certain conditions (Chen et al., 2015).

In order to inform and constrain models to realistic representations of aci, many observational studies find the susceptibility of a cloud characteristic to an aerosol perturbation. While a GCM can produce realistic global means, relationships between the cloud characteristics and aerosol reveals the true biases and error of a model (Carrier and Lenhard, 2019). By utilizing susceptibilities to judge GCM cloud parameterizations, the satellite observed global mean susceptibility of CRE regressed against an aerosol concentration proxy can be used as a comparison against a GCM simulated CRE against the same simulated proxy. This reveals if the magnitude and/or sign of the relationship within GCMs is correct (Ma et al., 2018). Even other relationship susceptibilities, such as the efficacy of precipitation regressed against aerosol in order to quantify the approximate magnitude of the second indirect effect, provide vital information on how well a GCM realistically produces these same relationships (Wang et al., 2012).

Recent work has suggested the aerosol concentration proxy chosen to estimate an ERFaci can skew the magnitude (Hasekamp et al., 2019). Many studies use aerosol optical depth (AOD) from MODIS to approximate aerosol concentration. AOD is only dependent on the amount of extinction within a column observed by MODIS, therefore if the aerosol is large but not abundant, or small and abundant, the AOD may be the same even if the properties of the aerosol are different. The aerosol concentration proxy should be equivalent to the amount of aerosol suitable to serve as a CCN, therefore using AOD may overestimate and underestimate the amount of suitable aerosol within the atmosphere. Aerosol index (AI) is a weighted measure of AOD by the turbidity of the layer defined by the Angstrom exponent (Bréon et al., 2002). The ERFaci decreases by  $.5 \text{ Wm}^{-2}$  when ERFaci is found using AOD vs. AI ( $-.33 \text{ Wm}^{-2}$  vs.  $-.80 \text{ Wm}^{-2}$ , respectively). So although observations can be used to find a "truth" estimate of the ERFaci and relationships between cloud properties and aerosol concentration, this "truth" value depends on how well the observed variables represent the desired quantities.

Not only do satellite-based trends in ACI depend on how well the observed variable represents the desired quantity, but how averaging may affect the robustness of the derived relationships (Grandey and Stier, 2010). In order to prove a relationship is not an artefact of the observations, the averaging scale of the observations should have very little impact on the susceptibility's magnitude and sign. Satellite studies cannot be used to find causality between aerosol and cloud properties, but robust

relationships can increase our confidence in our process based knowledge.

### 1.2.5 Constraining aerosol-cloud interactions

While regressing a cloud property against a proxy for aerosol concentration does provide an estimate of  $\text{aci}$ , it ignores the possible variation in the relationship due to confounding factors such as the environment or cloud state. The environment plays a leading role in determining how aerosol affects the cloud layer. The assumed first and second indirect relationships may only occur under ideal environmental conditions. Chen et al. (2012) found that closed cell marine stratocumulus dimmed as underlying ships loaded the clouds with aerosol. The environment controls the state of stratocumulus as either open or closed cell, and the variability of the cloud and its properties as it transitions between open to closed and the states in between, therefore the environment is directly moderating whether aerosol acts to increase or decrease the albedo (Stechmann and Hottovy, 2016). The relationship between a cloud property, such as cloud albedo, and aerosol concentration is only useful if the full context of the process leading to a change is understood. Regressing only the regional mean CRE against AI does derive a **mean** susceptibility, but would ignore minute responses such as the cloud dimming Chen et al. (2012) found in closed cell ship tracks. Lee et al. (2012) found the environment may act to "buffer" the cloud layer against aerosol perturbations. The morphology of a cloud and environment must be considered in order to isolate the roles of the environment and cloud state in buffering the system.

Stevens and Feingold (2009a) suggested a new framework had to be developed in order to properly characterize the range of responses clouds may have to aerosol beyond the mean susceptibility. In particular, "buffering," or a reduced response by the system through counteracting processes, may be why damped susceptibilities are observed in some regions, masking the true response of the cloud to aerosol. Chen et al. (2014) found when the stability and humidity above cloud are accounted for globally, there are a set of different susceptibilities of warm cloud CRE to aerosol depending on the environmental conditions. Further, the sign and magnitude of the LWP response to aerosol, one of the most pertinent cloud adjustments to understand as it links the cloud albedo to the second indirect effect, depends on the environment. Cloud dimming may be a response of the cloud to aerosol under certain environmental conditions, but may also be reflecting a decrease in LWP due to aerosol in other environmental conditions.

Regimes, or partitions of clouds based on their characteristics or the environment surrounding them, allow further inference on the behavior of particular clouds to aerosol loading. Regime specific behavior is pertinent to understand as well as quantify in order to better our cloud parameterizations and categorize the error in GCMs (Douglas and L'Ecuyer, 2019a). The extreme susceptibility of marine warm clouds to aerosol becomes apparent when cloud regimes are established based on cloud type alone (Gryspeerdt and Stier, 2012). However, cloud type itself can be influenced by aci. Gryspeerdt et al. (2013) found marine stratocumulus are more likely to form due to ACI compared to cumulus or stratus. Established regimes must go beyond cloud

type in order to account for covarying factors such as how aerosol may affect cloud type.

### **1.2.6 LWP: a confounding relationship**

LWP has been shown to have a non-linear relationship with aerosol. A single regression to find a susceptibility will show no correlation when in reality the LWP may first increase then decrease with increasing aerosol Gryspeerdt et al. (2019a). The second indirect effect dictates that aerosol will delay precipitation, which will increase the LWP and lifetime of the cloud, which should be a quasi-linear relationship if true (Albrecht, 1989). While there remains evidence that clouds do grow deeper and more extensive as aerosol increases, it remains unclear how aerosol affects the LWP (Christensen and Stephens, 2011, Goren and Rosenfeld, 2014).

Rosenfeld et al. (2019) found the LWP is extremely responsive to aerosol perturbations. In their satellite observation based study of warm, marine clouds, aerosol concentration, described by cloud drop concentrations  $N_d$ , can account for 25% of the variation in LWP and meteorology for the other 75%. They argue that the LWP does in fact increase as  $N_d$  increases, until the cloud has reached a critical point and additional aerosol leads to no impact on LWP. Rosenfeld et al. (2019) accounted for the environment by taking multivariate linear regressions of the cloud LWP and CRE against  $N_d$ , the stability of the boundary layer, and the cloud state defined by the thickness and cloud top cooling rate.

Contrary to Rosenfeld et al. (2019), Toll et al. (2019) found LWP is relatively unresponsive to aerosol loading in marine, warm clouds. Unlike Rosenfeld et al. (2019) which used a multivariate regression including environmental information, Toll et al. (2019) partitioned their observations by the source of the aerosol perturbing the cloud. They found the response of the cloud depth to aerosol depends on the type of aerosol introduced; the greatest deepening response occurred over land due to industry emissions. However, for all types of aerosol, the LWP showed no response compared to unpolluted, pristine control cases. This relationship and the associated processes behind the damped response of the LWP found by Toll et al. (2019) can only be hypothesized on a surface level as the environmental conditions between each response is unknown.

### **1.2.7 Inclusion of regimes within my work**

I focused on my work on only warm clouds in order to set a first order constraint on my analysis: all susceptibilities found were for only stratocumulus, stratus, or cumulus regime clouds. I then extended my regime framework to include environmental conditions described by the stability of the boundary layer and the relative humidity in the free atmosphere ( $RH_{700}$ ). These constraints are held constant throughout my work as the susceptibility of warm clouds varies in sign and magnitude as the stability and  $RH_{700}$  vary (Douglas and L'Ecuyer, 2019a). The confounding relationship between aerosol and LWP motivates my inclusion of limits on the LWP of the cloud.

Establishing regimes allows a process based understanding of the derived susceptibilities and the comparison to GCM related susceptibilities found within the same constraints.

## Chapter 2

### Data

Throughout my work, I utilized four years of satellite observations (2007 - 2010) from collocated sensors aboard the NASA A-Train constellation. Many of the same products were used throughout my chapters. I have summarized the main products and variables here along with a visualization (Figure 2.1). The products of the NASA A-Train were developed to provide information on radiation, clouds, and aerosols globally in a coordinated effort to improve our understanding of the Earth system (L'Ecuyer and Jiang, 2011).

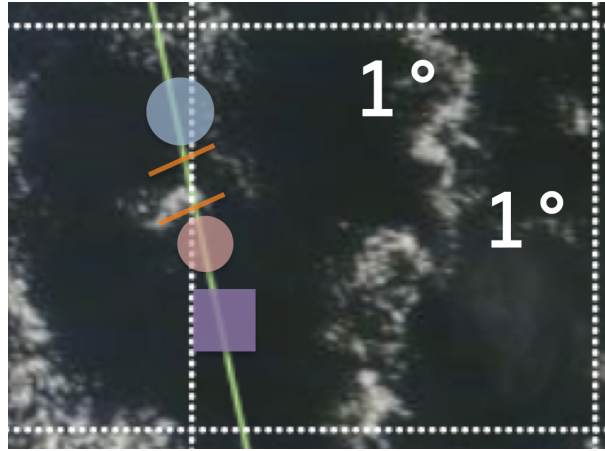


FIGURE 2.1: An example of the size of the footprints of the various sensors used along the CloudSat/CALIPSO track (green). The cloud fraction is at a 12 km, along track scale (distance between orange lines). The AMSR-E footprint for the 36.5 GHz channel is  $\sim 14$  km (blue circle). The CERES footprint is 12 km (red circle). MODIS aerosol information is provided at a 1 km x 1 km resolution. Within the purple square, there would be 25 observations of MODIS aerosol properties. MERRA-2 reanalysis is at  $.5^\circ \times .5^\circ$  resolution on the grid with the closest profile to each CloudSat pixel being chosen as the environmental state for that time.

## 2.1 Satellites used in analysis

### 2.1.1 CloudSat

All cloud properties including cloud top height, cloud fraction, and precipitation status utilized various CloudSat data products. Observations were limited to single layer warm clouds using 2B-CLDCLASS-LIDAR. This CloudSat product combines the radar returns from CloudSat's CPR with the CALIPSO lidar measurements in order to classify clouds by type. A benefit of combining radar and lidar measurements is even the thinnest of clouds with optical depths less than .03 are observed by the lidar (Sassen et al., 2008). Both the radar and lidar are able to distinguish multiple cloud layers within a single field-of-view, allowing us to limit our analysis

to only single layer clouds without overlying cirrus. Cloud top height is defined by 2B-CLDCLASS-LIDAR CloudLayerTop, which provides an estimate of the height of the cloud top defined by either CloudSat or CALIPSO. To limit our observations to warm clouds only, this height must be below the freezing level height from the European Centre for Medium-range Weather Forecasts (ECMWF) model included in the 2C-PRECIP-COLUMN product.

Cloud fraction is defined by averaging the number of warm, cloudy pixels within a 12 km segment along track. We chose 12 kms to approximate a scale close to that of boundary layer processes and divisible by the size of the CERES footprint. During preliminary analysis when applying our regime framework, we found that our results remain constant even as the cloud fraction is increased to 24 km and 96 km scales (Douglas, 2017). However, we chose to keep the scale at 12 km so even the smallest changes in cloud extent or cloud top height are captured and represented by our regressions (Jiang et al., 2009).

Precipitation is indicated by 2C-PRECIP-COLUMN Precip\_flag (Haynes et al., 2009). Precip\_flag indicates how certain CloudSat is of precipitation formation within the cloud layer: 0 indicates no precipitation of any type detected, 1 indicates rain possible, 2 indicates rain probable, and 3 indicates rain certain. In order to separate precipitating from non-precipitating, I chose to use Precip\_flag 3 as rain certain and Precip\_flag 0 as non-precipitating. This removes light drizzle and virga from results in Chapter 3, where the ERFaci is decomposed into environmental and cloud state

regimes, and from results in Chapter 5, where the effects of aerosol on rain processes are investigated.

The shortwave and longwave top-of-atmosphere fluxes for cloudy pixels only are provided by the CloudSat 2B-FLXHR-LIDAR product (L'Ecuyer et al., 2008). The shortwave top-of-atmosphere flux is weighted by the solar mean incoming flux to remove seasonal solar cycle biases. The 2B-FLXHR-LIDAR model estimates radiative fluxes using the liquid water content retrieved from CPR along with additional cloud and aerosol properties from collocated CALIPSO and MODIS retrievals. The ECMWF provides additional context on the atmospheric conditions for each derived flux profile. Precipitation within the cloud is provided by 2C-PRECIP-COLUMN.

### **2.1.2 Aqua**

The scene liquid water path is indicated by Advanced Microwave Scanning Radiometer for EOS (AMSR-E). AMSR-E is a twelve-channel passive radiometer aboard Aqua. LWP is determined by the 36.5 GHz channel (Wentz and Meissner, 2000). AMSR-E LWP has been shown to agree well with other satellite derived estimates of LWP for liquid, thin clouds ( $LWP < 300 \text{ gm}^{-2}$ ) (Stephens and Kummerow, 2007). The LWP product from AMSR-E is for all-sky (both cloudy and clear) pixels within its  $\sim 14$  km field-of-view.

Aerosol index is the product of the AOD at 550 nm and the Angstrom exponent from MODIS aboard Aqua. Aerosol index characterizes the size and concentration of

aerosol in the atmosphere. The Angstrom exponent is the slope of the AOD between 550 and 870 nm, which is inversely proportional to the size of the particles (Ångström, 1929). AI has been shown to be better correlated with the amount of CCN than AOD (Hasekamp et al., 2019, Stier, 2016). AI is not available in cloudy scenes from MODIS requiring us to interpolate AI between cloudy pixels.

### 2.1.3 CERES

The warm cloud radiative effect from CERES is used to define an overall susceptibility and ERF<sub>aci</sub>. CERES captures top-of-atmosphere radiative fluxes in total (.4 - 200  $\mu\text{m}$ ) and shortwave (.4 - 4.5  $\mu\text{m}$ ) channels (Loeb and Kato, 2002). The shortwave warm cloud radiative effect can be calculated using the all-sky CERES shortwave flux along with cloud fraction estimates from CloudSat.

$$F_{\text{All Sky}}^{\uparrow} - F_{\text{Clear Sky}}^{\uparrow} \times (1 - \text{CF}) = \text{CRE} \quad (2.1)$$

Where  $F^{\uparrow}$  is the outgoing shortwave flux, CF is the cloud fraction, and CRE is the calculated cloud radiative effect.

## 2.2 Reanalysis products used

MERRA-2 reanalysis provides temperature and humidity profiles (Gelaro et al., 2017). The relative humidity at 700 mb is used to define the humidity of the free atmosphere. Subsidence heating and other large scale dynamical effects may result in a drying or moistening of this layer, which would then impact how boundary layer entrainment at the cloud top affects the cloud. The estimated inversion strength is a measure of stability in the atmosphere highly correlated with low cloud extent (Wood and Bretherton, 2006). Similar to the lower tropospheric stability, or the difference in the potential temperature between the surface and the free atmosphere, the EIS includes the effect of moist processes on the stability of the boundary layer.

From Wood and Bretherton (2006):

$$\text{EIS} = \text{LTS} - \Gamma_m^{850}(z_{700} - \text{LCL}) \quad (2.2)$$

where  $\Gamma_m^{850}$  is the moist-adiabatic potential temperature gradient and LTS is the lower tropospheric stability.

## Chapter 3

# Decomposing the Shortwave Indirect Effect

### 3.1 Foreword

The work shown is currently under review with the Journal of Atmospheric Chemistry and Physics. Using satellite observations, I explore how the ERF<sub>aci</sub>, or the effective radiative forcing due to aerosol-cloud interactions since pre-industrial to present day times, may be estimated by summing its components the R<sub>Faci</sub> and cloud adjustments. Cloud adjustments are extremely difficult to quantify, as the LWP covaries with the R<sub>Faci</sub> and has a non-linear dependence on aerosol concentration. As such, the first constraint is placed on LWP in order to limit the non-linear, highly covarying factors between LWP, aerosol, the environment, and the resulting radiative forcing.

From there, I place an increasing number of constraints on the regressions used to define the ERFaci, cloud adjustments, and RFaci in order to understand how the environment, LWP, and regional dependencies alter the magnitude and the sign of forcings. Much of this work is based on my paper "Quantifying variations in short-wave aerosol–cloud–radiation interactions using local meteorology and cloud state constraints" where I first implemented and evaluated how the susceptibility of the warm cloud CRE depends on the environmental and cloud state regime.

## 3.2 Abstract

Aerosol-cloud interactions and their resultant forcing remains one of the largest sources of uncertainty of future climate scenarios. The effective radiative forcing due to aerosol-cloud interactions (ERFaci) is a combination of two different effects, how aerosols modify cloud brightness (RFaci, intrinsic) and how cloud extent reacts to aerosol (cloud adjustments CA, extrinsic). Using satellite observations of warm clouds from the NASA A-Train constellation from 2007 to 2010 along with MERRA-2 re-analysis and aerosol from the SPRINTARS model, we evaluate the ERFaci in warm, marine clouds and its components, the  $\text{RFaci}_{\text{warm}}$  and  $\text{CA}_{\text{warm}}$ , while accounting for the liquid water path and local environment. We estimate the  $\text{ERFaci}_{\text{warm}}$  to be  $-0.32 \pm 0.16 \text{ Wm}^{-2}$ . The  $\text{RFaci}_{\text{warm}}$  dominates the  $\text{ERFaci}_{\text{warm}}$  contributing 80% ( $-0.21 \pm 0.15 \text{ Wm}^{-2}$ ), while the  $\text{CA}_{\text{warm}}$  enhances this cooling by 20% ( $-0.05 \pm 0.03 \text{ Wm}^{-2}$ ). Both the  $\text{RFaci}_{\text{warm}}$  and  $\text{CA}_{\text{warm}}$  vary in magnitude and sign regionally, and can lead to opposite, negating effects under certain environmental conditions. Without

considering the two terms separately, and without constraining cloud-environment interactions, weak regional  $ERF_{aci_{warm}}$  signals may be erroneously attributed to a damped susceptibility to aerosol.

### 3.3 Introduction

Aerosol-cloud interactions (ACI) and their impact on cloud radiative effects are a vital component of Earth’s radiative balance. Warm clouds, in particular, are susceptible to aerosols, and due to their prevalence and role as “Earth’s sunblock”, these interactions are critical for regulating Earth’s surface temperature (Platnick and Twomey, 1994). Aerosols entering a cloud may become cloud condensation nuclei (CCN) initiating a domino effect wherein the cloud’s droplet number increases, reducing the mean droplet radius, brightening the cloud’s albedo, dampening its ability to precipitate, and, in theory, increasing its lifetime and radiative effect (Albrecht, 1989, Twomey, 1977b). However, it remains unknown to what degree aerosols alter warm cloud radiative forcing as models and observations disagree. Global climate models are prone to uncertainty due to their dependence on parameterizations and inability to explicitly represent all scales of ACI, while satellite observations have poor temporal resolution, and natural covariances with the environment may influence warm cloud response to aerosol (Stevens and Feingold, 2009b). In order to understand aerosol-cloud interactions and the resulting change in cloud radiative effect, observation-based methods must address the inherent limitations of satellite observations by creating a

framework to resolve the interplay between clouds, the environment, and aerosol-cloud interactions (Seinfeld et al., 2016).

Correctly quantifying the effective radiative forcing due to aerosol-cloud interactions (ERF<sub>aci</sub>) of warm clouds specifically is important to establish a climate sensitivity and identify cloud feedbacks (Bony and Dufresne, 2005, Boucher et al., 2013, Rosenfeld, 2006). It has been understood since the early 1990s that low, warm clouds play a leading role in determining future warming scenarios (Slingo, 1990). The micro- and macrophysical responses of warm clouds to ACI lead to numerous, poorly understood cloud feedbacks in the Earth system (Gettelman and Sherwood, 2016). Clouds do not exist in isolation (Stephens, 2005). Clouds are part of an interconnected system; changes to one aspect, such as particle size or liquid water content, has a ripple effect to other components of the Earth system. Likewise, clouds can be thought of residing in a “buffered system” where a clouds response to aerosol perturbations can be invigorated or diminished depending on the conditions in which it is initiated (Stevens and Feingold, 2009b). These interconnections lead to a range of cloud responses to aerosol that depend on the local meteorology and cloud state (Douglas and L’Ecuyer, 2019b). Both the short and long time scales of ACI and their radiative forcing are affected by the interconnections they exist in, meaning constraining the ERF<sub>aci</sub> of warm clouds must go beyond a single measure of the ERF<sub>aci</sub> globally and distinguish the individual components of the ERF<sub>aci</sub>, the radiative forcing due to aerosol-cloud interactions (RF<sub>aci</sub>) and cloud adjustments (CA). To account for the challenges in

estimating the cloud radiative response to aerosol, we constrain the influences of the local meteorology and cloud state using a method developed in Douglas and L’Ecuyer 2019, hereafter DL19. The  $ERF_{\text{Faci}_{\text{warm}}}$  is separated into the  $RF_{\text{Faci}_{\text{warm}}}$  and cloud adjustments determined with constraints on meteorology following DL19 and estimates of each effect are presented to find the relative contributions of the  $RF_{\text{Faci}_{\text{warm}}}$  and cloud adjustments to the  $ERF_{\text{Faci}_{\text{warm}}}$ . The present study expands upon work done in DL19 by specifying what aspects of the cloud lead to changes in the CRE, whether that be the brightness or cloud extent or both, and whether these changes can negate each other, such as when a cloud shrinks but the brightness increases.

Warm clouds, like marine stratocumulus and trade cumulus, are the prevailing cloud type over the oceans and dominate aerosol-cloud interactions (Gryspeerdt and Stier, 2012). Marine stratocumulus over the cold upwelling waters, such as off the west coast of Africa, persist for long periods of time in the stable, low marine boundary layers (Wood, 2012). Cumulus form from marine stratocumulus to cumulus transitions and in the equatorial region as trade cumuli (Sandu and Stevens, 2011). Warm clouds sheer abundance and bright albedo make them important to the radiative balance of Earth, and it should be no surprise that warm clouds contribute the largest amount of forcing to the  $ERF_{\text{Faci}}$  (Christensen et al., 2016). Marine stratocumulus have been the primary focus of aerosol-cloud-radiation interactions due to their sheet-like, “homogeneous” structure, pervasiveness ( $\sim 25\%$  of the Earth at any moment), location

near anthropogenic continental emissions, and susceptibility to changes in their CCN (Hahn and Warren, 2007b, Platnick and Twomey, 1994).

The warm cloud albedo has the largest response to aerosol compared to mixed phase or ice phase clouds (Christensen et al., 2016). Twomey was the first to hypothesize the high susceptibility of entirely liquid clouds to aerosol using a simple cloud model; work since then has confirmed this as the basis of RFaci (Twomey, 1977b). Observation- and model-based studies focus on the albedo effect because it is a macrophysical manifestation of microphysical processes. An increase in CCN and decrease in mean droplet radius greatly increases the cloud albedo, and, as such, has significant implications for the radiative balance. The radiative forcing of the albedo effect, or the sudden microphysical response to aerosol loading (RFaci), is dependent on the activation and eventual microphysical initiation of aerosol as cloud droplets, which can be influenced by local dynamics, the stability of the boundary layer, and the initial cloud state (Su et al., 2010). "Model" conditions simulated by Twomey only exist in the most pristine, stable southern oceans (Gryspeerd et al., 2017, Hamilton et al., 2014). Depending on the region studied, aerosol can increase the cloud albedo as expected, or in certain cases, lead to a dimming effect, such as when aerosol loading reaches a critical point or the local meteorology regulates the sign and/or magnitude of ACI (Christensen et al., 2014, Gryspeerd et al., 2019b). Studies conflict to what degree the RFaci dominates the ERFaci, in part because the cloud acts as a "buffered system" and mitigates the RFaci depending on the thermodynamic conditions, making

the quantification of the RFaci particularly challenging (Feingold et al., 2016, Goren and Rosenfeld, 2014, Stevens and Feingold, 2009b).

Efforts to understand the other component of the ERFaci, cloud adjustments, have been similarly clouded in uncertainty. Cloud lifetime and extent are highly susceptible to aerosol (Dagan et al., 2018b). Models have shown that aerosol affects the distribution of liquid throughout the cloud and vertical motion within the cloud, greatly perturbing the cloud’s lifetime, precipitation, and extent (Dagan et al., 2016, Ramanathan et al., 2001). Aerosol can act to increase the lifetime of clouds through delayed collision coalescence, or decrease the lifetime through evaporation-entrainment and induced cloud feedbacks (Albrecht, 1989, Small et al., 2009). A satellite observation-based study of ship tracks showed clouds experience a expansion or shrinking of cloud extent depending on whether the clouds are at an open or closed state and the background state of the aerosol (Chen et al., 2015). The cloud adjustment response depends on the cloud state and a sequence of reactions dictated by the environment (Gryspeerdt et al., 2019b). As such, cloud adjustments remain the largest source of variability of ERFaci in global climate models (Fiedler et al., 2019).

To account for influences and variation in the  $\text{ERFaci}_{\text{warm}}$ ,  $\text{RFaci}_{\text{warm}}$ , and warm cloud adjustments, we constrain the liquid water path, relative humidity of the free atmosphere, and stability of the boundary layer and covariances between them before evaluating the susceptibility of the effect in the same fashion as DL19. These constraints are held fixed first on a global and then on a regional basis to diagnose regime

specific then regionally specific responses. Finally, the decomposed  $ERFac_{warm}$ , or the sum of the  $RFac_{warm}$  and warm cloud adjustments, is calculated, with constraints on the environment and cloud state, for precipitating and non-precipitating scenes on a regional basis. Our methodology aims to reduce biases by accounting for the regionally specific aerosol and thermodynamic conditions (Feingold, 2003). The relationship between aerosol and cloud response has been proven to be sensitive to regional features like aerosol type or meteorology (Chen et al., 2014, Twohy et al., 2005)(DL19). Aerosol-cloud interactions experience a non-linear relationship with liquid water path therefore it is important to separate this complex relationship from ACI and the associated forcing in order to reduce the effects of this non-linear relationship on our results (Gryspeerd et al., 2019b).

## 3.4 Methodology and Observations

### 3.4.1 Data

Collocated satellite observations of cloud shortwave effect, cloud fraction, and aerosol index are obtained by NASA A-Train satellites Aqua, CloudSat, and The Cloud-Aerosol Lidar and Infrared Pathfinder Satellite Observation (CALIPSO) from 2007 to 2010. The NASA A-Train was intentionally created to maximize the synergy between different satellite products in order to improve our understanding of clouds, aerosols, and the environment (L'Ecuyer and Jiang, 2011). Observations of marine warm clouds and aerosols from the Cloud Profiling Radar (CPR) and Moderate Resolution Imaging

Spectroradiometer (MODIS) aboard CloudSat and Aqua, respectively, are utilized to evaluate the effects of aerosol-cloud interactions on the radiative properties of clouds including their albedo and extent.

CloudSat was launched to an orbit collocated with Aqua and other A-Train satellites in 2006. The CPR on CloudSat is a 94 GHz radar with a  $\sim 1.7$  km along track, 1.4 km cross track resolution, and 480 m vertical resolution (Stephens et al., 2018, Tanelli et al., 2008). A number of cloud properties can be inferred using the CPR backscatter including cloud top height, cloud type, and accompanying radiative effects.

An along track warm cloud fraction is defined using cloud top height from 2B-CLDCLASS-LIDAR and freezing level from 2C-PRECIP-COLUMN. 2B-CLDCLASS-LIDAR combines CloudSat's CPR with CALIPSO lidar observations in order to discern even the thinnest clouds. At each pixel, the cloud fraction is defined by the amount of cloud uptrack and downtrack of that pixel at a 12 km scale, chosen to approximate the scale of marine boundary layer processes and accentuate small scale changes in extent compared to other large sizes (e.g.  $1^\circ \times 1^\circ$ ). Using a smaller scale such as 12 kms for cloud fraction will allow even minute changes in the cloud extent to be detected by our methodology; using a larger size such as 96 km ( $\sim 1^\circ$ ) may diminish cloud breakup processes within large stratocumulus decks or minimize effects on trade cumuli. 2B-CLDCLASS-LIDAR includes collocated Cloud-Aerosol Lidar with Orthogonal Polarization (CALIPSO) satellite lidar backscatter measurements to identify thin, shallow clouds that may escape detection by the CPR (Sassen et al.,

2008). Cloud top heights from 2B-CLDCLASS-LIDAR, defined using a combination of collocated lidar and CPR measurements, are required to be below the freezing level (Haynes et al., 2009). The freezing level of 2C-PRECIP-COLUMN is obtained from European Centre for Medium-Range Weather Forecasts (ECMWF) analyses and is used to separate warm from mixed and ice phase clouds. Focusing only on warm phase clouds helps reduce the uncertainty associated with retrievals of mixed and ice phase clouds.

Cloud fraction is combined with shortwave top of atmosphere forcings from the Cloud-Sat 2B-FLXHR-LIDAR product to approximate the effect of aerosol on albedo. 2B-FLXHR-LIDAR uses a combination of CPR and CALIPSO measurements along with MODIS cloud properties and atmospheric conditions from ECMWF as input to a radiative transfer model that computes top of atmosphere shortwave fluxes that have been shown to agree well with CERES observations (Henderson et al., 2013). The mean shortwave flux at the top of atmosphere is weighed by a mean incoming solar radiation at the top of atmosphere in our analysis to account for diurnal variation of incoming solar radiation not sampled by the sun-synchronous A-Train orbit.

We use aerosol index (AI) as a proxy for aerosol concentration from MODIS. The AI is the product of the Angstrom exponent, calculated using aerosol optical depth (AOD) at 550 and 870 nm, and the AOD at 550 nm. AI has been shown to have a higher correlation with CCN compared to AOD (Hasekamp et al., 2019, Stier, 2016). Cloudy

scene AI is determined by interpolating between clear scenes along track. This interpolation may reduce the accuracy in completely overcast scenes, however for most scenes where cloud fraction is  $< 1$ , this interpolation should be sufficiently accurate. Aerosol swelling in high humidity environments also leads to some uncertainty in AI but should be limited to select high humidity environmental regimes. Pre-industrial aerosol information is provided by Spectral Radiation-Transport Model for Aerosol Species (SPRINTARS), an atmosphere-ocean general circulation model (Takemura et al., 2000). Pre-industrial aerosol errors lead to the majority of uncertainty in ACI due to uncertainties in transport, source, and concentration of pre-industrial aerosol conditions (Chen and Penner, 2005).

The sign and regional variations in susceptibilities found using MODIS AI shown within this study were evaluated against susceptibilities found using MACC and SPRINTARS aerosol in order to qualitatively scrutinize any error due to aerosol retrieval (Douglas, 2017). MACC and SPRINTARS provide independent aerosol estimates not susceptible to swelling, instrument sensitivity or retrieval error.. The fact that our results were qualitatively similar using modeled aerosol provides confidence that the derived susceptibilities shown are not simply an artifact of using satellite-derived AI.

The analysis is constrained to clouds with LWPs between  $0.02$  to  $0.4 \text{ kgm}^{-2}$  using the Advanced Microwave Scanning Radiometer for Earth Observing Satellite (AMSR-E), an instrument aboard Aqua that infers water vapor and precipitation amounts

using six microwave frequencies over a  $\sim 14$  km<sup>2</sup> area (comparable to the averaging scale of our cloud fraction) (Parkinson, 2003, Wentz and Meissner, 2007). While the footprints of CloudSat and AMSR-E do not perfectly overlap, the AMSR-E LWP is used to establish a scene based constraint on the clouds in order to better consolidate our observations into regimes. AMSR-E’s footprint is within  $\sim 2.5$  km of CloudSat’s track, meaning both sensors are observing the same, liquid clouds (Lebsock and Su, 2014). Imposing these LWP limits in place removes only  $\sim 1\%$  of observations leaving over 1.8 million satellite observations for analyses, but avoids possible skewing by extremely thick, bright clouds or extremely thin, dim clouds.

Environmental information to define local meteorological regimes is provided by the Modern-Era Retrospective analysis for Research and Applications, version 2 (MERRA-2) reanalysis (Gelaro et al., 2017). To broadly characterize large-scale environmental conditions, MERRA-2 temperature and humidity profiles are collocated by taking the environmental profile within 30 minutes of a CloudSat overpass and within  $\sim \frac{1}{2}^\circ$  latitude and longitude. Vertical profiles of humidity and temperature are used to calculate the estimated inversion strength (EIS) of the boundary layer and the relative humidity at 700 mb ( $RH_{700}$ ) to represent the humidity of the free atmosphere (Wood and Bretherton, 2006). By simultaneously stratifying the observations by LWP, RH, and EIS, the analysis directly accounts for covariability between LWP and the local environment by separately evaluating the susceptibility of each environmental regime within distinct LWP limits (Douglas and L’Ecuyer, 2019b).

Clouds are separated into precipitating and non-precipitating regimes using CloudSat’s 2C-PRECIP-COLUMN precipitation flag. Clouds with a 0 precipitation flag, no precipitation detected, are designated as non-precipitating. Precipitating clouds are separated using flag 3, where rain is certain (Haynes et al., 2009). Our precipitating clouds include a majority of the drizzling cases, as CloudSat’s 2C-PRECIP-COLUMN’s threshold for drizzle is -15 dB, which should capture all but the lightest drizzling clouds (Stephens and Wood, 2007).

### 3.4.2 Methodology

In DL19, environmental and cloud state regimes were imposed on a regional basis in order to identify regime specific behavior of aerosol-cloud-radiation interactions. Within each regime, we regressed the cloud radiative effect (CRE) against AI in order to find the susceptibility of warm cloud radiative properties to aerosol. We use these same susceptibilities within section 3.1 to quantify the total warm, marine  $ERF_{aci}$ . DL19 found that the susceptibility varies regionally and by regime, however the  $ERF_{aci_{warm}}$  depends on the magnitude to which aerosol has increased since pre-industrial times. Further, the  $ERF_{aci_{warm}}$  does not diagnose what characteristics of the cloud are causing the effect, prompting us within this paper to decompose the  $ERF_{aci_{warm}}$  into the effects on the albedo and the effects on cloud extent.

The mean shortwave flux at the top-of-atmosphere from CloudSat’s 2B-FLXHR-LIDAR along with our definition of warm cloud fraction from 60° S to 60° N are used to define the  $R_{Faci_{warm}}$  and cloud adjustment terms of the  $ERF_{aci_{warm}}$ . We first

calculate the  $\text{ERFaci}_{warm}$  on a regional basis with regime constraints using estimates of the susceptibility of the warm CRE to aerosol from DL19 and pre-industrial and present-day AI from SPRINTARS. We then use a partial derivative decomposition to separate out the  $\text{RFaci}_{warm}$  and cloud adjustment terms. These terms are evaluated globally as susceptibilities with constraints on the local meteorology and cloud state following the methodology of DL19. The  $\text{RFaci}_{warm}$  and cloud adjustments are evaluated regionally with constraints on cloud state and local meteorology. The decomposed  $\text{ERFaci}_{warm}$  is evaluated for precipitating and non-precipitating scenes to account for the potential effects of precipitation on ACI. Finally, the sum of the  $\text{RFaci}_{warm}$  and cloud adjustments, the decomposed  $\text{ERFaci}_{warm}$ , is compared against the first estimate of the  $\text{ERFaci}_{warm}$ .

### 3.4.3 Regimes

Following DL19, the  $\text{ERFaci}_{warm}$  and components are evaluated within a constrained space on both a global and regional scale. LWP is held approximately constant using a set of twelve LWP limits on a global basis and five LWP limits on a regional basis. This is in line with the original work of Twomey, who surmised that only for a fixed LWP will the cloud albedo increase in more polluted conditions. The local meteorology is defined by the stability of the boundary layer and the relative humidity of the free atmosphere. Both the stability, characterized by the estimated inversion strength, and the relative humidity of the free atmosphere, defined at the 700 mb level, have been shown to influence the sign and magnitude of the susceptibility of the CRE

to aerosol (Ackerman et al., 2004, De Roode et al., 2014, Wood and Bretherton, 2006). The resulting regimes isolate the susceptibility of the cloud to aerosol under controlled conditions. Buffering can entail the cloud being too thick and impervious to changes due to aerosol due to its high LWP, offsetting and opposite reactions of the cloud resulting in reduced mean signal, or the environment acting to damp the cloud reaction, such as an unstable boundary layer reducing the impact of aerosol on cloud lifetime (Fan et al., 2016, Stevens, 2007). Using EIS and  $RH_{700}$  does not guarantee to limit all covariability between the environment, aerosols, clouds, and their interactions. Some covariability may still exist, such as surface winds that may affect both clouds and aerosol (Nishant and Sherwood, 2017). These constraints only account for the major environmental controls on clouds and aerosol-cloud interactions, some more minor or less common environmental controls may still exert an influence on our results.

While binning our observations by environmental regime should control for some modulation the environment has on aerosol-cloud interactions, it does not fully capture aerosol-environment interactions. For example, in some regions such as off the coast of Africa, biomass burning results in smoke layers that absorb incoming radiation and warm the atmosphere (Cochrane et al., 2019). This could affect the humidity and temperature of the local environment. Environmental regime constraints would capture how the altered environment may regulate aerosol-cloud interactions, but separation into such regimes does not address how the aerosol has impacted the environment.

### 3.4.4 Decomposing the ERFaci

A Newtonian-based method is employed to represent the  $\text{ERFaci}_{warm}$  as a sum of its parts, the  $\text{RFaci}_{warm}$  and cloud adjustments. A positive  $\text{ERFaci}_{warm}$ ,  $\text{RFaci}_{warm}$ , or cloud adjustment denotes a damped cooling effect of the cloud while a negative sign denotes an additional cooling due to aerosol-cloud interactions. If the shortwave cloud radiative effect is the product of the cloud fraction (CF) and the cloudy sky shortwave flux at the top-of-atmosphere ( $\text{SW}_{Cloudy}$ ):

$$\text{CRE} = \text{CF} \times \text{SW}_{Cloudy} \quad (3.1)$$

then, taking the derivative of the CRE with respect to the log of aerosol index, we find the effective radiative forcing due to aerosol-cloud interactions ( $\text{ERFaci}_{warm}$ ) or the change in the CRE with respect to aerosol:

$$\text{ERFaci} = \frac{\partial \text{CRE}}{\partial \ln(\text{AI})} \times \Delta \ln(\text{AI}) \quad (3.2)$$

where  $\Delta \ln(\text{AI})$  is the change in  $\ln(\text{AI})$  from pre-industrial to present-day conditions derived from SPRINTARS. SPRINTARS is a 3-D aerosol model that includes emission,

advection, diffusion, chemistry, wet deposition, and gravitational settling of multiple species of aerosol driven by a general circulation model developed by the University of Tokyo (Takemura et al., 2005, 2000). The results shown herein depend on the emissions scheme from SPRINTARS; if the model were altered, it is possible the total forcing would change due to different  $\Delta\ln(\text{AI})$ .

All susceptibilities are found using MODIS AI, while only the  $\Delta\ln(\text{AI})$  term uses SPRINTARS modeled aerosol. The lowest 12% of aerosol indices are ignored when determining a susceptibility, as these have been shown to have little to no correlation with CCN compared to higher indices (Hasekamp et al., 2019). Error in MODIS AI estimates adds the greatest source of uncertainty in the observationally based portion of this study, however, signals derived are all robust enough to be observed even when random error is added to 10% of the AI estimates. The regressions within all regime constraints, from only meteorological to regional, remain robust for all susceptibilities when 10% of the AI estimates were randomly assigned. The same relationships can be qualitatively observed when SPRINTARS AOD is used in lieu of MODIS AI (Douglas, 2017).

The susceptibility ( $\frac{\partial\text{CRE}}{\partial\ln(\text{AI})}$ ) can be obtained directly from satellite estimates of top-of-atmosphere clear-sky and all-sky fluxes and aerosol index or further decomposed into separate albedo and cloud fraction responses using Equation 3.1. Applying the chain rule to equation 3.2, combined with the definition of CRE from Equation 1, gives:

$$\frac{\partial \text{CRE}}{\partial \ln(\text{AI})} = \frac{\partial \text{CF}}{\partial \ln(\text{AI})} \times \overline{\text{SW}}_{\text{Cloudy}} + \overline{\text{CF}} \times \frac{\partial \text{SW}_{\text{Cloudy}}}{\partial \ln(\text{AI})} \quad (3.3)$$

where the overbars represent means.

The sum of the right hand terms represent the decomposition susceptibility:

$$\text{Decomposition Susceptibility} = \lambda_{\text{Sum}} = \frac{\partial \text{CF}}{\partial \ln(\text{AI})} \times \overline{\text{SW}}_{\text{Cloudy}} + \frac{\partial \text{SW}}{\partial \ln(\text{AI})} \times \overline{\text{CF}} \quad (3.4)$$

The first term of Equation 3.4 represents the cloud adjustment susceptibility to aerosol, which to first order is the effect of aerosol on the cloud extent:

$$\text{Cloud Adjustment Susceptibility} = \lambda_{\text{CA}} = \frac{\partial \text{CF}}{\partial \ln(\text{AI})} \times \overline{\text{SW}}_{\text{Cloudy}} \quad (3.5)$$

The cloud adjustment forcing is the product of the cloud adjustment susceptibility  $\lambda_{\text{CA}}$  and the change in AI from pre-industrial to current times  $\Delta \ln(\text{AI})$ :

$$\text{Cloud Adjustment Forcing} = \lambda_{CA} \times \Delta \ln(\text{AI}) \quad (3.6)$$

The cloud adjustment susceptibility ( $\lambda_{CA}$ ) is described by its most notable effect, the enhancement and sustainment of clouds as a result of precipitation suppression. We define the cloud adjustments as the product of the change in cloud fraction with respect to aerosol index and the mean cloud shortwave forcing. By multiplying by the mean cloud shortwave forcing, a change in cloud extent is converted to a change in the reflected shortwave. While this term does not explicitly account for precipitation, we separate clouds by rain state and determine the difference in the  $\text{RFaci}_{warm}$  and cloud adjustments between precipitating/non-precipitating clouds; this difference is likely close to the overall effect of precipitation on aerosol-cloud-radiation interactions.

This cloud adjustment term accounts for the main process, the change in extent of clouds by aerosol, however many other studies define the cloud adjustment term by the change in LWP by aerosol. We choose to instead focus on the expansion or shrinking of clouds by aerosol and constrain any LWP effects. Research has yet to establish how and where LWP increases or decreases due to aerosol-cloud interactions; focusing on the changes to cloud extent reduces the error in the adjustment term due to this uncertainty.

The second term on the right hand side of Equation 3.4 represents susceptibility of warm cloud radiative forcing due to aerosol-cloud interactions (RFaci):

$$\text{RFaci Susceptibility} = \lambda_{RFaci} = \overline{\text{CF}} \times \frac{\partial \text{SW}_{\text{Cloudy}}}{\partial \ln(\text{AI})} \quad (3.7)$$

where the associated forcing is the product of the RFaci<sub>warm</sub> susceptibility  $\lambda_{RFaci}$  and the change in AI from pre-industrial to current times  $\Delta \ln(\text{AI})$ :

$$\text{Radiative Forcing due to aci} = \lambda_{RFaci} \times \Delta \ln(\text{AI}) \quad (3.8)$$

The RFaci<sub>warm</sub> susceptibility is the change in the shortwave effect owing to changes in cloud droplet radius, an immediate, fast response. The outgoing shortwave radiation for cloudy scenes depends on the cloud albedo; a brighter, whiter cloud will reflect more incoming solar radiation, increasing  $\text{SW}_{\text{Cloudy}}$  at the top of the atmosphere.  $\text{SW}_{\text{Cloudy}}$  is weighted by the annual solar insolation cycle in order to normalize the term and reduce the impact of changes in the incoming solar flux. RFaci<sub>warm</sub> is weighted by mean cloud fraction since the net effect of brighter clouds depends on how extensive they are.

Finally, to account for the dependence of each susceptibility (RFaci, CA, and total) on the meteorology and cloud state, each susceptibility ( $\lambda$ s from above) is evaluated in distinct EIS, RH, and LWP regimes regionally. The product of each susceptibility and  $\Delta\ln(\text{AI})$  is the resulting forcing of the aerosol-cloud-radiation interaction:

$$\text{Forcing} = \sum_{l=1}^{N_{\text{Reg}}} \sum_{k=1}^{N_{\text{LWP}}} \sum_{j=1}^{N_{\text{RH}}} \sum_{i=1}^{N_{\text{EIS}}} (\lambda_{i,j,k,l} \times W_{i,j,k,l}) \times \Delta(\ln(\text{AI})) \quad (3.9)$$

where  $W_{i,j,k,l}$  is the weighting factor,  $N$  is the number of limits imposed, and  $\lambda$  is the susceptibility being evaluated (ERFaci<sub>warm</sub>, RFaci<sub>warm</sub>, or CA) regionally ( $N_{\text{Reg}}$ ) with constraints on LWP, EIS, and RH<sub>700</sub>.  $W_{i,j,k,l}$  weights the ERFaci<sub>warm</sub>, RFaci<sub>warm</sub>, and cloud adjustments by the number of observations in each regime and also by the areal size of the region.

Constraints on LWP reduces the secondary effects of aerosol on LWP or LWP on susceptibility, as aerosol can result in thicker clouds and thicker clouds may have a damped reaction to aerosol. Constraining the meteorology separates signals forced by aerosol and the environment (Stevens and Feingold, 2009b). On a global scale the approach outlined in DL19 identifies regime specific behavior; when applied on regional scales, the regimes allow a process level understanding of the mean regional behavior (Mülmenstädt and Feingold, 2018). This approach is optimal for our satellite

based observations where larger scale parameters like AOD, AI, and cloud extent are less impacted by retrieval errors than specific properties of the aerosol.

The  $\text{RFaci}_{\text{warm}}$  and cloud adjustment susceptibilities are first understood with limits on the environment and cloud states on a global scale. Their individual forcings, or the product of the susceptibility and  $\Delta \ln(\text{AI})$ , are then found with constraints on the environment and cloud state regionally and contrasted against initial estimates of the  $\text{ERFaci}_{\text{warm}}$  evaluated under the same constraints. The susceptibility estimates are not forcings. Forcings are the product of the susceptibilities ( $\lambda_{\text{RFaci}}$  or  $\lambda_{\text{CA}}$ ) and the change in the aerosol index from pre-industrial times to current estimates ( $\Delta \ln(\text{AI})$ ). It is possible that even these estimates of forcing are slightly different than the definition of forcing from the IPCC or model based studies which difference top-of-atmosphere forcings in polluted vs. non-polluted GCM runs (Penner et al., 2011). The sum of these forcings, which we will term the decomposed  $\text{ERFaci}_{\text{warm}}$ , is contrasted against the simple expression for  $\text{ERFaci}_{\text{warm}}$  evaluated directly using Equation 3.2. By separating out the individual components of the  $\text{ERFaci}_{\text{warm}}$ , the physical processes of aerosol-cloud-radiation interactions can be better understood. The difference between the  $\text{ERFaci}_{\text{warm}}$  and the decomposed  $\text{ERFaci}_{\text{warm}}$  represents uncertainty in the linear decomposition owing to covariability, non-linearity, and other effects not quantified by our approach. In reality, there should be a covariability term at the end of Equation 3.4 to relate how a change in  $\text{RFaci}_{\text{warm}}$  may affect cloud adjustment processes or vice-versa, however a limitation of satellite observations are

that they cannot temporally relate events meaning covariance between the two terms cannot be accurately quantified (Seinfeld et al., 2016). We focus on the main cloud adjustment, the effect of aerosol on the cloud extent/lifetime, however other cloud adjustment effects exist that our simple calculation of a decomposed  $ERF_{aci_{warm}}$  misses, such as how precipitation suppression directly leads to changes in cloud extent or how suppression could lead to a later invigorated state of the cloud and faster dissipation.

Precipitation is indicated by the 2C-RAIN-PROFILE rain rate along the entire 12 km track segment (L’Ecuyer and Stephens, 2002). The decomposition susceptibility is found for precipitating and non-precipitating scenes globally using equation 3.9. Only the decomposition terms are found separately for precipitating and non-precipitating pixels. The CERES footprint is larger than the CloudSat’s, meaning while CloudSat could see an entire 12 km along track segment with no rain, the CERES footprint could still contain rain and influence the regression.

Uncertainty in each effect is found first by assuming the uncertainty in the observations lies in the AI, then by assuming a majority of the overall uncertainty in the  $ERF_{aci_{warm}}$  from error in the pre-industrial aerosol concentration estimates (Hamilton et al., 2014). Error is added randomly to AI to find how aerosol swelling or inaccurate retrievals of aerosol near cloud could alter susceptibility estimates. Aerosols swell in the vicinity of clouds, which increases their size and affects the MODIS retrieved AI (Christensen et al., 2017). To assess how significantly this may affect results we have randomly added errors of 10% to our AI estimates and re-derived all signals with all regime

constraints. Even with error in AI, the signals within our environmental and LWP regimes are robust. Uncertainty in the observations is most likely to come from the AI as CloudSat 2B-FLXHR-LIDAR fluxes have been shown to have at most  $\sim 10 \text{ Wm}^{-2}$  error in shortwave top-of-atmosphere fluxes (Henderson et al., 2013). The error from AI is then combined with randomly adding error to the pre-industrial AI estimates from SPRINTARS to quantify how error in the pre-industrial aerosol may lead to uncertainty in the  $\text{ERF}_{\text{aci}_{\text{warm}}}$ ,  $\text{RF}_{\text{aci}_{\text{warm}}}$ , and cloud adjustments. Overall, the majority of uncertainty in any  $\text{ERF}_{\text{aci}}$  estimate lies in the pre-industrial aerosol estimate (Carslaw et al., 2013, Chen and Penner, 2005, Stevens, 2013).

## 3.5 Results and Discussion

### 3.5.1 Estimate of the $\text{ERF}_{\text{aci}}$

The warm cloud  $\text{ERF}_{\text{aci}}$ , or the effective radiative forcing due to aerosol cloud interactions is  $-0.32 \text{ Wm}^{-2}$  when found with constraints on the liquid water path, stability, and free atmospheric relative humidity applied regionally. As stated before, a negative  $\text{ERF}_{\text{aci}}/\text{RF}_{\text{aci}}/\text{cloud}$  adjustment denotes additional cooling due to aerosol-cloud interactions. Figure 3.1 shows each component of Equation 3.9 and the resulting regional distribution of the  $\text{ERF}_{\text{aci}_{\text{warm}}}$ . The  $\text{ERF}_{\text{aci}_{\text{warm}}}$  is found applying Equation 3.2 regionally with regime constraints following DL19. This is within the range reported by the fifth IPCC report ( $-0.05 \text{ Wm}^{-2}$  to  $-0.95 \text{ Wm}^{-2}$ ) but suggests the net cooling effect is toward the lower end of the expected range. Note, however, that this

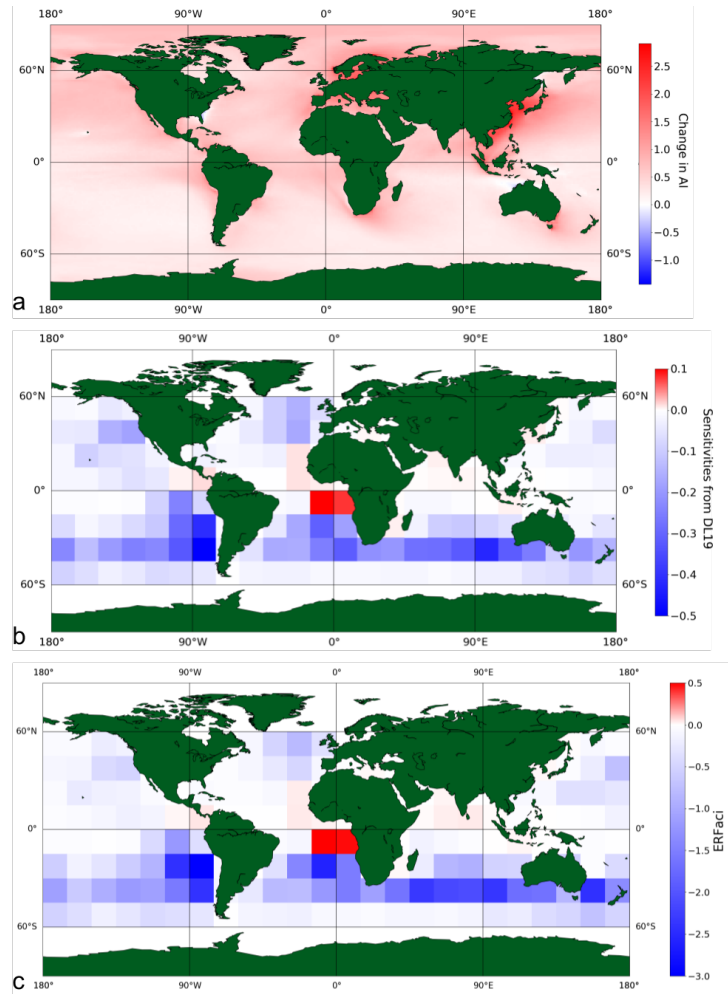


FIGURE 3.1: The change in aerosol index from SPRINTARS from the pre-industrial to present day (a),  $\frac{\partial \text{CRE}}{\partial \ln(\text{AI})}$  adapted from DL19 (b), and the associated  $\text{ERFaci}_{\text{warm}}$  found using Equation 3.2 found with constraints on LWP, EIS, and  $\text{RH}_{700}$  (c,  $-0.32 \pm 0.16 \text{ Wm}^{-2}$ ) using susceptibilities from DL19 (b) without areal weighting.

estimate neglects contributions from cold or mixed phased clouds and land regions (Boucher et al., 2013). This first estimate of the  $\text{ERFaci}_{\text{warm}}$  represents the sum of all effects of aerosol on the warm cloud radiative effect with no distinction between the  $\text{RFaci}_{\text{warm}}$  and  $\text{CA}_{\text{warm}}$  and is representative of how aerosol-cloud interactions may be altering the current radiative budget (Carslaw et al., 2013).

As expected, marine stratocumulus decks in the Southeast Pacific and South Atlantic exhibit the largest  $ERF_{aci_{warm}}$ , exceeding  $-3.0 \text{ Wm}^{-2}$  off the coast of Chile. The peak cooling is observed in the southern hemisphere, where the marine stratocumulus cloud decks subsist due to the strong inversions and cool sea surfaces (Wood, 2012). The storm tracks region in the north Atlantic exhibit a slight cooling, as do the marine stratocumulus off the coast of California, however the southern hemisphere dominates the cooling effect. Some regions where dimming occurs are amplified by the change in emissions of the region, such as the Asian coast.

Interestingly, ACI is responsible for a net warming of as much as  $0.6 \text{ Wm}^{-2}$  in the tropical Atlantic and Indian oceans. Diagnosing the cause of this warming cannot be done through the  $ERF_{aci_{warm}}$ , as it is impossible to accurately attribute it to a reduced albedo or cloud adjustment process. This signature, in particular, motivates decomposing the  $ERF_{aci_{warm}}$  into the  $RF_{aci_{warm}}$  and cloud adjustment components to allow the instantaneous albedo response to be separated from slower cloud processes. The physical processes resulting in a warming differ between the two components as the cloud adjustments are on a macrophysical scale while the  $RF_{aci_{warm}}$  is due to microphysical interactions between aerosol and CCN. The decomposition in Equation 3.3 allows the specific underlying physical processes responsible for this positive (warming) forcing to be assessed regionally.

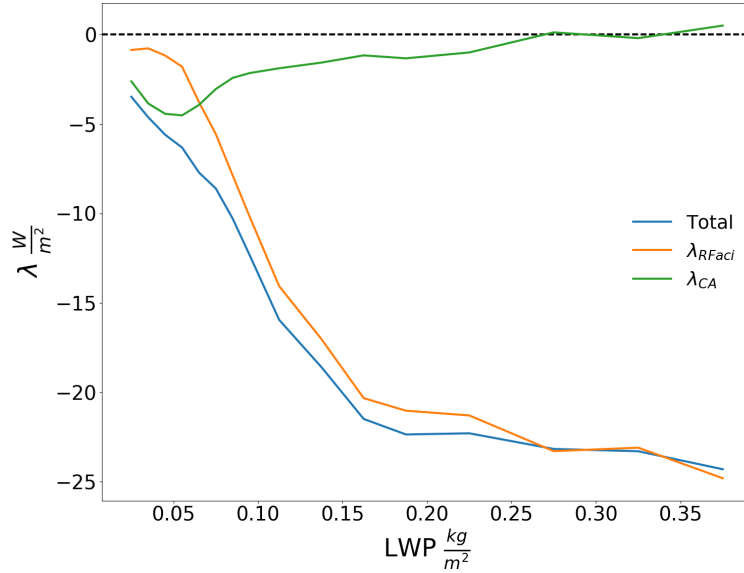


FIGURE 3.2: The  $\lambda_{RFaci_{warm}}$ , cloud adjustment, and sum of the two susceptibilities, decomposition susceptibility, found within regimes of cloud state defined by LWP. The total decomposition susceptibility is  $-7.04 \text{ Wm}^{-2}\ln(\text{AI})^{-1}$ .

The change in aerosol index is most notable off the coast of Asia and along the European coasts. Emissions from large coastal cities lead to large increases in AI, particularly changes in sulfuric aerosol (McCoy et al., 2017). The AI may have decreased off the coast of Australia due to the overall aerosol size increasing, which would decrease the Angstrom exponent and therefore AI (Carslaw et al., 2017). The northern hemisphere has had much larger changes in AI since pre-industrial times compared to the southern hemisphere due to the differences in anthropogenic activity between the two hemispheres. While the southern hemisphere has not experienced the same extreme changes in AI as the coast of Asia, the strong susceptibility of these warm clouds to aerosol combined with the local expansive clouds leads to a large cooling signal throughout the southern oceans.

### 3.5.2 Impact of LWP

Cloud LWP plays an integral role in modulating the strength of aerosol-cloud interactions. When first theorized by Twomey in 1977, the LWP of the cloud was considered to be constant as the first effect takes place. With this in mind, we first hold the LWP approximately constant and evaluate the decomposition susceptibility, Equation 3.4, within distinct LWP regimes. While both the  $\text{RFaci}_{\text{warm}}$  and cloud adjustments are dependent on LWP, they appear to have inverse relationships (Figure 3.2).  $\lambda_{\text{Sum}}$  is found to increase with increasing LWP, reaching a peak susceptibility between 0.06 and 0.15  $\text{kgm}^{-2}$  before asymptotically leveling off in the thickest LWP regime between 0.2 to 0.4  $\text{kgm}^{-2}$ . For the lowest LWPs, the cloud adjustment susceptibility dominates. This reverses in slightly thicker clouds at around 0.08  $\text{kgm}^{-2}$ . The  $\text{RFaci}_{\text{warm}}$  susceptibility grows to  $\sim 20 \text{ Wm}^{-2}\ln(\text{AI})^{-1}$  after 0.08  $\text{kgm}^{-2}$ , while the cloud adjustment susceptibility damps and oscillates around 0 after 0.25  $\text{kgm}^{-2}$ .

Thicker clouds are less susceptible to precipitation suppression, the key process to initiating many of the cloud adjustments (Fan et al., 2016, Michibata et al., 2016, Sorooshian et al., 2009). This is reflected in the very muted cloud adjustment susceptibility for higher LWPs past  $\sim 0.1 \text{ kgm}^{-2}$ . This inflection point is also where precipitation is more likely to occur in warm clouds and could be a sign of precipitation modulating the effects of aerosol on the cloud fraction (Lebsock et al., 2008, L'Ecuyer et al., 2009, Stevens and Feingold, 2009b). An alternative explanation is that thicker clouds with larger LWPs are more likely to precipitate, scavenging aerosol

and weakening the susceptibility. Aerosol-cloud-precipitation interactions complicate cloud adjustment processes in higher LWP clouds; the true susceptibility may be masked by covariance between aerosol and precipitation in these clouds. Precipitation would have an instantaneous effect on many cloud adjustment processes as major sink of liquid water within the cloud and therefore dampening process to other possible adjustments. Our framework for the cloud adjustment effect only considers processes which impact, either directly or indirectly, the cloud fraction. At higher LWPs, there are precipitation and other adjustment processes we do not account for that may later on change the radiative properties of the clouds, such as invigoration increasing the cloud depth and therefore both the longwave and shortwave cloud radiative effect (Koren et al., 2014, Rosenfeld et al., 2008).

Figure 3.2 confirms that LWP is intrinsically tied to the cloud albedo and extent necessitating the use of cloud state constraints on the decomposed  $ERF_{\text{aci}_{warm}}$ . While a change in LWP is itself considered a cloud adjustment, it is harder to establish a causal relationship between LWP and aerosol than cloud extent and aerosol due to the manifold of environmental parameters LWP depends on. LWP being held approximately constant in some subsequent analysis should therefore reduce the impact of the LWP adjustment on cloud extent. While LWP being held approximately constant accounts for some variability in the meteorology, explicitly holding the stability and free atmospheric contributions fixed within regimes of EIS and  $RH_{700}$  will further control modulation of  $\lambda$  by the environment. Modulation by the environment can include

the amplification of the reaction through a stable environment further prolonging the cloud lifetime and therefore extent.

While regime constraints on LWP do reduce the covariability between aerosol-cloud interactions and the role LWP plays in regulating these interactions, it does not remove all sources of covariability between LWP, aerosol, the environment, and cloud properties. Aerosol has been shown to negatively correlate with LWP (Gryspeerd et al., 2019a). It is possible that this relationship, and the inherent relationship between the environment and LWP, could affect results shown.

### 3.5.3 Constrained by local meteorology

When further separated by meteorological regimes defined by stability and  $\text{RH}_{700}$  of the free atmosphere, the influence of the environment becomes clearer as strong variations in both the sign and magnitude of  $\text{RFaci}_{\text{warm}}$  and  $\text{CA}_{\text{warm}}$  with environmental regime are evident (Figure 3.3). Both the  $\text{RFaci}_{\text{warm}}$  and cloud adjustment susceptibilities show warming responses in the most unstable, driest regimes. This is likely due to both the albedo and cloud extent being heavily influenced by entrainment-evaporation feedbacks (Christensen et al., 2014, Small et al., 2009).  $\lambda_{\text{CA}}$  shows a warming in the highest humidity, most stable regimes which may reflect cloud breakup processes like the stratocumulus to cumulus transition.

The total decomposed  $\text{ERFaci}_{\text{warm}}$  susceptibility, given by the sum of both the  $\text{RFaci}_{\text{warm}}$  and cloud adjustments within each individual stability and humidity regime, exhibits

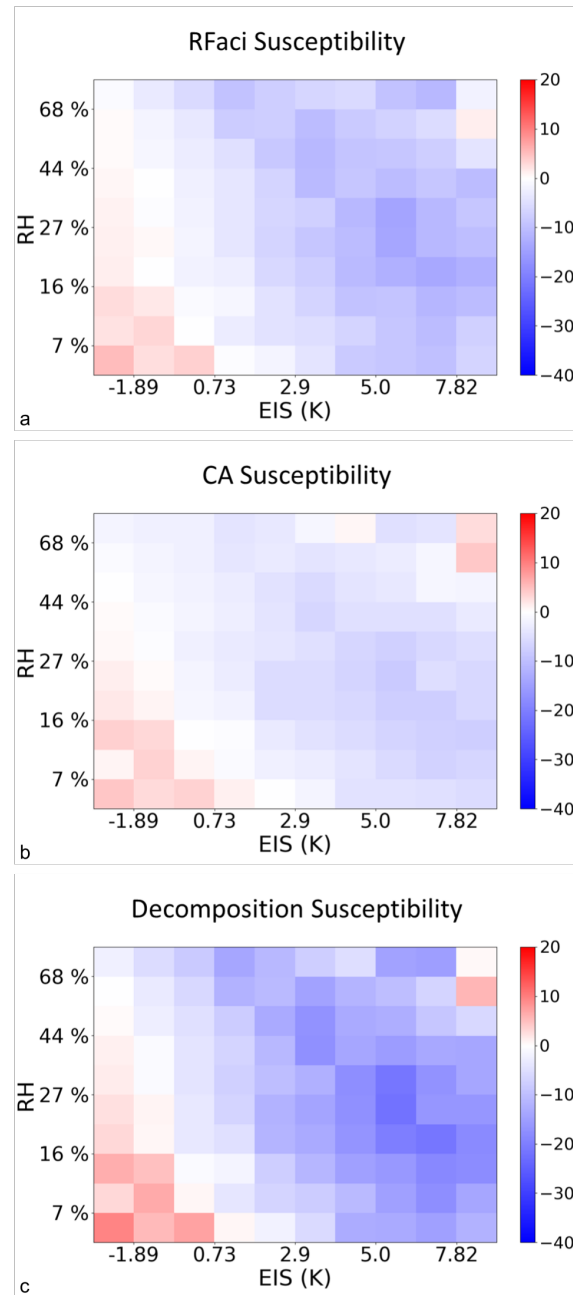


FIGURE 3.3: Variations in the a)  $\text{RFaci}_{warm}$  susceptibility ( $-5.26 \text{ Wm}^{-2}\ln(\text{AI})^{-1}$ ), b) cloud adjustment susceptibility ( $-2.88 \text{ Wm}^{-2}\ln(\text{AI})^{-1}$ ), and c) the sum of the two susceptibilities, the decomposed  $\text{ERFaci}_{warm}$  susceptibility ( $-8.22 \text{ Wm}^{-2}\ln(\text{AI})^{-1}$ ) with meteorological regimes defined by EIS and  $\text{RH}_{700}$ .

strong regime specific susceptibilities demonstrating the importance of understanding the total warm cloud radiative response to aerosol with consideration of the environment. Constraints on meteorology allow us consider how meteorology influences the cloud response to aerosol. Without these constraints, any derived susceptibilities could be attributed environmental responses. While cloud darkening occurs in only the most unstable regime ( $< -1.8$  K),  $\lambda_{CA}$  continues to show a warming response in moderately neutral environments ( $\sim 2$  K). This suggests that the instantaneous response ( $\lambda_{RFaci}$ ) is more sensitive to local meteorology than the slower cloud adjustments.

The dominant cooling of  $\lambda_{RFaci}$  and  $\lambda_{CA}$  in stable regimes illustrates the potential of a stable inversion to strengthen ACI. The peak cooling of  $\lambda_{CA}$  occurs in a relatively dry atmosphere  $\sim 27\%$  RH<sub>700</sub>. In this environment, the cloud extent rapidly increases as a response to aerosol, however the cloud is topped by a strong, stable inversion that prohibits much of an deepening of the cloud perhaps instigating the effect to push horizontally rather than vertically (Christensen and Stephens, 2011).  $\lambda_{RFaci}$  peaks in stable, but comparatively more moist environments where entrainment of moist air from the free atmosphere promotes activation of all available aerosol to CCN, rapidly increasing the albedo. This response may be similar to other regions where trade cumuli form and the FA is relatively moist (Koren et al., 2014).

Finally, while  $\lambda_{RFaci}$  shows less variation in sign, it exhibits more variation in magnitude between meteorological regimes indicating the importance of accounting for

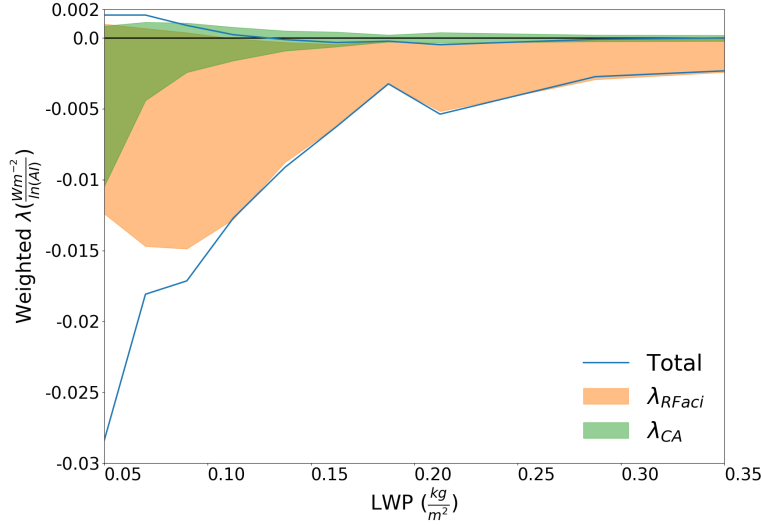


FIGURE 3.4: 10 to 90% range of the decomposition for 11 cloud states when found within 100 environmental regimes of EIS and  $RH_{700}$ . The  $\lambda_{RFaci_{warm}}$  (orange fill,  $\lambda_{RFaci}$ ) and cloud adjustment susceptibilities (green fill,  $\lambda_{CA}$ ) total  $-4.18 \text{ Wm}^{-2}\ln(\text{AI})^{-1}$  and  $-1.26 \text{ Wm}^{-2}\ln(\text{AI})^{-1}$ , respectively. The sum of the two from 10 to 90 percentiles, the decomposed susceptibility (blue line), totals  $-5.45 \text{ Wm}^{-2}\ln(\text{AI})^{-1}$ .

meteorological influences in order to capture this specific environmental regime dependence. It is possible with additional constraints, understanding how other components of the meteorology is affecting these terms would become more clear. It is also possible  $\lambda_{RFaci}$  is impacted by some semi-direct effects by smoke aerosol which would lead to a cloud dimming and positive susceptibility. Semi-direct effects are not accounted for by our methodology, however aerosol within the cloud layer could lead to cloud breakup processes, a dimmer albedo, and changes to the local environment by the absorbing aerosol.

### 3.5.4 Constraints on cloud state and local meteorology

As seen in Figures 3.2 and 3.3, the susceptibility of each component of the  $ERFac_{warm}$  varies with both cloud state and environmental regime. Therefore, when calculating each component of the  $ERFac_{warm}$ , both the meteorology and LWP must be accounted for. To accomplish this, the  $RFac_{warm}$  and  $CA_{warm}$  susceptibilities are found with constraints on both the LWP and environment (Figure 3.4). The shaded region of Figure 3.4 delineates the 10 to 90% range within each of the 11 cloud states of the susceptibility when further separated by the 100 environmental regimes used in Figure 3.3. Unlike Figures 3.2 and 3.3,  $\lambda$  is weighted by frequency of occurrence within each environmental state. This illustrates how the magnitude and sign of each susceptibility can vary by environmental regime even when LWP is held approximately constant. The weighted and summed susceptibility is  $-5.45 \text{ Wm}^{-2}\ln(AI)^{-1}$  with constraints on LWP, stability, and  $RH_{700}$  globally. This is slightly smaller than the susceptibility found in DL19, however that susceptibility took into account all changes in warm cloud CRE to aerosol while our decomposition only accounts for the two largest effects, the albedo and cloud extent susceptibilities to aerosol. The lowest LWP clouds ( $\leq 0.1 \text{ kgm}^{-2}$ ) contribute most to the net susceptibility due to their abundance but also exhibit the widest range in susceptibilities across different meteorological states.

The two components exhibit different behavior in terms of susceptibility to cloud state (defined here by LWP). The cloud adjustment susceptibility is largest for the lowest LWPs, while the  $RFac_{warm}$  susceptibility peaks around  $0.06 \text{ kgm}^{-2}$  and gradually

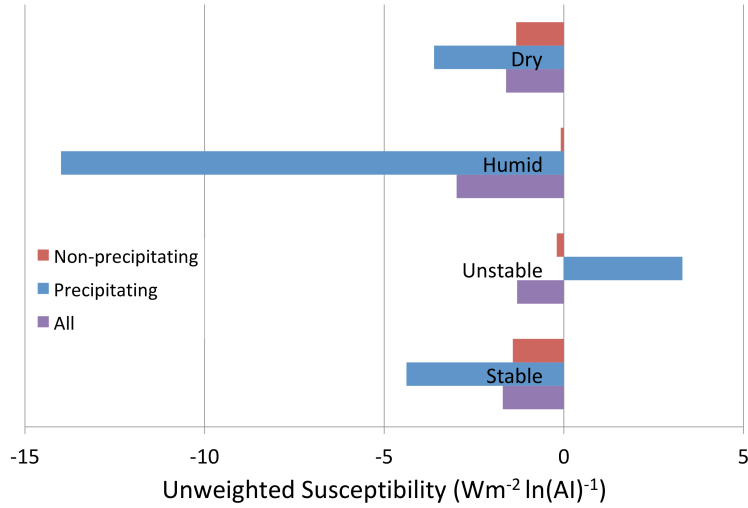


FIGURE 3.5: Globally summed and relatively weighted susceptibilities for different conditions when found within regimes of EIS, RH, and LWP on a regional basis.

declines. This may represent a “sweet spot” of cloud albedo susceptibility. Up to  $0.1 \text{ kgm}^{-2}$ , aerosol are easily activated and there are few processes beyond entrainment and activation to reduce the concentration within the cloud layer. Beyond  $0.1 \text{ kgm}^{-2}$ , where the  $\text{RFaci}_{\text{warm}}$  begins to decrease, the cloud may be influenced by precipitation formation, reducing the  $\lambda_{\text{RFaci}}$  within each environmental regime.

$\lambda_{\text{CA}}$  decreases in magnitude with LWP. Higher LWP clouds, independent of the environment, may be less susceptible to lifetime effects, as was seen in Figure 3.2. Precipitation suppression, the main driver of cloud adjustments, becomes less likely as LWP increases (Fan et al., 2016, Sorooshian et al., 2009). The thinnest and smallest clouds may have the the largest potential to experience a enhancement effect.

### 3.5.5 Impact of precipitation and environment on susceptibility

Precipitation formation within the cloud and the environment surrounding modulate the susceptibility. When weighted by the relative frequency of occurrence, rather than overall frequency of occurrence, the susceptibility of precipitating clouds is shown to be much higher in some environments than non-precipitating clouds (Figure 3.5). Precipitating clouds in humid environments especially, defined as having a  $RH_{700} > 44\%$ , have a much greater susceptibility than any other regime of clouds. Unstable clouds show a reduced susceptibility in all cases, with precipitating clouds showing a warming effect in these environments while non-precipitating clouds experience an extremely damped cooling effect. Unsurprisingly, in dry environments and stable environments, precipitation does less to magnify the susceptibility and the difference between precipitating and non-precipitating susceptibilities is reduced.

Precipitating clouds reduce the amount of aerosol available to interact with warm clouds through wet scavenging, yet still may induce several other processes within the cloud that stimulate a response Gryspeerd et al.. These include stabilizing the boundary layer through virga, increasing the EIS and therefore susceptibility (Figure 3.3). Precipitation formation within the cloud induces vertical motion and mixing of the cloud layer, increasing turbulence and mixing of the layer which may increase activation of aerosol and therefore the response of the cloud. Further work must

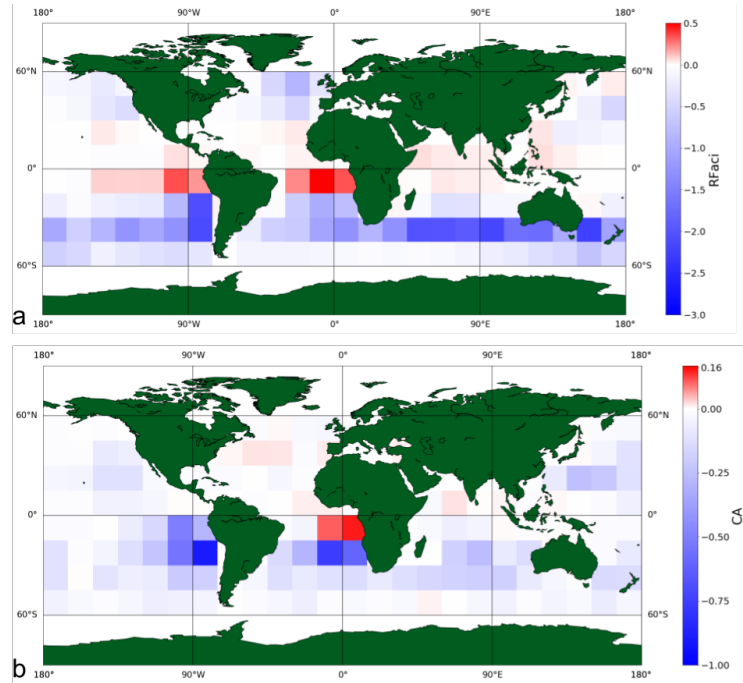


FIGURE 3.6: The radiative forcing due to aerosol-cloud interactions (RFaci) (top,  $-0.21 \pm .12 \text{ Wm}^{-2}$ ) and cloud adjustments (bottom,  $-0.05 \pm .03 \text{ Wm}^{-2}$ ) found on a regional basis with constraints on LWP, EIS, and  $\text{RH}_{700}$  without weighting by area. Note the colorbar for  $\text{CA}_{\text{warm}}$  (bottom) is 1/3 of the magnitude of  $\text{RFaci}_{\text{warm}}$  (top).

be done to resolve how and to what magnitude precipitation alters the warm cloud radiative susceptibility to aerosol.

### 3.5.6 Contribution of RFaci and cloud adjustments to global $\text{ERFaci}$

With these considerations in mind, the sum of the  $\text{RFaci}_{\text{warm}}$  and CA, or the decomposed  $\text{ERFaci}_{\text{warm}}$  as we will refer to it, is  $-0.26 \pm .15 \text{ Wm}^{-2}$  found using Equation 3.9 (Figure 3.7). The components of the  $\text{ERFaci}_{\text{warm}}$ , the  $\text{RFaci}_{\text{warm}}$  and cloud adjustments, are found using Equations 3.5 and 3.7 and shown in Figure 3.6. The  $\text{ERFaci}_{\text{warm}}$  from Figure 3.1 is slightly larger in magnitude than the decomposed

ERFaci<sub>warm</sub>. Overall, their regional variations and magnitudes are extremely similar, suggesting the linear decomposition captures a majority of the ERFaci<sub>warm</sub>. The southern ocean dominates the decomposed ERFaci<sub>warm</sub>, as is expected based on the susceptibilities. The difference in overall magnitude stems from a stronger dimming effect evaluated in the decomposed ERFaci<sub>warm</sub> (Figure 3.6). In the decomposed ERFaci<sub>warm</sub>, more regions experience a decrease in CRE with increasing AI compared to the ERFaci<sub>warm</sub>. This may be due to the definition of the decomposed ERFaci<sub>warm</sub> that allows either the RFaci<sub>warm</sub> or CA<sub>warm</sub> to reduce cooling.

A reduced albedo, or positive RFaci, has been noted by other observation based studies before (Chen et al., 2012). A positive RFaci<sub>warm</sub> can be caused by multiple processes. A semi-direct effect, where non-activated aerosol acts to decrease the total albedo of the cloud in the case of smoke, reducing the CRE of the cloud and therefore the RFaci<sub>warm</sub> (Johnson et al., 2004). A decrease in the RFaci<sub>warm</sub> may also be due to any changes to the distribution of liquid water throughout the cloud layer. In certain environmental conditions, an increase in aerosol may lead to sedimentation within the cloud throughout the entrainment zone, which could decrease the cloud albedo and therefore CRE (Ackerman et al., 2004). If these two effects combined under the "perfect storm" of aerosol and environmental conditions, the RFaci<sub>warm</sub> would have a large, positive effect.

The cloud adjustment term likewise undergoes a positive, or damped cooling, response in certain regions. A reduced cloud fraction due to aerosol-cloud interactions has been

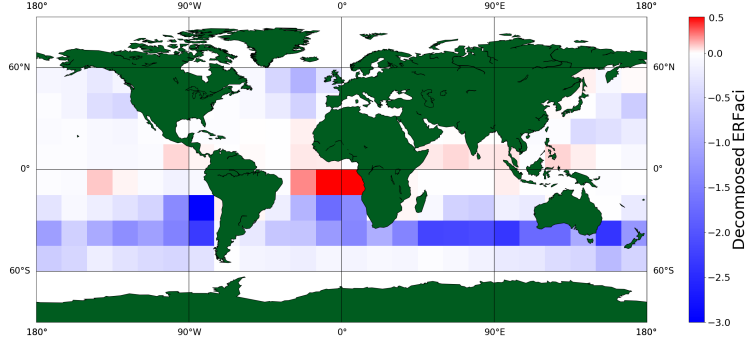


FIGURE 3.7: The  $ERFaci_{warm}$  found as a sum of the  $RFaci_{warm}$  and cloud adjustments (Figure 3.6) with constraints on the LWP, EIS, and  $RH_{700}$  on a regional basis ( $-0.26 \text{ Wm}^{-2}$ ) without areal weighting.

noted before by others (Small et al. (2009), Gryspeerdt et al. (2016)). Chen et al. (2014) noted a decrease in LWP due to an increase in AI in their observationally based study, while other studies have indicated the LWP response and therefore cloud fraction response can be either positive or negative (Gryspeerdt et al., 2019a). Any process that alters the cloud’s liquid water path, such as evaporation-entrainment, may lead to a decrease in cloud fraction given certain environmental conditions.

The discrepancy between the two estimates of  $ERFaci_{warm}$  ( $0.065 \text{ Wm}^{-2}$ ) may be cloud adjustment effects or covariance between  $RFaci_{warm}$  and  $CA_{warm}$  not captured by the simple regression employed here. The error between the two lies well within the bounds of error of both estimates ( $\pm 0.16$  and  $\pm 0.15$ ). While cloud extent changes are the dominant cloud adjustment effect, changes in liquid water path due to precipitation suppression will have an impact on the radiative forcing as well. Future work on understanding and evaluating the  $ERFaci_{warm}$  must include other cloud adjustments and explicitly account for covariance between the  $RFaci_{warm}$  and cloud adjustments.

Although they occur on different time scales, the  $\text{RFaci}_{warm}$  could be thought of as reactive to cloud adjustments. So while the cloud adjustment process may take hours, an albedo adjustment occurs simultaneously.

### 3.5.7 Regional variation due to precipitation

Figure 3.5 clearly demonstrates that precipitation plays a leading role in modulating the magnitude of aerosol-cloud interactions and their resultant forcing. The contribution of precipitating and non-precipitating clouds to the  $\text{ERFaci}_{warm}$  is presented in Figure 3.8. Precipitation has a large impact on both the  $\text{RFaci}_{warm}$  and warm cloud adjustment processes, indicated by the difference in global magnitudes between the two  $\text{ERFaci}_{warm}$  when separated by precipitation ( $-.21 \text{ Wm}^{-2}$ ) and not separated by precipitation (Figure 3.7  $-.26 \text{ Wm}^{-2}$ ). Precipitating clouds exhibit different microphysical processes and therefore pathways of aerosol-cloud interactions that lead to an increased susceptibility ( $-43. \text{ Wm}^{-2}\ln(\text{AI})^{-1}$  vs.  $-30. \text{ Wm}^{-2}\ln(\text{AI})^{-1}$  weighed individually). However, on average only  $\sim 30\%$  of warm clouds observed by CloudSat are precipitating, leading to a smaller net contribution to the total  $\text{ERFaci}_{warm}$  shown in Figure 3.8. If in future climates, warm clouds rain more frequently, it is possible that the decomposed  $\text{ERFaci}_{warm}$  could increase due to precipitating clouds higher susceptibilities, given the environmental conditions (EIS and RH) remain constant.

In regions where trade cumulus are more prevalent and the marine boundary layer is more unstable, precipitation clouds have the capacity to greatly decrease the cooling due to  $\text{ERFaci}_{warm}$  (Figures 3.5, 3.8). However, this positive  $\text{ERFaci}_{warm}$  is balanced

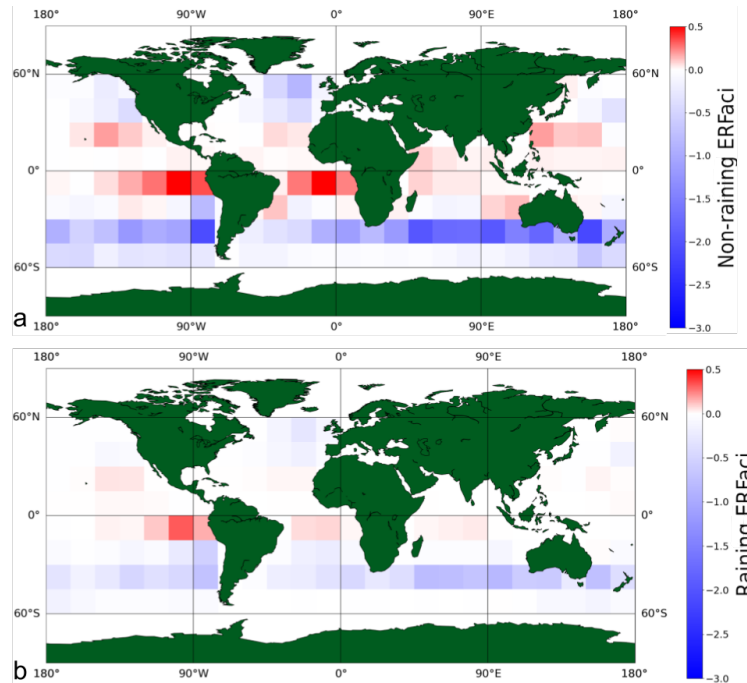


FIGURE 3.8: The decomposed effective radiative forcing due to aerosol-cloud interactions found as a sum of its components on a regional scale within regimes of EIS, RH, and LWP for a) non-raining clouds ( $-0.147 \text{ Wm}^{-2}$ ) and b) raining clouds ( $-0.06 \text{ Wm}^{-2}$ ).

by their expansive cooling throughout the southern ocean. More regions experience a cooling due to ACI when clouds are precipitating than not precipitating. Further, due to wet scavenging of aerosol, it is possible that precipitating clouds could reduce semi-direct or direct effects and remove aerosol that could otherwise warm the atmosphere. The possible feedbacks or consequences of changes in precipitation require further research, especially since precipitation is heavily controlled by aerosol type as well as concentration.

### 3.6 Conclusions

The global distribution of the warm, marine cloud ERF<sub>aci</sub> and its components, the RRF<sub>aci<sub>warm</sub></sub> and cloud adjustments, are found with constraints on cloud state and local meteorology following the methodology of DL19. The total effective radiative forcing due to aerosol-cloud interactions is  $-0.32 \pm 0.16 \text{ Wm}^{-2}$ . The radiative forcing due to aerosol-cloud interactions is  $-0.21 \pm 0.12 \text{ Wm}^{-2}$ . The forcing due to cloud adjustments from aerosol-cloud interactions is  $-0.05 \pm 0.03 \text{ Wm}^{-2}$ . In all cases, constraining the environment and cloud state are found to be critical for reducing error in misrepresenting aerosol-environment effects as aerosol-cloud interactions. Our estimations of the ERF<sub>aci<sub>warm</sub></sub>, as a sum and/or single term, agrees with other estimates of the warm cloud ERF<sub>aci<sub>warm</sub></sub> such as Chen et al. who estimated  $-0.46 \text{ Wm}^{-2}$ , and with Christensen et al. who estimated  $-0.36 \text{ Wm}^{-2}$ . The latter further showed liquid clouds dominate the ERF<sub>aci<sub>warm</sub></sub> over mixed-phase and ice phase aerosol-cloud-radiation interactions. Thus changes in the warm cloud susceptibility to aerosol perturbations could substantially alter the radiative balance due to the warm cloud dominance of the ERF<sub>aci<sub>warm</sub></sub>.

Regionally, the ERF<sub>aci<sub>warm</sub></sub> derived from the linear decomposition into RRF<sub>aci<sub>warm</sub></sub> and cloud adjustments agrees moderately well with that derived directly from the SW CRE, proving our method of decomposing the ERF<sub>aci<sub>warm</sub></sub> to the first order components does capture the main effects adequately. Globally, the ERF<sub>aci<sub>warm</sub></sub> is

dominated by the  $\text{RFaci}_{warm}$ , however the cloud adjustment term is found to contribute  $\sim\frac{1}{5}$  of the total forcing. The cloud adjustments vary regionally in sign and magnitude, meaning in some regions the two effects are additive, while in others they may cancel each other out. In the south Atlantic, both effects lead to a warming, or positive, forcing as clouds both shrink and dim in this region, most likely due to the prevalence of a drier free atmosphere and unstable boundary layer in this region. In the tropical Pacific, clouds dim while the cloud extent swells, leading to an overall muted cooling effect. Regions like this where the two signals have opposing signals are prime examples of why a decomposition of the  $\text{ERFaci}_{warm}$  into its components is necessary. The muted signal in the tropical Pacific would most likely be attributed to offsetting reactions in the  $\text{RFaci}_{warm}$  and  $\text{CA}_{warm}$ , as this region shows a damped signal of  $\text{ERFaci}_{warm}$ , if not for the knowledge that the  $\text{RFaci}_{warm}$  and  $\text{CA}_{warm}$  have opposing responses in this region.

It is possible our simple methodology to evaluate cloud adjustments underestimates the possible forcing due to other adjustment processes or the possible covariance with the  $\text{RFaci}_{warm}$ . If the difference between the  $\text{ERFaci}_{warm}$  and the sum of the  $\text{RFaci}_{warm}$  and cloud adjustments is assumed to arise from the missing forcing from other adjustments, the total contribution of the  $\text{CA}_{warm}$  to the  $\text{ERFaci}_{warm}$  would increase to  $-0.11 \text{ Wm}^{-2}$ , or nearly a third, of the  $-0.32 \text{ Wm}^{-2}$ . This would be consistent with a recent estimate by Rosenfeld et al. which found the relationship between  $\text{Nd}$  and cloud fraction, when constrained by LWP, still had a significant signal. Cloud

adjustments are found to dominate over the  $\text{RFaci}_{\text{warm}}$  at the lowest liquid water paths. Thus in regions or climate conditions that support enhanced prevalence of thin clouds, the cloud adjustment term would increase at the expense of the  $\text{RFaci}_{\text{warm}}$ .

The southern hemisphere dominates the global  $\text{ERFaci}_{\text{warm}}$  due ubiquitous marine stratocumulus in the South Pacific and South Atlantic. The northern hemisphere storm tracks region in the North Atlantic and marine stratocumulus off California exert  $\sim \frac{1}{5}$  the magnitude of forcing observed from the southern hemispheres pristine warm clouds. Warm clouds in the southern hemisphere are predisposed for aerosol-cloud-radiation interactions.

Cloud adjustments and  $\text{RFaci}_{\text{warm}}$  varying regionally in sign and magnitudes implies that there are regions and conditions where the two components could effectively cancel each other out, thwarting short term, observation-based attempts at discerning a noticeable change in cloud radiative effects due to aerosol. Moreover, the character of the clouds does not remain constant. Aerosol interactions that result in brighter clouds covering a smaller area, or dimmer clouds covering a larger area, represent important physical responses that may be masked by direct assessment of  $\text{ERFaci}_{\text{warm}}$  from CRE alone. In these regions especially, care should be given to discerning which effect is dominating and to what magnitude.

## Chapter 4

# Exploring the Longwave Indirect Effect

### 4.1 Introduction

#### 4.1.1 Background

Aerosols released from natural and anthropogenic activity interact with clouds within the atmosphere by acting as a cloud condensation nuclei (CCN) within the cloud. As the amount of aerosol increases, the number of CCN increases, reducing the mean droplet size of the cloud for a fixed LWP. ACI lead to a delay in collision coalescence, as the likelihood of drops colliding and gathering enough mass to fall out decreases as the mean drop size decreases, resulting in longer lived clouds (Albrecht, 1989). The longer

lived clouds grow larger and taller than their non-perturbed, pristine counterparts, increasing the cloud longwave radiative effect and resulting in a slight warming of the atmosphere and surface in what is known as the longwave indirect effect. Another pathway of increasing the longwave (LW) CRE is through the reduced droplet size, which alters the emissivity in the cloud and increases the LW CRE. These effects on the LW CRE are amplified by changes in the cloud extent due to an increased lifetime, as the size of the cloud increases (as shown in Chapter 3), and additionally increases the overall LW CRE of the cloud.

The longwave indirect effect has remained outside of the realm of interest of the aerosol-cloud interactions community. Studies investigating whether clouds may experience an increase in their longwave emission due to aerosol-cloud interactions focus on the arctic, where the radiative balance must be precisely quantified in order to determine the effects of climate change on the ice sheet (Lubin and Vogelmann, 2006). The slight warming due to raised cloud tops and smaller droplet sizes, increasing the thermal emission of the clouds back to the surface, can have large consequences on the ice mass in the arctic, however this warming may be so insignificant compared to the shortwave cooling induced by aerosol-cloud interactions in other regions that it can be assumed to be zero (Christensen et al., 2016). Nonetheless, as anthropogenic emissions alter the Earth system, the sign and magnitude of the longwave indirect effect must be evaluated in order to determine how it may impact the total effective

radiative forcing due to aerosol cloud interactions (ERFaci) and whether cloud deepening, which drives a longwave indirect effect, is occurring, as this may signal other aerosol driven changes to the cloud's precipitation state.

### 4.1.2 Motivation

L'Ecuyer et al. (2009) found evidence of cloud deepening due to precipitation suppression, providing evidence of one pathway to increase the LW CRE of warm clouds. There has been further evidence of cloud deepening due to ship track emissions within marine stratocumulus (Christensen and Stephens, 2011). Similar to L'Ecuyer et al. (2009), the degree of deepening depended on the environmental conditions of the boundary layer, as stability strongly modulates whether the cloud is at an open or closed state and therefore its response, and the free atmosphere, as aerosol emissions sometimes induced greater rates of entrainment at the cloud top and a drier free atmosphere deteriorated the cloud layer. Further, the deepening due to ship track emissions is extremely localized within  $\sim 3$  kilometer vicinity of the ship. While many studies have theorized the cloud top height should increase due to aerosol-cloud interactions, as a cloud adjustment to precipitation suppression, many studies have focused on how the LWP response instead of the cloud depth response (Rosenfeld et al., 2019, Toll et al., 2019).

Whether the indirect effect leads to cloud deepening or not has been eschewed by the aerosol-cloud interactions community, as attempting to answer this question leads to questions of invigoration of the cloud. Rosenfeld et al. (2008) postulated that clouds

will deepen due to aerosol-cloud interactions, leading to enhanced precipitation formation rates and greater turbulence within the cloud, a process now collectively known as invigoration. Invigoration has yet to be thoroughly proven or disproven by observations, though modeling efforts reaffirm the process is possible in both convective and warm cloud types (Fan et al., 2016).

Here I investigate the susceptibility of the longwave indirect effect by decomposing it as a sum of its parts (and susceptibilities), the change in the longwave cloud radiative effect through deepening and the change in the longwave cloud radiative effect due to cloud extent. The susceptibilities are found with constraints on the environment and cloud state following Douglas and L’Ecuyer (2019a). Further, the effect of the diurnal cycle on deepening is investigated, as the cloud adjustment process may be sensitive to changes in the solar insolation and nighttime boundary layer dynamics. Finally, the implications of cloud deepening, whether it occurs or not, are evaluated as they link aerosol-cloud interactions with invigoration and cloud feedbacks.

## **4.2 Data & Methods**

### **4.2.1 Data**

The susceptibility of the longwave indirect effect is decomposed into its components, the change in longwave forcing due to cloud deepening and increased cloud extents, using four years of satellite observations from the NASA A-Train constellation. Cloud

properties including cloud fraction (CF) and the cloud longwave outgoing top-of-atmosphere flux (CLW) are provided by CloudSat. Aerosol index, a proxy for aerosol concentration, is provided by MODIS aboard the Aqua satellite. Regimes used to constrain covarying processes are defined using LWP from AMSR-E aboard Aqua and the estimated inversion strength (EIS) and relative humidity of the free atmosphere ( $RH_{700}$ ) from MERRA-2 reanalysis. The regime framework from Douglas and L’Ecuyer (2019a) is followed here to similarly quantify the susceptibilities on a regional basis within regimes of LWP, EIS, and RH.

Cloud fraction is defined by the number of cloudy pixels flagged by 2B-CLDCLASS-LIDAR in each 12 km section of the satellite’s track (Sassen et al., 2008). Cloud top height in km is indicated by 2B-CLDCLASS-LIDAR cloud layer top. Clouds must lie below the freezing level defined by comparing the cloud top temperature from 2B-CLDCLASS-LIDAR and the freezing level from 2C-PRECIP-COLUMN. The cloud longwave outgoing top-of-atmosphere flux is from the 2B-FLXHR-LIDAR product, which models the cloud’s radiative effect using the returns from the cloud profiling radar aboard CloudSat and two stream radiative transfer model.

### **4.2.2 Decomposing the longwave susceptibility**

A susceptibility is defined as the regression of a cloud property against the natural log of AI.

$$\frac{\delta \text{Cloud Property}}{\delta \ln(AI)} = \text{Susceptibility} \quad (4.1)$$

The natural log of AI is used as many cloud processes scale logarithmically with aerosol concentration (Sorooshian et al., 2009).

The longwave cloud radiative effect (CLWRE) susceptibility to aerosol is therefore defined as the change in the CLWRE with respect to  $\ln(AI)$ :

$$\frac{\delta CLWRE}{\delta \ln(AI)} = \text{Susceptibility of the Longwave Cloud Radiative Effect to Aerosol} \quad (4.2)$$

Assuming that the changes are to a first order controlled by the change in cloud deepening due to aerosol and greater cloud extents due to aerosol, the CLWRE susceptibility can be decomposed into the sum of these susceptibilities weighted accordingly:

$$\frac{\delta CLWRE}{\delta \ln(AI)} = \frac{\delta CTH}{\delta \ln(AI)} \frac{\delta CLW}{\delta CTH} \times CF + \frac{\delta CF}{\delta \ln(AI)} \times \overline{CLW} \quad (4.3)$$

Where CTH is cloud top height, CLW is the cloud longwave outgoing top-of-atmosphere flux, and  $\overline{CLW}$  is the mean CLW. The first susceptibility term in Equation 4.3 is the deepening term, relating a change in cloud top height due to aerosol with a change

in CLW. The second susceptibility term in Equation 4.3 is similar to the cloud adjustment term in Chapter 3, though now weighted by the mean CLW to translate a change in cloud cover to a change in the outgoing longwave. A positive susceptibility implies warming, or the longwave CRE increases and more longwave is being emitted both out to space and back to Earth.

### 4.2.3 Establishing constraints with regimes

Regimes are structured following Douglas and L'Ecuyer (2019a) (see Appendix A). Environmental regimes are defined on a regional basis using 20 percentile bins of EIS and  $RH_{700}$ . The LWP is used to define cloud state regimes on a regional basis. The LWP bins are kept constant across the regions, while the environmental bins depend on the distribution of the environmental conditions within that region. The LWP bin limits are defined as:

- $.02 < \text{LWP} < .06$
- $.06 < \text{LWP} < .1$
- $.1 < \text{LWP} < .2$
- $.2 < \text{LWP} < .4$

where LWP is in units  $\text{kgm}^{-2}$ . The limits are chosen to separate thinner clouds ( $<.2$ ) into more regimes as warm clouds have an average LWP  $\sim .06 \text{ kgm}^{-2}$ . However, the limits are broad enough to ensure the regional environmental regimes have at least 50 observations per regime to perform regressions.

The regional susceptibility is found by summing and weighting the susceptibilities within each environmental and cloud state regime:

$$\text{Susceptibility} = \sum_{EIS}^5 \sum_{RH}^5 \sum_{LWP}^4 \frac{\delta \text{Cloud Property}}{\delta \ln(AI)} \times W_{EIS,RH,LWP} \quad (4.4)$$

where  $W$  is the frequency of observations within a regime of  $EIS$ ,  $RH_{700}$ , and  $LWP$  for that region.

## 4.3 Results and Discussion

### 4.3.1 The longwave susceptibility to aerosol

The global mean susceptibility of the longwave decomposed indirect effect during the day is  $.3 \text{ Wm}^{-2}\ln(AI)^{-1}$ . To compare, the mean susceptibility of the shortwave indirect effect found under the same constraints and time is  $-10.13 \text{ Wm}^{-2}\ln(AI)^{-1}$ , or about 30x larger (Douglas and L'Ecuyer, 2019a). While the longwave mean is an order of magnitude smaller than the shortwave susceptibility, in some regions the two are of comparable magnitudes. The eastern coast of Asia shows a negative, or cooling, susceptibility of  $\sim 1.5 \text{ Wm}^{-2}\ln(AI)^{-1}$ , comparable to the slight warming shortwave susceptibility when found under the same conditions (Douglas and L'Ecuyer, 2019a). The net zero impact of aerosol-cloud interactions on the cloud radiative effect in this region is due to the offsetting balance of the longwave and shortwave effects whereby

the longwave leads to a cooling due to reduced thermal emissions at the cloud top and the shortwave leads to warming due to the decreased albedo in the same region.

If the global AI increases by 1 unit from the pre-industrial to present day times, the longwave indirect radiative effect would contribute  $.3 \text{ Wm}^{-2}$  of warming to the global radiative balance. The contribution is due to a combination of increased cloud extents, trapping more outgoing longwave radiation, and greater cloud depths, increasing the longwave CRE. In order to properly diagnose how cloud deepening may affect the longwave emissivity of warm clouds, we evaluate the first term of Equation 4.3.

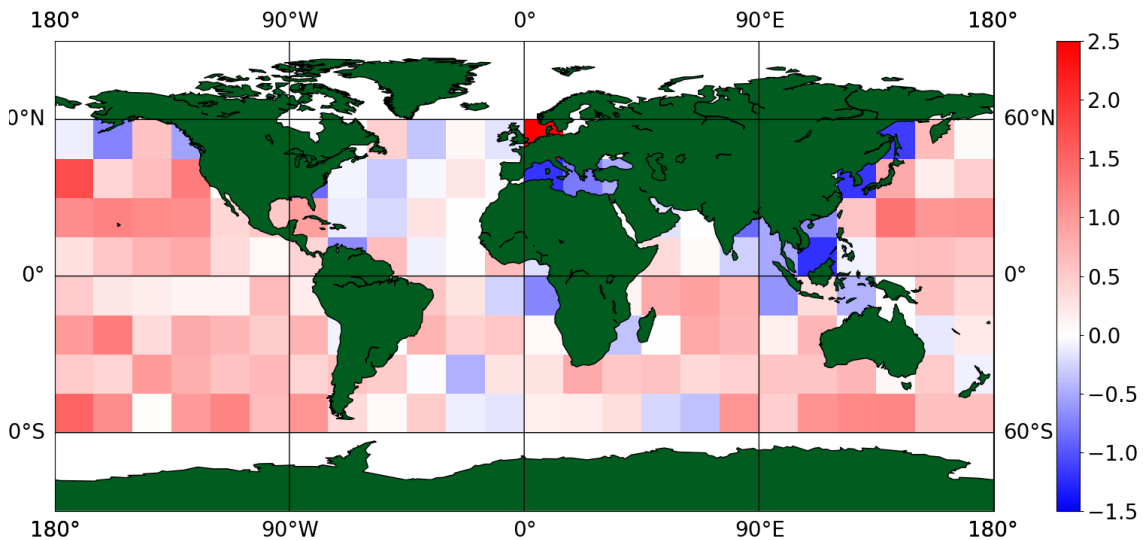


FIGURE 4.1: The susceptibility of decomposed longwave indirect effect to aerosol when found with constraints on LWP, EIS, and  $\text{RH}_{700}$  during the daytime.

### 4.3.2 The cloud deepening susceptibility

The cloud deepening and subsequent increase in the longwave CRE due to aerosol-cloud interactions forms the basis of the longwave indirect effect. Globally, the mean

susceptibility of the cloud top height per unit AI is only  $\sim .05$  km, however the local amplitude can be much larger. In regions of stable stratocumulus and much of the southern ocean, the cloud top height is susceptible to deepening due to aerosol-cloud interactions (figure 4.2).

Not all marine stratocumulus regions behave in the same manner; the marine stratocumulus in the Angola basin off of the coast of Africa display a cloud thinning response due to aerosol-cloud interactions, counter to the deepening susceptibilities in the California and Peruvian marine stratocumulus. These may be indicated by the negative mean susceptibilities in Figure 4.3, right where some high stability, low humidity regionally based regimes display a thinning response. The greatest thinning susceptibility is in the tropics, where cumuli dominate the warm cloud type. These are likely indicated by clouds in the slightly thicker regime in Figure 4.3, left whereby the thinning response is more prevalent for all stabilities. In some regions, the cloud depth is unresponsive to aerosol. The storm tracks region of the north Atlantic displays a noticeably damped susceptibility where cloud top heights imperceptibly increase. Globally, the mean reaction of warm clouds is to deepen as aerosol concentrations increase. Further, these susceptibilities are likely close to the true response of the cloud as the effects of LWP, the stability and boundary layer depth, and effects of entrainment are constrained by our regime framework.

The stratocumulus depth response, both magnitude and sign, depend on the type of

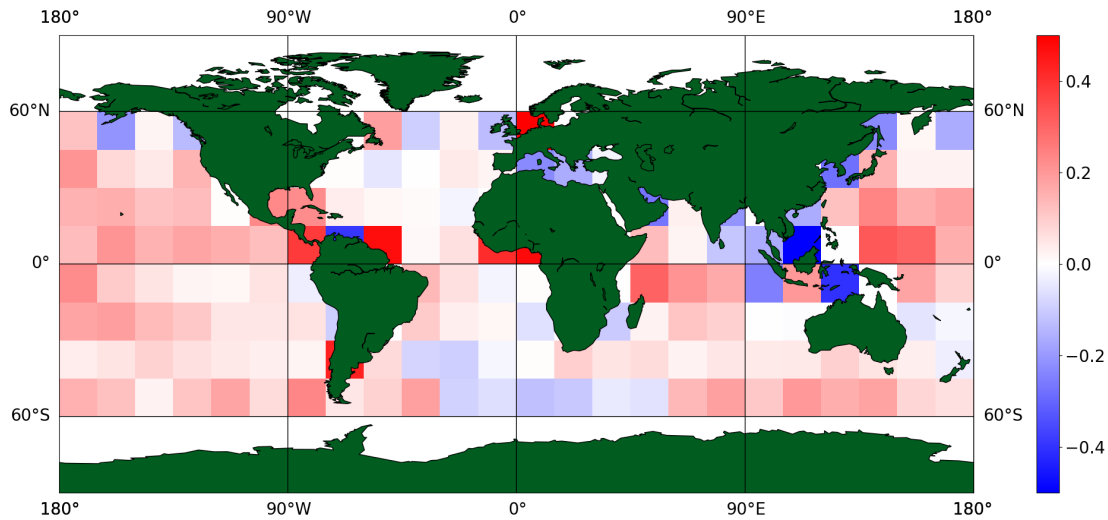


FIGURE 4.2: The susceptibility of cloud top height to aerosol when found with constraints on LWP, EIS, and  $RH_{700}$  during the daytime.

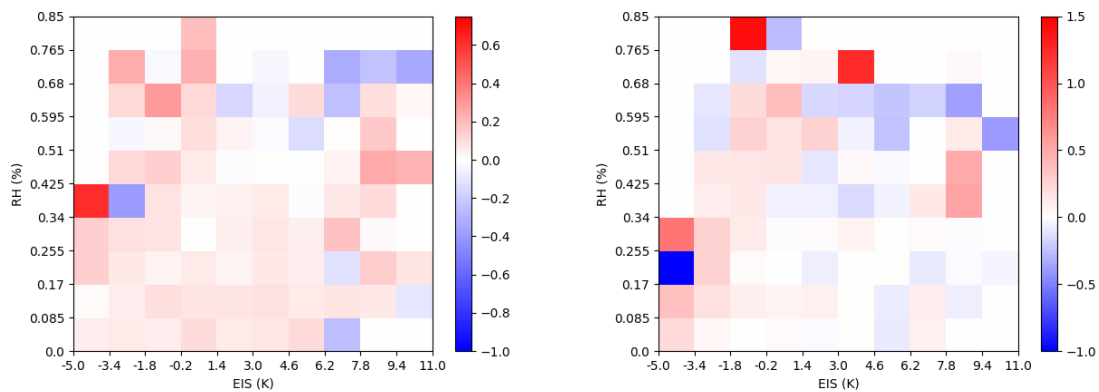


FIGURE 4.3: The daytime susceptibility of cloud top height to aerosol for LWPs between  $20$  to  $60 \text{ gm}^{-2}$  and  $60$  to  $100 \text{ gm}^{-2}$  evaluated on a regional basis and averaged into global bins. (Note the adjusted colorbars)

cellular convection. Closed cellular convection, where the cloud appears to be one continuous layer and the independent cells are hard to distinguish, are known to have a damped deepening response to aerosol (Christensen and Stephens, 2011). Conversely,

open cellular convection is extremely conducive to aerosol-forced deepening. In stratocumulus regions such as off the California coast, the mean susceptibility is likely a combination of these two modes.

Tropical cumuli appear more susceptible to experience a thinning response due to evaporation-entrainment (Jiang et al., 2009). Within shallow cumuli, enhanced evaporation at the cloud top due to entrainment of dry air leads to cloud thinning, eventually breaking up the cloud. The negative susceptibilities in the tropics may be due to this effect. As aerosol increases in the cloud layer, cumuli experience enhanced turbulence, increasing the amount of entrained air from the free atmosphere and more readily evaporating the smaller drops within the cloud's entrainment zone (Small et al., 2009). While stable environments cap the clouds under an inversion, minimizing the possible effects increased turbulence may have on the cloud layer, cumuli in unstable environments do not experience this limiting factor and therefore are more likely to experience evaporation-entrainment thinning.

### **4.3.3 The cloud extent susceptibility**

The mean global response of warm clouds to aerosol loading is to increase in size with a mean susceptibility of 3% cloud fraction increase per unit AI (Figure 4.4). In some regions of tropical cumuli, the cloud fraction decreases as aerosol increases. Warm clouds off the coast of Africa decrease in size, however this may be due to semi-direct effects leading to cloud breakup rather than aerosol-cloud interactions. Our regime constraints account for the effects of the environment, but lack constraints

on additional aerosol effects on the cloud layer. Aerosol not fully activated within a cloud may absorb incoming solar radiation, heating the cloud layer and leading to cloud break up (Johnson et al., 2004).

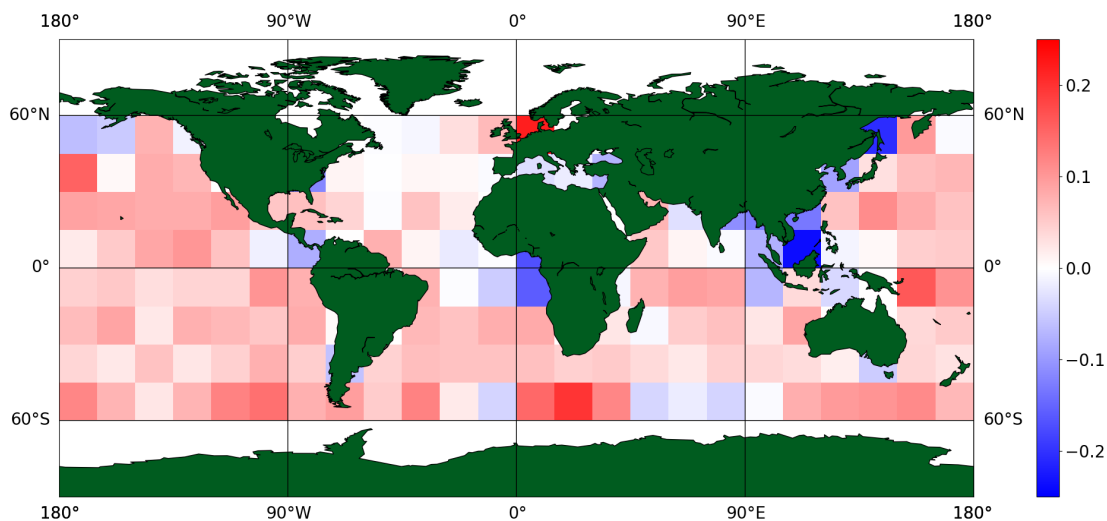


FIGURE 4.4: The susceptibility of cloud fraction to aerosol when found with constraints on LWP, EIS, and  $RH_{700}$  during the daytime.

#### 4.3.4 Diurnal influence on susceptibilities

The nighttime response to aerosol vary in sign and magnitude much more than the daytime responses (Figure 4.5). At night, many of the marine stratocumulus decks appear to decrease in height as aerosol concentration increases. This may be due to the dependence on nighttime turbulence on precipitation within marine stratocumulus. Drizzling processes can lead to the thinning of the cloud while higher rain rates lead to a deeper cloud column (Chen et al., 2011). The decrease in the California and Peruvian depths may be a sign that these stratocumulus cloud decks do not experience heavy enough precipitation to sustain their depth or deepen. The change in sign from

a deepening to thinning response can be seen in the summative global regime bins (Figure 4.7). As the cloud top cools unimpeded by any solar warming, the inversion increases in strength, capping any deepening.

The trade cumuli in the Atlantic experience a deepening as aerosol concentration increases. A number of low stability bins show an extreme deepening response (Figure 4.7). These clouds are more likely to precipitate and at higher rain rates; it is possible that aerosol delays precipitation within trade cumuli, increasing their LWP over time (L'Ecuyer et al., 2009, Sorooshian et al., 2009). At night when the cloud is most likely to precipitate, the enhanced latent heating due to the greater number of cloud droplets within the cloud then leads to higher cloud top heights (Koren et al., 2014).

While the cloud top height response is extremely sensitive to precipitation and the inversion strength, the cloud extent response appears more consistent over time (Figure 4.6). While the response is damped compared to the daytime response (Figure 4.4), a majority of warm clouds experience an increase in extent as aerosol increases at night. A cloud depth response depends on the in-cloud turbulence, while the cloud extent response is more likely linked to the stability of the boundary layer at night (Wood, 2012, Wood and Bretherton, 2006). The possibility of evaporation-entrainment breaking up the cloud layer decreases at night without solar insolation. In the regions where cumuli are the dominant cloud type, the decrease in cloud fraction may be due to the clouds aggregating, whereby the clouds become smaller, but taller in size.

Variance in the sign and magnitude of the susceptibilities of cloud top height and extent (Figures 4.5, 4.6) may be due to the timing of diurnal processes. The A-Train constellation passes over the region at 1:30 am local time, meaning in some regions the sun has been set for over six hours. In that time, it is possible the cloud has already adjusted and reached equilibrium with the nighttime boundary layer and any aerosol present. Without incoming solar radiation, the turbulence of the cloud increases as the cloud top cools unimpeded. This may quicken the rate at which the cloud reaches its new equilibrium to any additional aerosol (Dagan et al., 2017). Further study of diurnal aerosol-cloud interactions must include more observations beyond the ones taken at 1:30am in order to capture any adjustments undergone by the cloud layer prior to the satellite overpass.

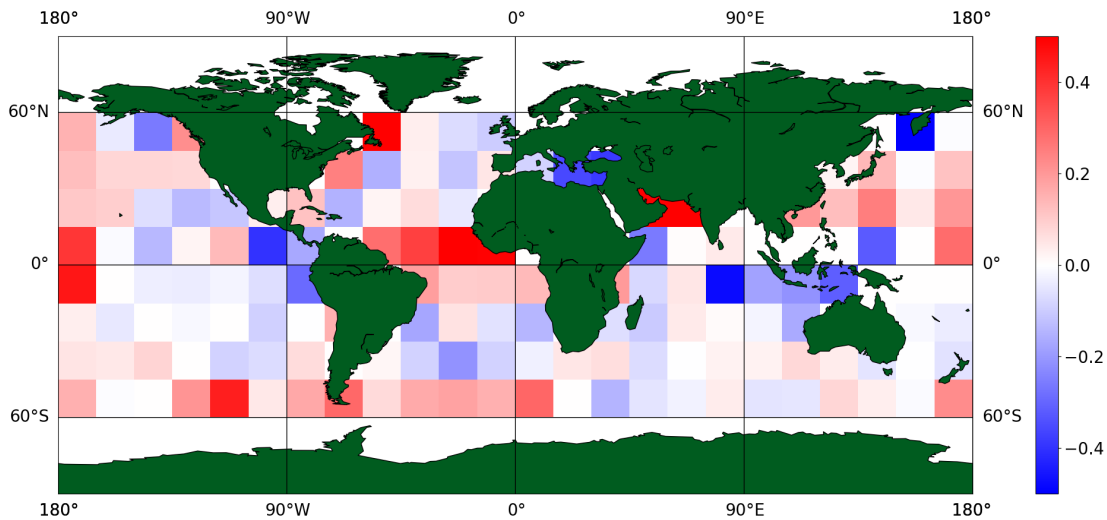


FIGURE 4.5: The susceptibility of cloud top height to aerosol at night when found with constraints on LWP, EIS, and  $RH_{700}$ .

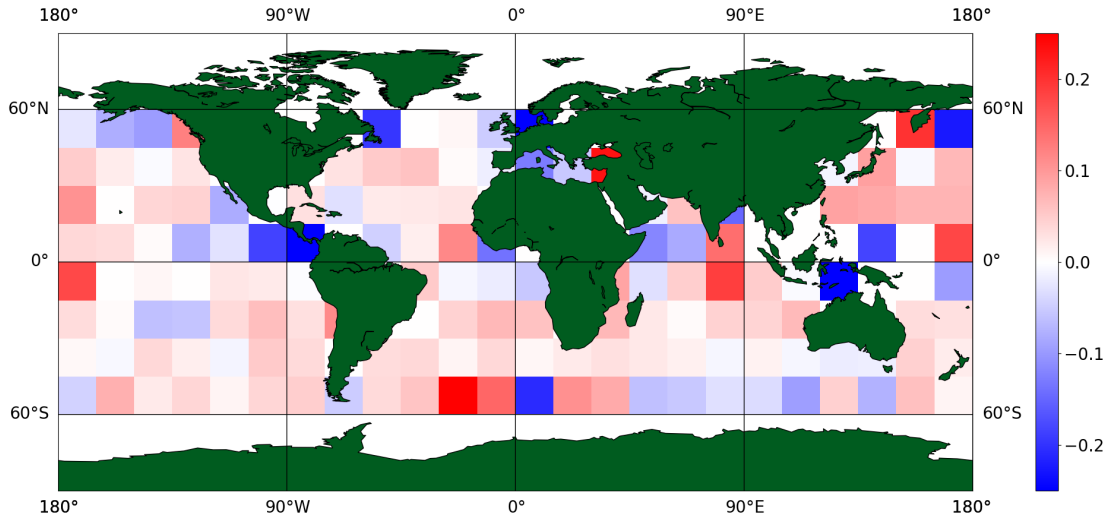


FIGURE 4.6: The susceptibility of cloud fraction to aerosol at night when found with constraints on LWP, EIS, and  $RH_{700}$ .

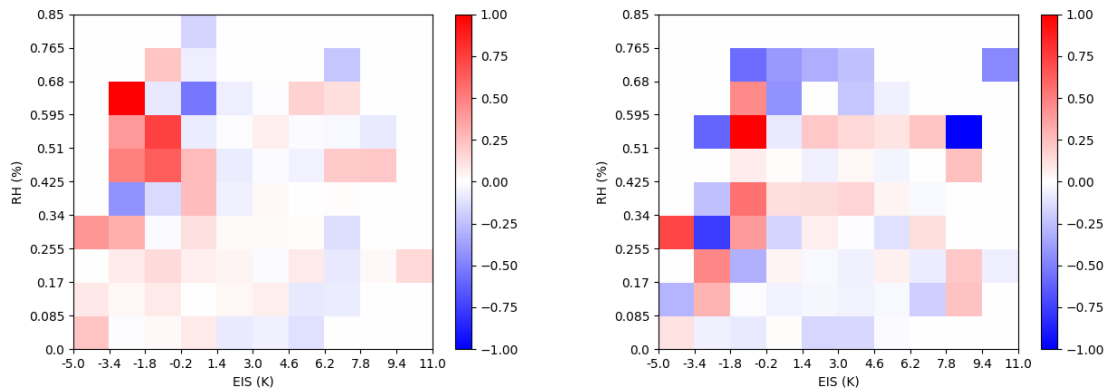


FIGURE 4.7: The nighttime susceptibility of cloud top height to aerosol for LWPs between 20 to 60  $\text{gm}^{-2}$  and 60 to 100  $\text{gm}^{-2}$  evaluated on a regional basis and averaged into global bins.

### 4.3.5 Inducing cloud feedbacks

There are possible cloud feedbacks that could be induced by aerosol-cloud interactions altering the cloud extent and/or the cloud longwave CRE. As the cloud extent decreases, the amount of outgoing longwave radiation increases, venting and cooling

the surface. If aerosol-cloud interactions lead to smaller pre-convective clouds, the mature, convective type have a decreased size as well, increasing the total amount of cooling at the surface due to venting. Cumuli may be more susceptible to this process as night. Further analysis must uncover how the diurnal cycle affects precipitation formation and how this may alter the physical processes controlling depth and extent of pre-convective warm clouds.

If aerosol-cloud interactions do lead to a deepening effect, this may suggest an invigoration of the cloud whereby the cloud experiences greater precipitation formation rates, turbulence or flow, and changes to the structure of the cloud (Altaratz et al., 2014). The cloud deepening effect seems to strongly depend on the stability (Figure 4.2), as more unstable regions showed a greater susceptibility. Future climates may lead to destabilizing of the boundary layer; as the sea surface temperature warms, the inversion strength capping and maintaining marine stratocumulus diminishes (Schneider et al., 2019). The dominant cloud type is currently stratocumulus globally, any shift in the dominant regime will have drastic consequences on both possible invigoration of cumuli precipitation and the radiative balance (Hahn and Warren, 2007a).

## 4.4 Conclusions

The longwave indirect effect, whereby an increase in cloud top height and extent increases the overall LW CRE, is explored here by evaluating the susceptibility of the

deepening effect and cloud extent effect within regime. The sum of these susceptibilities, the longwave indirect effect susceptibility, is found on a regional basis within regimes of stability, free atmospheric relative humidity, and the LWP of the cloud to assess how the longwave indirect effect compares to the shortwave indirect effect in magnitude and sign (Figure 4.1). It is possible in some regions for the two to effectively cancel each other out, resulting in no discernible change in the total radiative balance due to ACI, as is found off the coast of Asia. Interestingly, the longwave susceptibility is negative, or has a cooling signal, in this region, suggesting the cooling effect from a reduce LW CRE may offset the warming susceptibility of the shortwave indirect effect, caused by a cloud darkening in the same region (Douglas and L'Ecuyer, 2019a).

The cloud deepening found during the daytime and in selection regions at night (Figures 4.2, 4.5) suggests precipitation suppression leads to macrophysical changes to the cloud enhancing the LW CRE. The magnitude and sign, whether the cloud significantly depends or thins, depends on the region and whether it is day or night. The structure of the boundary layer, particularly the effects of the diurnal cycle on the capping inversion, play a role in determining whether the cloud is able to deepen or thin and to what degree. Warm cloud types such as trade cumuli are not as impacted by the inversion as marine stratocumulus; their response is therefore controlled by the amount of turbulence ACI can induce within the cloud to instigate a deepening response.

The response of the cloud extent to aerosol shows the same dependencies on region and nighttime conditions as the cloud top height (Figures 4.4, 4.6). The mean daytime response of warm clouds to aerosol is an increase in cloud fraction, while the nighttime response is more varied. In some regions, a decrease in cloud extent at night would lead to a venting of the surface, as the thermal emissions are not "trapped" by any cloud cover. Aggregation, or the possibility of changes to the organization and total cloud cover, may be induced in certain conditions by ACI. Inducing cloud feedbacks such as aggregation or invigoration through indirect effects is an emerging field; further work should be done on investigating what conditions induce these behavior or strengthen the feedback.

Many cloud feedbacks related to ACI may be heavily dependent on precipitation formation, or lack thereof, within the cloud. The delay of precipitation is suggested to result in invigoration of the cloud; a pathway our results support as cloud deepening is one of the strongest signals of invigoration within the cloud. How the diurnal cycle may affect precipitation suppression remains unknown. Our results suggests in some regions of marine stratocumulus where drizzle is known to occur at night that precipitation plays a leading role in determining the cloud's macrophysical response to aerosol (Wood, 2012). The role of precipitation in determining the susceptibilities of the longwave CRE to aerosol is vital to determine in future work, especially if aerosol-cloud-precipitation-environment interactions can inhibit or induce cloud feedbacks (Fan et al., 2016).

## Chapter 5

# Invigoration of Warm Rain due to Aerosol-Cloud Interactions

### 5.1 Foreword

The work shown is currently under review with the Proceedings of the National Academy of Sciences of the United States of America. Cloud deepening is a sign of invigoration of the cloud state, wherein the rain formation rates and turbulence within cloud increase due to aerosol-cloud interactions. In order to evaluate how aerosol-cloud interactions may alter precipitation formation, mixing with the atmosphere, and vertical motion within the cloud we utilize the Wisconsin Algorithm for Latent heating and Rainfall Using Satellites product described herein (Nelson et al., 2016). The same interactions that result in cloud deepening and an increased longwave

indirect effect of the cloud may also result in invigoration of the cloud's precipitation processes. Building on our knowledge of how the environment modulates aerosol-cloud interactions (Chapter 3), and how it directly regulates cloud deepening (Chapter 4), Chapter 5 shows the culmination of this work to explore invigoration signals within the cloud while accounting for the environment and constraining the cloud LWP.

## 5.2 Significance Statement

Here we show the first observational evidence of invigoration due to anthropogenic emissions within warm clouds. Invigoration, or greater rain rates, higher cloud tops, and faster wind speeds within the cloud, greatly affects both the hydrological cycle and climate system. While the invigoration hypothesis was postulated over 30 years ago, it has proven challenging to observe evidence of invigoration beyond a cloud deepening response. Our work illustrates that emissions can increase the rate of warm rain formation, affect cloud lifetime processes, and induce flow within the cloud. However, these effects all depend on the environment around the cloud. Without accounting for how the environment interacts with invigoration, discerning signs of invigoration is impossible.

## 5.3 Abstract

Aerosol-cloud-precipitation interactions can lead to a myriad of responses within cumulus clouds including an invigoration response, whereby aerosol loading results in a

higher rain rate, more turbulence, and deepening of the cloud layer, but have found indications that invigoration occurs. Observation based studies have generally focused on only the deepening response. Here, we show the first evidence of invigoration beyond a deepening response. Using latent heating and vertical motion profiles derived from CloudSat radar observations, we show warm clouds in unstable, polluted environments exhibit a marked increase in precipitation formation rates, cloud top entrainment rates, and induced flows. However, invigoration is only discernible when the stability of the boundary layer is explicitly accounted for in the analysis. Without this environmental constraint, the mean polluted and pristine cloud responses are indiscernible from each other due to offsetting, opposite reactions. Signs of invigoration, or lack thereof depending on the environment, may induce possible feedbacks in both stable and unstable conditions that could subdue or enhance these effects, respectively. The invigoration response is found to additionally depend on the organization of the cloud. The size of the warm rain system controls the magnitude of all invigoration signals. Modeling parameterizations must account for not only the possibility of an invigorated cloud state, but also the dependence of this state on the environment and the organization of the rain system.

## 5.4 Introduction

Aerosol-cloud interactions remain one of the largest sources of uncertainty in future climate projections (Boucher et al., 2013). Further, their role in climate feedbacks,

particularly how they affect low clouds, controls the magnitude of the climate sensitivity (Zelinka et al., 2020b). However, despite the importance of tropical low clouds to the global climate, understanding their response to anthropogenic activity including aerosol loading remains a challenge (Bony and Dufresne, 2005). In particular, invigoration, or the enhanced size, precipitation rate, or turbulence, of low clouds was hypothesized as a potential outcome of aerosol-cloud interactions decades ago but remains relatively unconfirmed from observations (Pincus and Baker, 1994, Rosenfeld et al., 2008). Invigoration of warm cloud thermodynamics has the potential to alter deep convection, making eventual storms more intense and turbulent (Chen et al., 2017).

Many have focused on detecting cloud deepening as a signal of invigoration, as it theoretically implies increased turbulence and precipitation within the cloud (Altaratz et al., 2014). L'Ecuyer et al. (2009) showed warm, polluted precipitating clouds grow deeper than those in more pristine environments. Christensen and Stephens (2011) found as ships passed below marine stratocumulus, the locally affected clouds deepened. Kubar et al. (2009) found evidence of cloud deepening in highly polluted environments in all warm cloud types. Yuan et al. (2011) found evidence of cloud deepening in trade cumulus when interacting with nearby volcanic emissions. However, Dey et al. (2012) found no evidence of cloud deepening in the smallest clouds studied, only an increase in extent. While observational studies have been able to

discern a cloud depth response, few have included the environment within their estimates in order to certify that this response is due to aerosol-forced invigoration and not environmentally forced. Additionally, a deepening cloud does not conclusively prove an increased turbulence and precipitation formation rate, only another cloud adjustment process.

Modeling efforts have proven more promising in, at least hypothetically, demonstrating invigoration of warm clouds is possible by aerosol. Heiblum et al. (2019) used a LES model to show that clouds formed in higher aerosol environments release more latent heat and promote a larger rain cell size. Jiang et al. (2009) similarly used a LES and found clouds in polluted environments produced more evaporation at the cloud edge in simulated trade cumuli, producing more vertical motion. Clouds formed in polluted environments may experience an increase in droplet mobility, which delays collision coalescence and changes the organization of liquid water within the cloud to a more invigorated state reaffirming Albrecht's original theory of a second aerosol indirect effect (Albrecht, 1989, Berg et al., 2008, Koren et al., 2015). Depending on the environmental conditions, the liquid water path of the cloud may decrease, signaling a curtailment, not invigoration, response (Jiang et al., 2006).

The environment plays a strong role in modulating warm rain processes and therefore must be considered when using observations to imply aerosol-forced invigoration of warm clouds (Stevens and Feingold, 2009a). Prior work has shown that the environment controls the amount of suppression within the cloud, which may modulate the

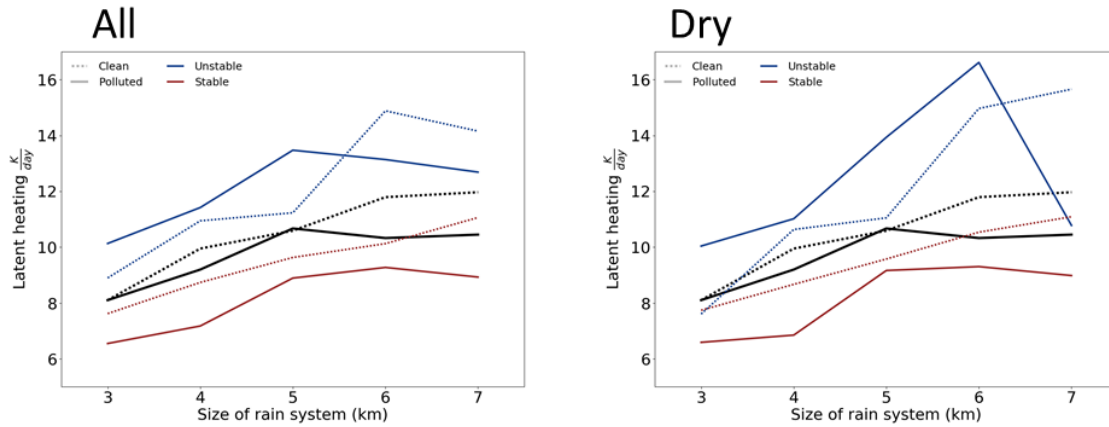


FIGURE 5.1: The maximum rate latent heat release due to precipitation within the cloud against the size of the rain system for all (top) and dry (bottom) warm clouds with an extent of 15 km. Black is for all stabilities, blue is for unstable environments, red is for stable environments; dashed represents pristine and solid represents polluted surroundings.

amount of invigoration (L'Ecuyer et al., 2009). The strength of the marine boundary layer inversion controls cloud top height in many warm clouds (Wood, 2012). This inversion strength has been shown to heavily influence rain formation rates in warm clouds (Nelson and L'Ecuyer, 2018). The magnitude and sign of warm cloud aerosol-cloud interactions is likewise heavily modulated by both the inversion strength and free atmosphere (Douglas and L'Ecuyer, 2019a). The humidity of the free atmosphere affects how aerosol impacts the distribution of liquid water throughout the cloud layer due to entrainment processes (Ackerman et al., 2004). Both are considered within this study in order to constrain these confounding factors.

The liquid water path controls to a first degree the probability of a cloud raining (Berg et al., 2006, L'Ecuyer et al., 2009). Aerosols in turn impacts the liquid water path as part of a cloud adjustment process, which then further alters the probability

of precipitation. The relationship between aerosol-cloud interactions and the cloud liquid water are not universal nor well known. In order to reduce the uncertainty interpreting our results, we limit our observations to clouds with liquid water paths in a narrow range between 150 to 200 g/m<sup>2</sup>. In doing so, we focus only on how aerosol alters the organization of rain formation and evaporation within the cloud layer, not its influence on cloud liquid water. Invigoration in this context includes how aerosol enhances rain formation within the cloud, alters evaporation in the entrainment zones, and induces more turbulence.

Using latent heating and vertical motion profiles from the Wisconsin Algorithm for Latent heating and Rainfall Using Satellites (WALRUS), we show that there is a discernible signal of invigoration in warm clouds due to aerosol. Observations are limited to cumulus clouds using CloudSat cloud information. The Moderate Resolution Imaging Spectroradiometer (MODIS) aerosol index (product of aerosol optical depth and Angstrom exponent) is used as a proxy for how aerosol concentrations affect the number of cloud condensation nuclei. A series of constraints are implemented in order to account for the role of stability in modulating invigoration.

## **5.5 Results and Discussion**

### **5.5.1 Aerosol Effects on Rain Formation**

Warm rain invigoration predicts that in a more polluted environment, the rate of collision coalescence and therefore precipitation production increases. Our analysis

suggests clouds in polluted environments on average do not show an increased rate of precipitation formation relative to pristine environments (black solid line, figure 5.1). The difference between polluted (solid) and pristine (dashed) is minimal when only the mean is considered. However, when separated the stability, it is evident that the reason for this is not that the warm rate intensity is unaffected by aerosol loading, it is that clouds in polluted scenarios react differently under stable and unstable conditions. In unstable environments, polluted conditions lead to a marked increase in precipitation rate relative to unstable, pristine conditions until rain system grows beyond  $\sim 6$  km. Conversely, stable, polluted conditions lead to a decrease in precipitation rate relative to stable, pristine conditions. The opposite reactions in stable vs. unstable conditions offset each other, giving the mean impression that warm rain is unaffected by aerosol loading when in actuality its sensitivity is simply environmentally dependent. A sign of invigoration is only identifiable when stability is accounted for.

Pristine clouds show a strong dependence on the size of the warm rain system compared to polluted clouds. While polluted clouds have a non-linear relationship between the size of the rain system and the maximum rain formation rate, pristine clouds show a steady, linear increase in the rate as the size of the rain system grows. Polluted clouds have an inflection point whereby after that size they show much greater rates of rain formation, and this inflection point depends on both the stability of the boundary layer and the humidity of the free atmosphere. Pristine conditions do not show this acceleration.

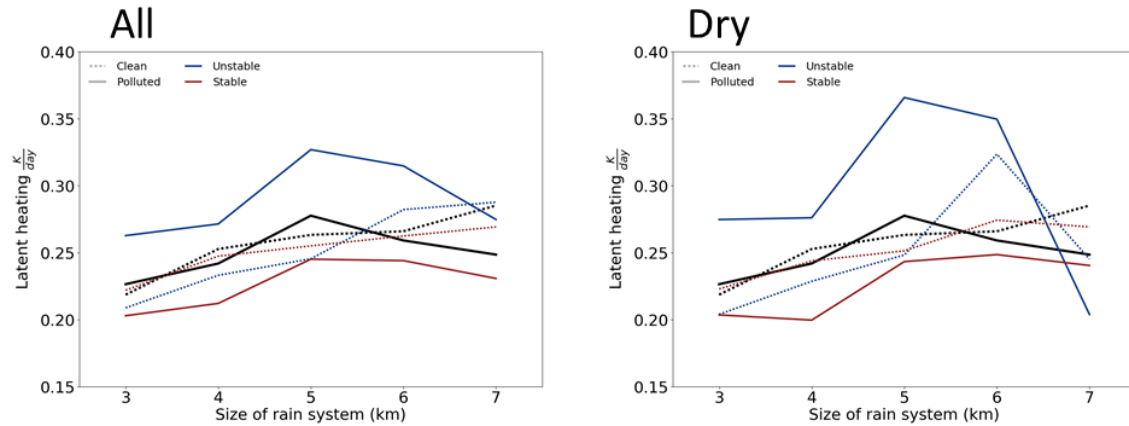


FIGURE 5.2: The mean amount of latent heating released due to precipitation formation rate in the geometrical center of the rain system against size of the rain system for all (top) and dry (bottom) warm clouds with an extent of 15 km. Black is for all stabilities, blue is for unstable environments, red is for stable environments; dashed represents pristine and solid represents polluted surroundings.

The core of a warm convective system should theoretically show the greatest sign of invigoration of precipitation. Our results indicate this is correct, as invigoration of the warm rain formation rate due to aerosol is most pronounced in the geometrical center of the rain system (figure 5.2). The mean precipitation rate increases in the center in unstable, polluted clouds relative to both cleaner and more stable conditions. This effect is exacerbated in dry conditions until the rain system seems to hit a size inflection point around 7 km. While instability in polluted clouds leads to greater formation rates in the center, clouds in stable but equally polluted environments show a decrease in rain production relative to pristine conditions. This reverse behavior is seen regardless of the effects of the free atmosphere, as clouds in a dry environment (figure 5.2 right) show the same behavior as all clouds (figure 5.2 left).

### 5.5.2 Aerosol Effects on Evaporative Processes

However, that is not to say that the free atmosphere does not play a role in altering the thermodynamics or possible invigorate state of warm rain systems. Evaporative processes link entrainment, below cloud evaporation, precipitation formation, and the energy budget of a cloud. When focusing on how aerosol may affect entrainment, the free atmosphere's relative humidity becomes a controlling factor. A drier atmosphere leads to greater evaporation rates above the cloud in more polluted environments (figure 5.3). While increased mixing with the free atmosphere may lead to cloud deepening, it may also lead to an early onset of cloud breakup processes through evaporation-entrainment (Small et al., 2009). Increased entrainment and evaporation at the cloud top could lead to reduced cloud top heights, opposite of an invigoration effect (Xue and Feingold, 2006). Whether the cloud deepens or shallows may depend on the distribution of liquid water near the cloud top and the ability of the cloud to penetrate the free atmosphere.

A drier atmosphere reverses this behavior in only unstable conditions; stable clouds are unaffected by a drier free atmosphere. This is likely due to the stronger capping inversion in stable conditions which limits mixing with the dry free atmosphere, limiting its effects on the cloud layer and, by extension, the invigoration process (Christensen and Stephens, 2011). While stable clouds have had similar responses in precipitation formation rates, the inversion's role in limiting effects is most pronounced in evaporation due to entrainment mixing. By limiting the amount of mixing with the free

atmosphere, the inversion damps the ability of stable, polluted clouds to experience a cloud deepening effect compared to unstable, polluted clouds. While these clouds do not show signs of invigoration, stable, polluted conditions may prolong cloud lifetime by lessening cloud thinning processes (Van der Dussen et al., 2014).

That the core of dry, polluted, unstable systems experience significantly greater rain formation rates than all other environments may suggest these clouds undergo some aggregation process focusing the majority of precipitation formation within the core of the cloud. This results agrees with a theoretical model posed by Morrison (2017), where entrainment of dry air leads to narrowing effect on the cumuli and enhancement of the core. Aerosol may act to invigorate this specific response by increasing the entrainment-evaporation at the cloud top, promoting turbulence within the cloud layer.

Below cloud evaporation and its associated cooling destabilizes the boundary layer, which could then further invigorate the cloud layer through amplified turbulence (Xue and Feingold, 2006). Figure 5.4 demonstrates that larger warm rain systems exhibit considerably more below cloud evaporation than smaller systems. The steep increase in dry, unstable environments may signal the size inflection point where evaporation goes from a slow to rapid process. Polluted clouds exhibit less below cloud evaporation in regardless of the stability. This may imply that pristine conditions destabilize the boundary through below cloud cooling.

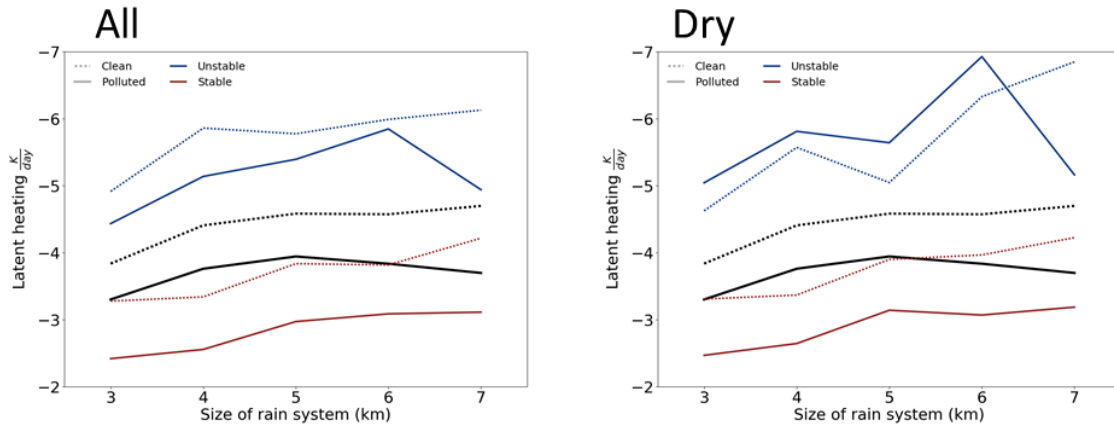


FIGURE 5.3: The maximum rate latent heating released due to evaporation above the cloud against size of the rain system for all (top) and dry (bottom) warm clouds with an extent of 15 km. Black is for all stabilities, blue is for unstable environments, red is for stable environments; dashed represents pristine and solid represents polluted surroundings.

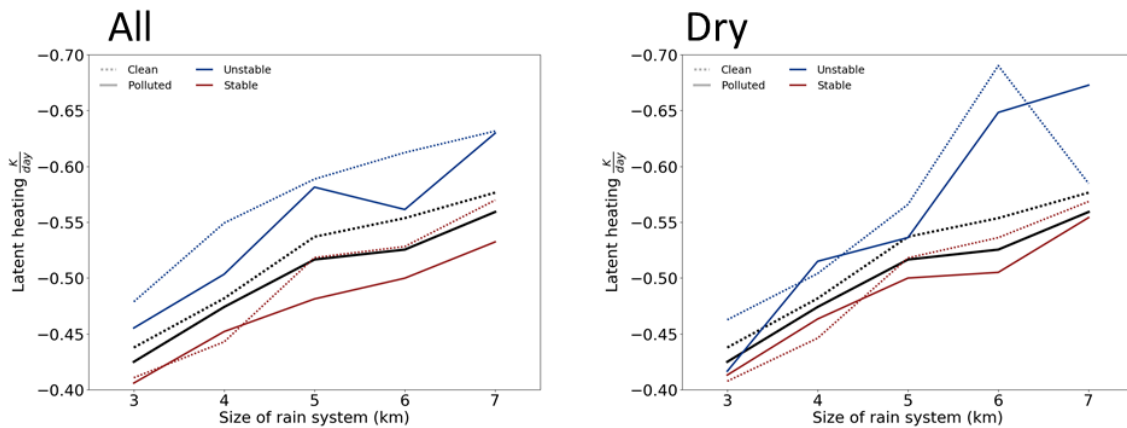


FIGURE 5.4: The mean rate of latent heating due to evaporation below the cloud vs size of the rain system for all (top) and dry (bottom) warm clouds with an extent of 15 km. Black is for all stabilities, blue is for unstable environments, red is for stable environments; dashed represents pristine and solid represents polluted surroundings.

In environments with drier free atmospheres, unstable clouds (both pristine and polluted) have much greater rates of evaporation below the cloud (figure 5.4 left). This implies that the increased evaporation due to entrainment (figure 5.3) leads to more mixing throughout the cloud layer, more collision-coalescence, and may decrease the mean drop size, increasing the rate of evaporation below the cloud. Interestingly, this increases the rate of evaporation more in pristine than polluted environments, which may be due to efficiency of evaporation. In polluted, unstable, dry environments, the smaller droplets (relative to pristine conditions) may evaporate more efficiently, increasing the humidity of the lower boundary layer and decreasing the rate of evaporation as the cloud continues to precipitate (Jiang et al., 2009, Pincus and Baker, 1994). Stable, polluted boundary layers show the lowest rates of below cloud evaporation. This agrees with the original hypothesis of Albrecht (1989), whereby aerosol works to increase cloud lifetime. However, in this context stable, polluted boundary layers work to increase cloud lifetime through a possible feedback whereby there is less below cloud evaporation, therefore the boundary layer remains more stable, which in turn decreases the amount of below cloud evaporation and increases the lifetime of the cloud.

### **5.5.3 Aerosol Effects on Vertical Motion**

Our results are consistent with the hypothesis that invigoration will increase turbulence, indicated by changes in vertical motion, within the cloud layer due to greater amounts of latent heat release (Rosenfeld et al., 2008). Polluted environments display

higher updraft speeds within the cloud layer than pristine environments (figure 5.5). This reaffirms others' hypothesis that cloud deepening is driven by enhanced updrafts (Christensen and Stephens, 2011). Aerosol may act to redistribute water throughout the cloud resulting in changes to the distribution of latent heating (Dagan et al., 2018a). Modifying where latent heat is released, especially increasing the difference between the center where rain formation is occurring and edge evaporation due to cloud edge entrainment, alters turbulence and flow within the cloud layer. While it remains unclear how aerosol may affect the absolute amount of water within a cloud, it is clear aerosol affects how water is distributed within the cloud (Rosenfeld et al., 2019, Toll et al., 2019).

When separated into stable and unstable environments (figure 5.5) it becomes obvious how *strongly* stable environments damp invigoration. While unstable environments intensify the turbulence within the cloud layer, stable environments show only a faint increase in turbulence at the middle of the cloud. This may explain why stable, polluted environments also manifest the smallest rates of evaporation due to cloud top entrainment, as these clouds have less overturning motion near the cloud tops. Though stable, polluted environments displayed a reduced core precipitation formation rate compared to their pristine counterparts, the reduced size of the polluted droplets may allow greater mobility and therefore rates of vertical motion (Koren et al., 2015). Unstable, large rain systems ( $\sim 6$  km) may have downdrafts within the cloud due to enhanced evaporation entrainment, leading to more in-cloud turbulence, overturning

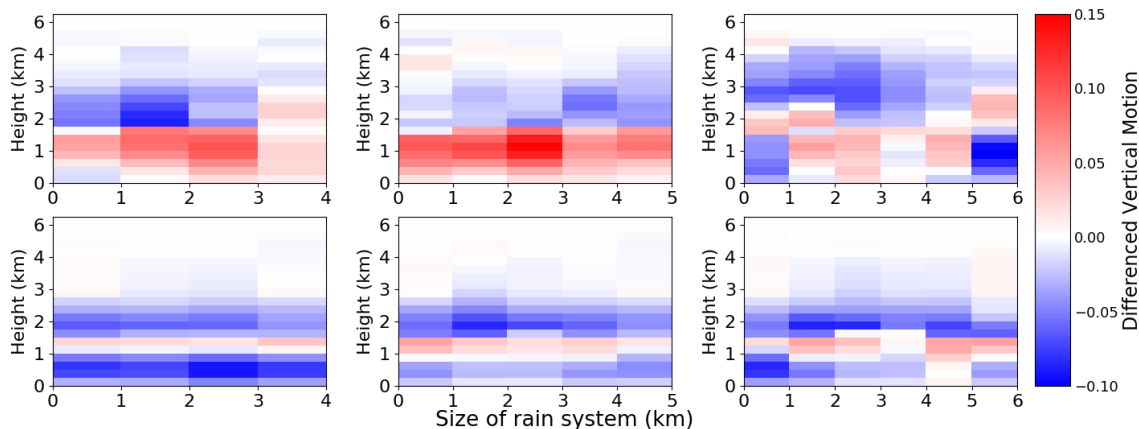


FIGURE 5.5: The difference (polluted - pristine) in vertical motion in unstable environments in unstable (top) and stable (bottom) environments for clouds of rain size 4 km (left), 5 km (middle), and 6 km (right).

motion, and mixing.

It should be noted that increased rates of rain formation in unstable clouds could induce a positive feedback: latent heating increases from faster rain formation which leads to more vertical motion and turbulence, greater updraft speeds, more entrainment and therefore buoyancy fluctuations within the cloud, which in turn leads to more collision-coalescence and latent heating. This could explain both the greatly enhanced rain formation rates in the center (figure 5.2) and intensified turbulence (figure 5.5). However, this feedback may be particularly sensitive to the size of the rain system, as larger systems may decrease the chance of the feedback occurring. The scattered increases in turbulence seen in rain systems of size 6 km and the sloping off of rain formation rates at the same size imply a sensitivity to the size and organization of the system (Fan et al., 2016).

## 5.6 Conclusions

Cumulus clouds in polluted, unstable environments display greater rates of peak and core precipitation formation along with greater amounts of vertical motion and therefore turbulence within the cloud. Dry environments act to increase this response, along with inducing further invigoration effects by increasing the amount of entrainment mixing. Stable environments act to dampen invigoration by capping entrainment effects and reducing precipitation formation rates. In polluted environments, a stable boundary layer and strong inversion acts to inhibit rain production relative to pristine environments. This reverse response may be driven by reduced amounts of vertical motion in polluted cloud tops and bases, hindering precipitation formation throughout the cloud.

Invigoration is an "elusive" effect in the aerosol-cloud interaction community perhaps because observing it depends on the definition. Based on our definition, whereby aerosol loading of warm clouds increases the precipitation formation rate and in-cloud turbulence, there is evidence invigoration may occur. However from the results shown, two important aspects of invigoration emerge:

1. The magnitude of invigoration in marine cumuli is extremely dependent on the size of the cloud. As the rain system grows, all possible signs of invigoration, from more rain formation to increased turbulence, vary with the rain system size. Further, this implies the organization of the

cloud plays a role in defining how aerosol loading may impact aspects of invigoration. The dependence of these processes on the size of the system may explain why many components of invigoration (LWP response, cloud deepening, etc) are non-linear when regressed against aerosol alone.

2. Stability can reduce and/or reverse all aspects of invigoration within the cloud layer. The mean warm cloud signal of invigoration is completely buffered by the environment unless stability is accounted for.

Even with stability and the environment accounted for through sets of constraints, our observations are limited by liquid water path in order to derive a signal of invigoration. Without these constraints, invigoration would be indiscernible. The formation rate in polluted environments closely tracked the mean pristine rate (figures 5.1, 5.2). Analysis of invigoration must account for these relationship when deriving aerosol impacts on precipitation.

Our analysis is based on latent heating and vertical motion derivations from WALRUS. As such, some amount of uncertainty remains due to the nature of WALRUS as a satellite-based algorithm of latent heating. Additionally, our study is limited to only a "snapshot" view of clouds, unable to account for the individual lifetimes of each cumuli. Future analysis should include the state of the cloud throughout its lifetime in order to understand how the trajectory of a cloud affects its response to aerosol loading.

## 5.7 Data and Methods

All observations are from instruments aboard NASA A-Train satellites from 2007 to 2010 and from 60° south to 60°. Aerosol index (AI) from MODIS serves as our aerosol concentration proxy. The AMSR-E provides the mean cloud liquid water path of the scene. CloudSat’s cloud profiling radar (CPR) is used to define cloud extent. We employ the WALRUS algorithm, derived from CloudSat CPR and reanalysis, to infer changes in latent heating and vertical motion within cloud profile.

Aerosol index is the product of the Angstrom exponent and the aerosol optical depth measured at 550 nm and is better correlated with cloud droplet concentrations than AOD (Ångström, 1964, Hasekamp et al., 2019). MODIS AI is available in clear sky scenes over the ocean, meaning cloudy AI is calculated using interpolation (Levy et al., 2010). We remove AI within 2 km of the clouds in order to reduce the influence of aerosol swelling in high humidity scenes (Christensen et al., 2017). We define pristine conditions as those with an AI less than .042 and polluted as those with an AI higher than .09. These roughly correspond to the lower and upper 20 percentiles of our dataset. Avoiding intermediate AIs reduces the possibility our analysis captures possible transition states as clouds move out of the aerosol limited regime (Koren et al., 2014).

Clouds are limited to LWPs between 150 to 200  $\text{gm}^{-2}$  LWP using AMSR-E (Wentz and Meissner, 2007). Although AMSR-E LWP is derived using a larger field-of-view,

this is a rough constraint; discrepancies between the AMSR-E LWP and CloudSat's footprint should not impact results. The liquid water path is used as an approximate constraint on cloud depth, which is further enforced by limiting the observations by the size of the cloud using CloudSat CPR and the height of the cloud. Cloud extents are defined using CloudSat's 2B-CLDCLASS-LIDAR product by limiting the analysis up to 15 contiguous, cloudy pixels (Sassen et al., 2008). This cloud based partitioning is analogous to the cloud object based partitioning used by Igel et al. (2014) except while Igel et al. (2014) focused on convective systems, our clouds are constrained to shallow convective types. We are focusing on cumulus warm clouds, rather than stratus or stratocumulus, in order to focus on shallow convection.

Environmental information is provided by MERRA-2 reanalysis. We define the stability of the atmosphere using the estimated inversion strength (EIS) (Wood and Bretherton, 2006). Stability of the boundary layer controls the depth of the cloud making it imperative that this relationship is constrained in order to separate aerosol effects from environmental forcings (Zuidema et al., 2009). Unstable environments are defined as having an EIS below 1 K while stable environments are defined as having an EIS above 3 K. This partitions environments into two main regimes: trade cumuli (unstable) and cumuli from stratocumulus to cumulus transitions (stable). A dry free atmosphere alters the distribution of liquid throughout the cloud layer, thereby directly impacting precipitation formation processes as well. In order to control for these interactions, clouds are further subset into a dry regime whereby the  $RH_{700}$  is

below 30% to analyze how dry air entrainment may impact invigoration processes.

The Wisconsin Algorithm for Latent heating and Rainfall Using Satellites (WALRUS) provides information on the latent heating and vertical motion profiles in the atmosphere. The model uses CloudSat's CPR along with warm rain states from the Regional Atmospheric Modeling System (RAMS) in order to emulate realistic latent heating rates and related vertical motion (Nelson et al., 2016). WALRUS limits our analysis to maritime clouds with heights less than the freezing level and only rain certain, therefore our results do not include the effects of drizzle on possible invigoration processes. This should also focus our results on only the growing and mature stages of shallow convection. Signals of invigoration are derived based on changes in the latent heating within the cloud. Precipitation formation rates correspond to the latent heat release within the cloud, while evaporation due to entrainment at the cloud top or vigra below the cloud are indicated by cooling from WALRUS. Turbulence, or the change in velocity, is determined by the difference in vertical velocity between polluted and pristine environments.

WALRUS employs a Bayesian Monte Carlo method in order to derive probabilistic latent heating profile. While precipitation amounts alone can be used to infer total latent heating of the cloud, this type of methodology allows the inference of the distribution of latent heating throughout the profile, below, within, and above the cloud. The Bayesian Monte Carlo method relies on an a priori distribution of possible characteristics to connect to the CloudSat observations. The a priori database is

created using the RAMS model with simulations based on the Atlantic Trade Wind Experiment field campaign. The model is run at a 250 m horizontal and 100 m vertical resolution for a set of sea surface temperatures (293 K, 298 K, and 303 K). Quick Beam produces radar reflectivity profiles and attenuation signals from the RAMS simulation, which are sampled every 40 minutes for the database. Overall, WALRUS had 1.4 million possible a priori distributions. WALRUS derives physically realistic latent heating and associated vertical motion rates. For more information and the full validation please refer to Nelson et al. (2016).

# Chapter 6

## Synthesis

### 6.1 Motivation

The effective radiative forcing due to aerosol-cloud interactions is the leading source of uncertainty in determining a climate sensitivity (Boucher et al., 2013). The effects of aerosol on clouds, and how this influences their overall radiative impact, remains uncertain due to our inability to accurately model these interactions within global climate models or observe these interactions with both high spatial and temporal resolutions. Aerosols act as CCN within a cloud, altering the cloud's albedo and ability to precipitate as more drops take longer to collision coalescence (Albrecht, 1989, Twomey, 1977a).

Longer lived and brighter clouds will increase the amount of cooling by reflecting more incoming solar insolation, however these interactions additionally alter the longwave impact and precipitation properties of clouds. Altering cloud precipitation has immediate implications to the hydrological cycle, changing where, when, and how much a cloud will precipitate. It is vital not just to quantify the change in the radiative balance due to  $a_{ci}$ , both in the shortwave and longwave, but to understand how the magnitude and the sign of these changes is modulated by the cloud state and environment. Moreover, the effects on precipitation must be understood with the same attention paid to the environmental factors, as changes in the hydrological cycle can further add uncertainty to the climate sensitivity Watanabe et al. (2018).

## **6.2 Investigating the effects of aerosol-cloud interactions on warm cloud properties**

The shortwave indirect effect is decomposed and evaluated with constraints on the stability of the boundary layer, free atmospheric relative humidity, and the liquid water path. The constraints are meant to identify regime specific behavior, as the environment and LWP of the cloud determine the strength and magnitude of the effect (Douglas and L'Ecuyer, 2019a, Stevens and Feingold, 2009a). By decomposing the shortwave indirect effect, the two components, the radiative forcing due to aerosol-cloud interactions (RF $_{aci}$ , albedo component) and the cloud adjustments (CA, lifetime component), can be compare and contrasted to find regions where the two effectively

cancel each other out.

With regime constraints in place, the RFaci dominates over CAs globally. In many regions, the two have the same negative effect on the radiative balance leading to a cooling effect. The RFaci leads to a cooling effect due to a higher albedo in regions of marine stratocumulus, however in some regions where semi-direct effects compromise the albedo effect, a cloud dimming is found. Regions with extreme amounts of pollution, such as the coast of Asia and the gold coast of Africa, show cloud dimming that offsets any cooling due to larger cloud extents. Without decomposing the shortwave indirect effect, these regions would show no change in CRE due to aerosol loading, erroneously attributing the null signal to a damped susceptibility.

The magnitude of warm cloud adjustments may double when effects of LWP are quantified. The LWP effect covaries with the albedo, cloud extent, and many other effects, and therefore may increase the overall magnitude of the ERFaci beyond the CA. In order to reduce uncertainty in our estimates, we chose not to include a change in LWP within our decomposition as studies disagree on the magnitude and sign to the point of denying the effect exists (Rosenfeld et al., 2019, Toll et al., 2019). If the LWP effect was just as large as the effect on cloud extent, the total cooling due to CAs would increase to  $-0.1 \text{ Wm}^{-2}$  and contribute  $\frac{1}{3}$  of the total ERFaci.

While warm clouds have warm cloud tops and therefore a small longwave cloud radiative effect, deepening due precipitation suppression and increased LWP would decrease

the cloud top temperature, increasing the overall longwave CRE. The global susceptibility of the longwave CRE to aerosol is  $.3 \text{ Wm}^{-2}\ln(\text{AI})^{-1}$ , or  $\frac{1}{30}$  the magnitude of the shortwave CRE susceptibility (Douglas and L'Ecuyer, 2019a). Nonetheless, the regional magnitude and sign vary significantly, and in some regions the longwave indirect effect has the potential to offset the shortwave indirect effect. Further, the longwave indirect effect can evaluate to a negative or cooling signal, whereby aerosol leads to a decrease in cloud top height, and can amplify the overall cooling due to indirect effects or offset slight warming due to cloud dimming.

Cloud deepening occurs globally during the daytime and in regions of cumuli at night. Cloud deepening due to aerosol indirect effects is controlled by the strength of the inversion of the boundary layer and precipitation. At night, in regions where the boundary layer increases in strength cloud deepening is damped in marine stratocumuli, while in regions trade regions and other regions where the boundary layer is less affected by diurnal effects the cloud is free to deepen. Cloud deepening is a sign of invigoration of the cloud state, whereby ACI lead to a deeper cloud, more precipitation formation, and increased turbulence within the cloud.

In order to expand upon the sign of invigoration found when decomposing the longwave indirect effect, the effect of aerosol on precipitation formation and turbulence is evaluated using model and CloudSat derived estimates of latent heating within warm clouds. All constraints from the previous estimate are because the stability of the boundary layer, the free atmospheric relative humidity, and the LWP of the cloud are

proven to influence how the cloud reacts to aerosol. The constraints are less refined than previous work due to the reduced number of usable observations, with only two stability regimes (stable and unstable) and one  $\text{RH}_{700}$  regime (dry).

Without regime separation into stable and unstable, the mean precipitation formation rates between polluted and pristine environments would be indistinguishable. The differences are only apparent when separated by stability. It becomes clear that polluted, unstable environments experiences much greater rates of precipitation formation than their pristine or stable counterparts. The  $\text{RH}_{700}$  is important when considering effects of aerosol on cloud top entrainment, reversing the behavior of unstable clouds whereby in drier, polluted environments experience more above cloud evaporation. The enhanced precipitation formation within the cloud and above cloud evaporation due to entrainment drive changes in turbulence throughout the cloud layer, however these changes are size and stability dependent. The size of the cloud determines the magnitude of the increased turbulence, with a peak near clouds with rain core sizes of 5 km and a sharp drop off with increasing size thereafter.

The dependency of the changes to precipitation formation and evaporation throughout the cloud profile on the stability,  $\text{RH}_{700}$ , and size of the rain system may contribute to the non-linear behavior of the LWP to indirect effects. This pattern is seen time and time again when evaluating indirect effects, whether invigoration or the radiative impact. The environment and state of the cloud determine not just the magnitude but the sign of the response. The global means often obfuscate the range of responses.

It is only when constraints are put into place that the true range of responses and non-linear dependencies on the environment and cloud state are apparent.

### 6.3 Future work

In order to expand my results on the regime framework used in Chapters 3 and 4, I plan to find the pre-industrial environmental regime distributions to compare against the present day distributions. If the environment of clouds has shifted since pre-industrial times, this shift can be used to better estimate the ERFaci by adding a term to the ERFaci equation in Chapter 3 to include a change in the distribution. Further, the change in aerosol must include how the distribution has changed from pre-industrial to present day times to better reduce any uncertainty in ERFaci estimates.

While the use of constraints through regimes captures the range of possible responses, these responses only reveal the state of the cloud during the time of the CloudSat overpass, not the processes responsible for the response. In my future work, I hope to integrate the history of a cloud when determining the response to aerosol through back trajectory analysis and machine learning techniques. The state of the environment, combined with cloud properties from geostationary satellites (15 minute resolution) or MODIS (4x daily resolution), can be used as a feature in machine learning. The entire history of the cloud, the environment, and aerosol can then be used to determine the response. My work so far is a step into understanding the many pathways responsible

for the response of cloud to aerosol; integrating more advanced methods of regression beyond linear methods are necessary to capture the range of responses seen.

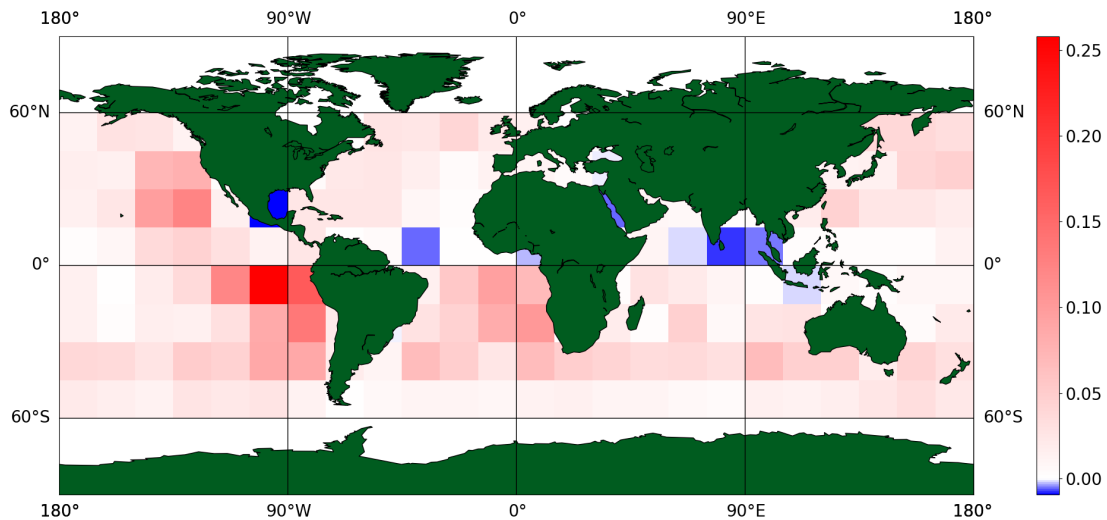


FIGURE 6.1: The change in cloud fraction (all - pristine) using modeled pristine cloud fraction at 12 km estimates.

As a proof of concept, I implemented a random forest regressor to predict the pristine environment cloud fraction using the same four years of CloudSat observations used throughout this work. I used the same environmental information as my inputs (EIS,  $RH_{700}$ ) along with the sea surface temperature and LWP. The random forest is trained with pristine environmental cloud fraction estimates and then forced to predict the cloud fraction for all aerosol conditions. Because it is trained using only pristine cloud fraction estimates, the predicted cloud fraction estimate should be close to the cloud fraction of that scene if aerosol was decreased to pristine conditions.

These initial results agree well in magnitude and sign with the results from Chapter 2. Further, they have proven to be robust to changes in the observational scale.

When the scale is upped to 48 or 96 km, the change remains constant at around a 5% global increase in cloud fraction due to aerosol loading. The next steps of this work are to incorporate the cloud, environment, and aerosol history trajectories as features in order to see how the interactions before a CloudSat overpass may be affecting the response.

# Appendix A

## Appendix of Information

Recreated here with permission of the journal of Atmospheric Chemistry and Physics.

Quantifying Variations in Shortwave Aerosol-Warm Cloud-Radiation Interactions Using Local Meteorology and Cloud State Constraints. Douglas, A., L'Ecuyer, T.S. 2019. Atmospheric Physics and Chemistry.

### **A.1 Abstract**

While many studies have tried to quantify the sign and the magnitude of the warm marine cloud response to aerosol loading, both remain uncertain owing to the multitude of factors that modulate microphysical and thermodynamic processes within the cloud. Constraining aerosol-cloud interactions using the local meteorology and cloud

liquid water may offer a way to account for covarying influences, potentially increasing our confidence in observational estimates of warm cloud indirect effects. Four years of collocated satellite observations from the NASA A-Train constellation, combined with reanalysis from MERRA-2, are used to partition marine warm clouds into regimes based on stability, the free atmospheric relative humidity, and liquid water path. Organizing the sizable number of satellite observations into regimes is shown to minimize the covariance between the environment or liquid water path and the indirect effect. Controlling for local meteorology and cloud state mitigates artificial signals and reveals substantial variance in both the sign and magnitude of the cloud radiative response, including regions where clouds become systematically darker with increased aerosol concentration in dry, unstable environments. A darkening effect is evident even under the most stringent of constraints. These results suggest it is not meaningful to report a single global sensitivity of cloud radiative effect to aerosol. To the contrary, we find the sensitivity can range from  $-.46$  to  $.11 \frac{\text{W m}^{-2}}{\ln(\text{AI})}$  regionally.

## A.2 Introduction

Warm clouds play an important role in Earth's radiative balance. Cooling the atmosphere and covering 25% of the Earth's surface on average and reflecting incoming shortwave radiation, any changes to their radiative properties should be well quantified and understood (Hahn and Warren, 2007b). These clouds are most prevalent off the western coasts of continents as marine stratocumulus, near the tropics as trade cumulus, and in the storm track regions as stratus (?). Perturbations in aerosol, whether

from natural sources like sea spray or anthropogenic activities like biomass burning, lead to cloud-aerosol interactions that alter cloud radiative properties through two main effects, the albedo and the cloud lifetime effects. First termed by Twomey in 1977, the albedo effect, or the first indirect effect as it's also known, suggests that clouds will become brighter as a result of aerosol loading. For a fixed liquid water path, increased aerosol within a cloud increases the number of cloud condensation nuclei (CCN), forcing the mean drop size to decrease, resulting in a brighter, more reflective cloud. The second indirect effect, or the cloud lifetime effect, proposed by Alrecht (1989) builds on this idea, noting that a decrease in mean drop size due to aerosol-cloud interactions may also delay the onset of collision coalescence, suppressing precipitation and, in turn, allowing the cloud to survive longer, grow larger, and ultimately reflect more shortwave radiation. Early estimates of the indirect effect estimated including the cloud lifetime effect may increase it by 1.25x (Penner et al., 2001). Work since then has concentrated on decreasing the range of uncertainty rather than separating the effects in observation based studies, as without explicit constraints in place on the cloud water, the two effects are intrinsically related through the liquid water content of the cloud (Mülmenstädt and Feingold, 2018).

However, observing the indirect effect is not as straight forward as looking out your window trying to spot brighter clouds. The magnitude and sign of the indirect effect is extremely sensitive to the method used to quantify it. As a result, the Intergovernmental Panel on Climate Change (IPCC) has low confidence in the current estimate

of the global aerosol indirect effect (AIE) (Boucher et al., 2013). An accurate assessment of the total indirect effect will reduce error in climate sensitivity and further our understanding of the role of clouds in future climates (Bony and Dufresne, 2005).

Historically, methods of estimating the AIE employ a single linear regression of either the cloud’s radiative effect or droplet radius against a proxy for aerosol concentration (Christensen et al., 2016, Platnick and Twomey, 1994, ?). This method ignores all possible covariances between the cloud, aerosol, and any processes that may affect both and assumes one linear regression captures all effects, disregarding the role played by the local environment as a strong modulator of warm cloud properties and responses (Stevens and Feingold, 2009b). Constraining the local meteorology, or the characteristics of the environment around the cloud, as well as cloud type can significantly alter the magnitude of the AIE compared to single, unconstrained global linear regression (?). Regional analyses, such as treating the marine stratocumulus cloud decks off the west coasts as a homogeneous sample, instead capture assorted responses and magnitudes as they fail to extricate covariance with local meteorology (?). Observationally-based estimates simply cannot “turn off” the effects of entrainment or other environmental effects like a model, therefore observation based approaches must prescribe a way to diminish the effect of these influences on cloud radiative effects, even at a regional scale.

Modeling provides one pathway for estimating the global AIE that explicitly accounts for local meteorological conditions, however low clouds are one of the largest sources

of error in current global climate models (GCM) (Williams and Webb, 2009). In particular, GCMs tend to overestimate liquid water path (LWP) in low clouds, which leads to an overestimation of the albedo (Nam et al., 2012). The artificially elevated LWP impacts the sensitivity to aerosol by assessing it under unrealistic conditions. Further, entrainment and precipitation are artificially dampened as a result of incorrect cloud parameterizations in GCMs (Tsushima et al., 2016, ?). Many cloud-aerosol processes are explicitly resolved in large eddy simulation (LES) models, but these are limited to small scales. LES can prescribe exact environments, but again these are limited to idealized meteorologies, only realistic to small regions on Earth. The microphysical processes of aerosol activation, nucleation, and eventual raindrop formation can only be parameterized in current GCMs and will remain so for the foreseeable future. The resolution is too coarse to emulate all scales of aerosol-cloud interactions hence the dependence on parameterizations and large uncertainty in model-derived estimates (Wood et al., 2016). A solution to this problem is a combination of global climate modeling guided by observation-based analysis and coordinated LES modeling to understand and quantify the AIE (Stephens, 2005).

Observation-based methods must avoid the pitfalls of historical evaluations and define a clear methodology to limit covariance with local environmental conditions or buffering by the cloud. Buffering is when the cloud state and/or environment work to reduce the impact of aerosols on the cloud Stevens and Feingold (2009b). Cloud characteristics, such as LWP, and the local meteorology, like stability, can compound

uncertainty in evaluating the AIE because they influence both radiative properties and susceptibility to aerosol (??). The AIE is specifically defined as the cloud response to aerosol and the resulting effects on the radiative properties. Any quantification of the AIE must avoid including the effects of the local environment on the cloud radiative properties. When the local meteorology was accounted for, Gryspeerdt et al. (2016) found the sensitivity of cloud fraction to aerosol loading was reduced by 80%. Quantifying the AIE therefore requires separating and constraining all processes that moderate cloud radiative properties from those specifically due to aerosol-cloud radiation interactions (Stevens and Feingold, 2009b). Organizing clouds into constrained, bounded spaces based on the external and internal covarying conditions can improve aerosol-cloud-radiation impact estimates (Ghan et al., 2016).

This study examines the sensitivity of the shortwave radiative forcing of warm clouds to aerosol by employing a methodology that attempts to adequately constrain external influences while maintaining sufficiently robust statistics. Our methodology takes advantage of the vast sampling provided by satellites to systematically hold environmental conditions and cloud state approximately constant. We quantify the warm cloud sensitivity to aerosol for clouds of similar properties within similar environments. While most satellite studies of aerosol-cloud interactions are by necessity correlative, the more covarying factors that are controlled (at the individual cloud level), the more closely we can approximate a causal relationship. Although we cannot confirm causation due to the temporal resolution of the observations, some studies

have begun utilizing the high temporal resolution of geostationary satellites to augment A-Train observations and fix this ongoing problem (?). In our study, a set of environmental conditions and cloud state parameters is referred to as a regime. This idea of stratifying observations into regimes has been successfully implemented before to analyze cloud processes (Chen et al., 2014, Gryspeerdt and Stier, 2012, Oreopoulos et al., 2016, Williams and Webb, 2009).

The environmental and cloud state regimes adapted here are designed to homogenize the clouds and processes occurring, reducing covariance the cloud radiative response to aerosol and other influences. Observationally-based, regime-dependent cloud processes have been discerned most often over large regional scales, however, divergent signals can be lost depending on the size of the region analyzed (Grandey and Stier, 2010). Even on small, local scales, variance in the meteorology alters the strength of the observed effects (Liu et al., 2016). A study using satellite observations with regime constraints, for example, found a definite relationship between the warm cloud AIE varies and atmospheric stability on a global scale (Chen et al., 2014).

One important meteorological influence is the stability of the boundary layer. LES of warm clouds have further shown that environmental instability can alter the effects of aerosol loading on warm clouds (Lee et al., 2012). The need to incorporate stability into AIE estimates has also been noted in prior observational studies (L'Ecuyer et al., 2009, Sorooshian et al., 2009, Su et al., 2010). Warm clouds in stable environments

may show an increasing LWP with respect to aerosol loading while unstable environments may exhibit a decrease in LWP (Chen et al., 2014). Su et al. (2010) found the stability and rate of subsidence work to modulate aerosol-cloud-radiation interactions in warm clouds.

The effects of large scale subsidence and entrainment can be captured by the relative humidity ( $RH_{700}$ ) in the free atmosphere, known to exert a powerful influence on warm cloud characteristics (Wood and Bretherton, 2004). Entrainment of free atmospheric air furthers the decoupling process by increasing the temperature and humidity gradients at the cloud top (?). Including  $RH_{700}$  in aerosol sensitivity studies accounts for some decoupling influence. Models affirm the effects of entrainment on the cloud layer depend in part on  $RH_{700}$ , as LES have shown RH differences moderates cloud feedbacks in low warm cloud simulations (Van der Dussen et al., 2015). De Roode et al. (2014) showed that  $RH_{700}$  plays a significant role in modulating the liquid water path, which could then modulate the strength of any aerosol-cloud interactions. This modulation is likely due to the entrainment of dry air from the free atmosphere which alters the distribution of liquid water within a cloud (Ackerman et al., 2004, Bretherton et al., 2007).

In his original work, Twomey postulated that cloud albedo ought to increase with aerosol provided LWP is held fixed, after all, albedo is dependent on the optical depth and effective radius. The LWP has been shown to clearly control the second AIE via its influence on precipitation suppression (L'Ecuyer et al., 2009, Sorooshian et al.,

2009). Field campaign observations have noted this relationship as well. For example, the Atmospheric Radiation Measurement Mobile Facility Azores campaign found the cloud radiative response depended largely on the LWP (Liu et al., 2016). LWP is intrinsically tied to the magnitude of the AIE. Failing to distinguish clouds by LWP will lead to large covariance and/or buffering in the system by the LWP.

For these reasons, we adopt the boundary layer stability and relative humidity of the free atmosphere in conjunction with LWP to segment observations into regimes at the individual satellite pixel scale. To illustrate the impact of these specific buffering factors, we sequentially increase constraints on the regression of the warm cloud radiative effect against aerosol, what we refer to as the sensitivity or  $\lambda$ . First, the sensitivity is constrained by only LWP to demonstrate the importance of accounting for cloud state alone when estimating aerosol response. Next, environmental regimes of stability and relative humidity are used to segment warm clouds and, within each regime, the sensitivity of the cloud radiative effect to aerosol is assessed. These environmentally regimented observations are then further separated into LWP regimes to control for cloud state and environment simultaneously. Finally, the warm cloud sensitivity with all regime constraints is derived on a regional basis to account for local influences not captured by the global regime partitions.

## **A.3 Methods**

### **A.3.1 Data**

The effect of aerosol on marine warm cloud shortwave radiative properties is diagnosed from observations collected by the NASA A-Train constellation from 2007 to 2010. The A-Train is a series of synchronized satellites which allow for collocated observations from a variety of instruments (L'Ecuyer and Jiang, 2011). Environmental information is provided by collocated reanalysis data from the Modern-Era Retrospective analysis for Research and Applications Version 2 (MERRA-2). Collocated observations from multiple instruments, combined with high resolution reanalysis at the pixel scale, allows an extensive view of the roles the environment and cloud state play in modulating the warm cloud sensitivity to aerosol concentration.

### **A.3.2 Cloud**

The Cloud Profiling Radar (CPR) on CloudSat and the Cloud-Aerosol Lidar and Infrared Pathfinder Satellite (CALIPSO) are used to restrict analysis to single-layer, marine warm clouds between  $60^\circ$  N and  $60^\circ$  S. All data is interpolated down to CloudSat's  $\sim 1$ km footprint. The CloudSat 2B-CldClass-Lidar product that classifies cloudy pixels based on their vertical structure from merged radar and lidar observations is leveraged to filter out ice phase and multilayered cloud systems (Sassen et al., 2008, ?). All observations are restricted to below the freezing level of CloudSat which is determined using an ECWMF-AUX collocated reanalysis dataset and set where ECWMF

determines the  $0^\circ$  isotherm. The Advanced Microwave Scanning Radiometer - Earth Observing System (AMSR-E) liquid water path (LWP) aboard the Aqua satellite is then used to limit observations to scenes where the LWP is above  $.02 \frac{\text{kg}}{\text{m}^2}$  and below  $.4 \frac{\text{kg}}{\text{m}^2}$  (Wentz and Meissner, 2007). Very thin clouds below  $.02 \frac{\text{kg}}{\text{m}^2}$  are likely thin veil clouds with low albedos that are not the focus of this analysis (?). An along-satellite track cloud fraction is determined by finding the average number of warm cloud pixels that satisfy these criteria (seen by CloudSat or CALIPSO, below the CloudSat determined freezing level, and LWP between  $.02$  and  $.4 \frac{\text{kg}}{\text{m}^2}$ ) over each 12 km segment of the CloudSat track on a pixel by pixel basis, a scale that represents both the local scale length of the boundary layer and field-of-view used to define cloud radiative effects from Clouds and the Earth's Radiant Energy System (CERES) (?). Marine warm clouds fitting these parameters reside within the boundary layer. Even with these initial constraints on LWP and height, there were 1.8 million satellite observations fitting these parameters within the time period.

The warm cloud shortwave radiative effect is found by combining this along track warm cloud fraction with top of atmosphere (TOA) radiative fluxes from CERES. CERES has a total ( $.4 - 200 \mu\text{m}$ ) and shortwave channel ( $0.4 - 4.5 \mu\text{m}$ ) that allow outgoing shortwave and longwave fluxes at the top of the atmosphere to be estimated using appropriate bi-directional reflectance models. All-sky radiances from CERES are not restricted to any type of scene and include the raw radiances observed by CERES. The shortwave warm cloud radiative effect (CRE) is then defined in terms

of the all sky and inferred clear sky forcings from CERES and warm cloud fraction from CloudSat. The clear sky flux ( $F_{\text{Clear Sky}}^{\uparrow}$ ) is a regional, monthly mean estimate of cloud free outgoing shortwave radiation. Writing the all-sky net SW radiation at the top of the atmosphere as:

$$(F_{\text{SW}}^{\downarrow} - F_{\text{SW}}^{\uparrow})_{\text{All Sky}} = (F_{\text{SW}}^{\downarrow} - F_{\text{SW}}^{\uparrow})_{\text{Clear Sky}} \times (1 - \text{CF}) + (F_{\text{SW}}^{\downarrow} - F_{\text{SW}}^{\uparrow})_{\text{Cloudy}} \times \text{CF} \quad (\text{A.1})$$

It is easy to show that for shortwave radiances:

$$F_{\text{All Sky}}^{\uparrow} - F_{\text{Clear Sky}}^{\uparrow} \times (1 - \text{CF}) = \text{CRE} \quad (\text{A.2})$$

where the warm  $\text{CRE}_{\text{SW}} = \text{CF} \times F_{\text{Cloudy}}^{\uparrow}$

The instantaneous CRE for each warm cloud observation is used in conjunction with aerosol information and corresponding instantaneous cloud state and meteorological state constraints to derive the sensitivity of the cloud radiative effect to aerosol loading.

### A.3.3 Aerosol

Aerosol index (AI) is used to characterize the concentration of aerosol in the atmosphere. AI is the product of the Angstrom exponent (found using AOD at 550 and 870 nm) and AOD at 550 nm, both of which are derived from the Moderate-Resolution Imaging Spectroradiometer (MODIS) aboard the Aqua satellite. The Angstrom exponent, a measure of the turbidity of the atmosphere, is derived from multiple estimates of aerosol optical depth (AOD) (Ångström, 1929, ?). The MODIS Angstrom exponent provides information about the size of the observed aerosol as well as concentration (Levy et al., 2010). MODIS AI is derived from the auxiliary dataset (MOD06-1km-AUX) developed from the overlap of the CloudSat CPR footprint and the MODIS cloud mask at pixel level. Although AI is not a direct measurement of CCN in the air, it has a higher correlation with CCN compared to the AOD and is therefore more suitable for aerosol-cloud interaction studies (Dagan et al., 2017, Stier, 2016). While AOD and the Angstrom exponent from MODIS are not available in cloud scenes, the collocated dataset interpolates these between clear sky scenes in order to infer a cloudy AI. For lower cloud fraction scenes, this interpolation is more accurate, however it is possible that in higher cloud fraction scenes, the accuracy of AI is reduced. This is a source of uncertainty within our results. AI can be affected by aerosol swelling in the most humid environments. All results have some amount of uncertainty due to this effect (?). This is minimized in the driest  $RH_{700}$  regimes, however the most humid  $RH_{700}$  regimes may be affected by aerosol swelling. The effect will be largest in the

cloudiest regions such as the marine stratocumulus decks in the South Atlantic, Southeast Pacific, and off the California coast because aerosol measurements near clouds (15 km) are subjected to the largest amount of swelling (Christensen et al., 2017). It has been suggested using AI underestimates the strength of the indirect effect; our estimates of sensitivity of the warm cloud radiative effect to aerosol could be thought of a lower bound on the warm cloud indirect effect sensitivity (Penner et al., 2011). Another source of uncertainty is that the aerosol may not be located at the same height as the warm, boundary layer clouds we are evaluating. Aerosol should ideally be located near the cloud base in order to be fully activated and initiate the indirect effect (?).

### **A.3.4 Regimes**

#### **A.3.4.1 Environmental Regimes**

MERRA-2 reanalyses collocated with each CloudSat footprint is used to define local thermodynamic conditions that distinguish environmental regimes. The environmental regimes employed here provide a crude representation of the local meteorology acting to inhibit or invigorate the cloud response. While these states, defined from percentile bins of the estimated inversion strength (EIS) and relative humidity at 700 mb ( $RH_{700}$ ), do not capture the complete range of environmental factors that influence warm cloud development, they have been shown to provide fairly robust bulk classification for sorting satellite observations into meteorological regimes (Chen et al.,

2014, L'Ecuyer et al., 2009, Sorooshian et al., 2009). Here, EIS is calculated using MERRA-2 temperature and relative humidity profiles and indicates the stability of the boundary layer. EIS incorporates effects of water vapor on the lower tropospheric static stability and is better correlated for all cloud types with cloud fraction.

From Wood and Bretheron (2006):

$$\text{EIS} = \text{LTS} - \Gamma_m^{850}(z_{700} - \text{LCL}) \quad (\text{A.3})$$

where  $\Gamma_m^{850}$  is the moist-adiabatic potential temperature gradient and LTS is the lower-tropospheric stability.

The relative humidity at 700 mb is used as a measure of the effect of entraining free tropospheric air (?). As the height of the 700 mb isobar is included in the equation for EIS, there is some covariability between EIS and  $\text{RH}_{700}$ . Some processes involved in altering the height at 700 mb will also affect  $\text{RH}_{700}$  and vice versa, therefore there is some covariability between our two meteorological variables. When referring to the effects of entrainment, it means the effects of  $\text{RH}_{700}$ . All observations within the 5% - 95% percentiles of both EIS and  $\text{RH}_{700}$  are partitioned into regimes of percentile limits. The bin limits depend on the number of bins implemented, which is varied in the results to establish the degree to which the environment must be constrained to accurately characterize sensitivity. For example, with 100 environmental regimes, the observations will be binned from by 10 percentile limits of both EIS and  $\text{RH}_{700}$ .

Within each row of  $RH_{700}$  of the environmental regimes, there are the same number of observations as within each column of EIS, however, within each individual environmental regime of both EIS and  $RH_{700}$ , the number of observations is dependent on the distribution of both EIS and  $RH_{700}$ .

### **A.3.4.2 Cloud States**

Cloud states are defined by the LWP. Although there are other definitions of cloud regimes and cloud states used in other studies (e.g. ?), throughout ours cloud state or cloud morphology refers to the set of observations binned by liquid water path. Environmental stability and entrainment directly affect the LWP so these parameters are not independent. In what follows, however, we consider the LWP separately from the local meteorology to separately evaluate two aspects of the indirect effect formulation. Since Twomey’s original hypothesis of the aerosol indirect effect was based on holding LWP constant, we first examine the impact of increasing stringent constraints on LWP. Constraining LWP diminishes the effects of aerosol on cloud LWP itself allowing the sensitivity of the warm cloud CRE to aerosol to be isolated (Gryspeerd et al., 2019b). More recently, numerous others have extensively demonstrated that aerosol indirect effects can be buffered by other environmental conditions. Since EIS and RH have been frequently adopted as proxies for these buffering effects, we further examine the impact of increasingly stringent constraints on these environmental characteristics. Our separation of ‘cloud regimes’ and ‘meteorological regimes’ is made

only to contrast the magnitudes of their effects and does not imply that LWP is independent of EIS or RH. Ultimately it will be shown that all three factors must be accounted together to adequately constraint the warm cloud radiative sensitivity to aerosol. LWP responds the humidity of the free atmosphere and the inversion strength (De Roode et al., 2014). It has been shown that the free atmospheric relative humidity can increase the sedimentation rate at the top of the cloud, altering the distribution of liquid throughout the cloud’s vertical profile (Ackerman et al., 2004). Final results have constraints on LWP, EIS, and  $RH_{700}$  to account for relationships between meteorology and LWP. For the sake of clarity, we consider the LWP separately from  $RH_{700}$  and EIS, however we acknowledge that LWP is directly affected by the meteorology of the boundary layer. LWP is intrinsic to the second indirect effect, where aerosol acts to suppress precipitation and enhance the cloud lifetime, however quantifying exactly how LWP responds to aerosol has remained up for debate.

AMSR-E liquid water path, derived from the 19, 23, and 37 GHz channels, is used to separate observations into cloud state regimes (Wentz and Meissner, 2007). AMSR-E LWP is most accurate for low, marine warm clouds (Juárez et al., 2009, ?). 99% of observations fell below a LWP of  $.4 \frac{\text{kg}}{\text{m}^2}$  and analysis was restricted to observations with LWP below this limit. Since CRE is proportional to the optical depth of a cloud, which is directly related to the LWP, the sensitivity has a strong covariance with LWP (Wood, 2012, ?, ?). Holding LWP effectively constant is therefore essential to estimating the AIE (?). The number of LWP bins decreases from global to regional

analysis due to sampling; on a global scale, seven LWP regimes are used, while on a regional scale, only four LWP regimes are used. Limits are placed to separate out the signals of low LWP clouds vs. high LWP clouds, as low clouds may be affected by evaporation-entrainment feedbacks while high LWP clouds may be affected by precipitation (Jiang et al., 2006, L'Ecuyer et al., 2009). While the environmental regimes are established on a percentile basis, cloud state regimes are set by having an increased number of bins for the lowest LWP clouds and a bin limit always set at  $.15 \frac{kg}{m^2}$  to delineate clouds which are extremely unlikely to precipitate ( $< .15 \frac{kg}{m^2}$ ) and clouds more likely to precipitate ( $> .15 \frac{kg}{m^2}$ ) (L'Ecuyer et al., 2009). When environmental regimes are combined with cloud state constraints, the environmental regime limits remain constant throughout all cloud state regimes. The difference in the sensitivity of the warm cloud radiative effect to aerosol in one environmental regime versus another environmental regime at a constant LWP can therefore be more accurately attributed to aerosol.

### **A.3.5 Sensitivity**

The warm cloud radiative sensitivity to aerosol, or  $\lambda$ , is defined as the linear regression of the shortwave CRE against  $\ln(AI)$ . While other studies have called similar metrics a susceptibility, we use the term sensitivity. The natural log of AI is used to better represent the effects of the smallest particles, which are more likely to act as CCN within a cloud (?). The sensitivity is evaluated within environmental and cloud state regime frameworks on both global and regional scales. The observations are binned by

15 percentile bins of  $\ln(\text{AI})$ . The AI bins are defined by the set of observations being regressed. The sensitivity is only calculated if there are 100 observations within the regime to ensure an adequate number of observations to regress against, and the linear regression Pearson correlation coefficient is greater than .4 to ensure the slope is a good fit within each regime. Throughout the study, although environmental and cloud state impacts are constrained through regimes, it cannot be stated with certainty that the observed changes in CRE are due to aerosol, only correlated with aerosol.

The unconstrained sensitivity, or the sensitivity of the warm cloud shortwave radiative effect to  $\ln(\text{AI})$  without limits on region, LWP, stability, or  $\text{RH}_{700}$ , is computed as:

$$\lambda_0 = -\frac{\partial \text{CRE}}{\partial \ln(\text{AI})} \quad (\text{A.4})$$

The partial derivative in this equation implies influencing factors other than aerosols should be held fixed. Here this is accomplished by evaluating the sensitivity with increasing constraints on the partial differential through regimes.

To hold the cloud state fixed, the sensitivity is found for seven distinct LWP regimes (k) and summed to yield a mean sensitivity:

$$\lambda_{LWP} = \sum_{k=1}^{N_{LWP}} \left( - \frac{\partial \text{CRE}}{\partial \ln(\text{AI})} \right)_k W_k \quad (\text{A.5})$$

Where  $W_k$  is fraction of observations in cloud state  $k$ :

$$W_k = \frac{\text{Number in Cloud State } k}{\text{Total Number}} \quad (\text{A.6})$$

In our results, we evaluate the efficacy of increasing and decreasing the number of cloud states.

Similarly, the sensitivity within environmental regimes, defined by the estimated inversion strength and relative humidity of the free atmosphere, can be computed, weighted, and summed to account for meteorological covariability with ten regimes of each EIS ( $i$ ) and  $\text{RH}_{700}$  ( $j$ ), where  $W_{i,j}$  is the weighting factor for each environmental regime:

$$\lambda_{ENV} = \sum_{j=1}^{N_{RH}} \sum_{i=1}^{N_{EIS}} \left( - \frac{\partial \text{CRE}}{\partial \ln(\text{AI})} \right)_{i,j} W_{i,j} \quad (\text{A.7})$$

Where  $W_{i,j}$  is the fraction of observations in environmental regime  $i,j$ :

$$W_{i,j} = \frac{\text{Number in Environmental Regime } i,j}{\text{Total Number}} \quad (\text{A.8})$$

By extension, both cloud and environmental conditions can be controlled via:

$$\lambda_{BOTH} = \sum_{k=1}^{N_{LWP}} \sum_{j=1}^{N_{RH}} \sum_{i=1}^{N_{EIS}} \left( -\frac{\partial \text{CRE}}{\partial \ln(\text{AI})} \right)_{i,j,k} W_{i,j,k} \quad (\text{A.9})$$

Where  $W_{i,j,k}$  is fraction of observations in both cloud state  $k$  and environmental regime  $i,j$ :

$$W_{i,j,k} = \frac{\text{Number in Environmental Regime } i,j \text{ and Cloud State } k}{\text{Total Number}} \quad (\text{A.10})$$

Finally, it is recognized that these bulk constraints do not fully capture all of the local factors that influence aerosol-cloud interactions. AI alone does not fully constrain the effect of aerosol composition which varies regionally. Thus, to control for these

unaccounted for local effects, the sensitivity is further constrained by finding Eqn (A.9) on a  $15^\circ$  by  $15^\circ$  scale with four cloud state regimes (k), five regimes of stability (i), and five regimes of  $\text{RH}_{700}$  (j) for each of the 152 regions (l).

$$\lambda_{ALL} = \sum_{l=1}^{N_{\text{Reg}}} \sum_{k=1}^{N_{\text{LWP}}} \sum_{j=1}^{N_{\text{RH}}} \sum_{i=1}^{N_{\text{EIS}}} \left( -\frac{\partial \text{CRE}}{\partial \ln(\text{AI})} \right)_{i,j,k,l} W_{i,j,k,l} \quad (\text{A.11})$$

Where  $W_{i,j,k,l}$  is fraction of observations in region l in both cloud state k and environmental regime i,j.

## A.4 Results

### A.4.1 Unconstrained Sensitivity

The global sensitivity of warm cloud SW forcing to aerosol without any constraints described by Equation (A.4) is  $-12.81 \frac{\text{W m}^{-2}}{\ln(\text{AI})}$  (Figure A.1). This seems to capture the warm cloud AIE, after all the shortwave CRE increases with aerosol loading as expected. However, this unconstrained estimate ignores the roles of buffering and covariance. The indicated variation of SW CRE within each  $\ln(\text{AI})$  bin alludes to variation in the overall effect not captured by a single linear regression. Although the  $R^2$  is high, without constraints the increase in shortwave CRE cannot be attributed to only aerosol. Furthermore, from this estimate, no information is made known on

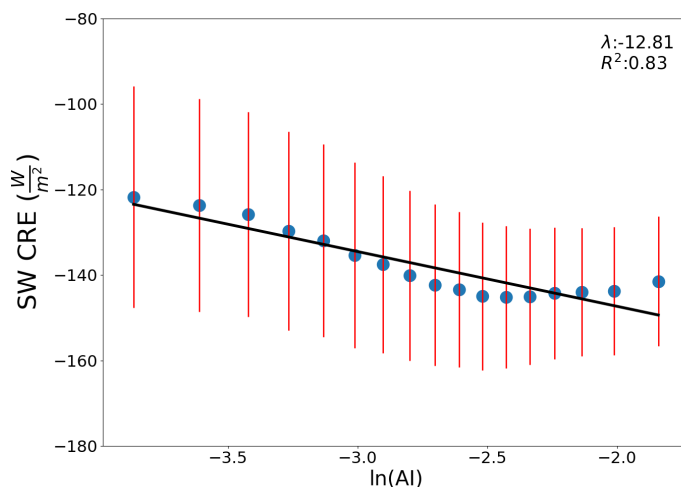


FIGURE A.1: The sensitivity of CRE to aerosol ( $\lambda_0$  from equation (A.4)) found globally from the mean SW CRE for each  $\ln(\text{AI})$  bin (blue dots) without constraints on the environment, cloud state, or region. The red lines represent the standard deviation within each bin of  $\ln(\text{AI})$ .

how the sensitivity varies regionally, how cloud processes affect the AIE, or whether particular cloud states may be influenced more strongly by aerosol than others.

#### A.4.2 Sensitivity to Cloud State

The original description of the albedo effect by Twomey (1977) specified holding the LWP of the cloud constant. Following Twomey's original hypothesis, when warm clouds are separated by LWP into cloud states, it is clear that cloud morphology plays a role in modulating the magnitude of the sensitivity (Figure A.5). The total weighted, summed sensitivity is  $-13.12 \frac{\text{W m}^{-2}}{\ln(\text{AI})}$  for seven cloud states. From Figure A.5, the lowest cloud states are less sensitive to aerosol, with a steep increase at  $\sim 0.8 \frac{\text{kg}}{\text{m}^2}$ . The sensitivity increases with LWP, peaking for LWPs between .1 and .15  $\frac{\text{kg}}{\text{m}^2}$ . Beyond .15  $\frac{\text{kg}}{\text{m}^2}$ , the trend reverses and the sensitivity decreases with LWP, consistent with the fact that

thicker clouds are already bright and less susceptible to aerosol-induced changes (Fan et al., 2016). The non-linear relationship along with the known covariance between LWP and the AIE make it a vital component of the regime framework proposed here (Feingold, 2003). Constraints on LWP limit these influences (Feingold, 2003).

The key to implementing appropriately stringent regime constraints is to determine the minimum number of cloud states required to adequately capture LWP modulation of the total sensitivity. We will be using seven cloud states throughout our global analysis as it appears to capture the impact cloud state exerts on the sensitivity while permitting ample sampling for further division of observations throughout environmental regimes. The number of cloud states are steadily increased from 3 to 7 to 11 to 23 partitions to follow a progressive increase in the number of bin limits from 4 to 8 to 12 to 24 limits, respectively. Overall,  $\lambda_{LWP}$  exhibits a similar trend regardless of partitioning. The peak sensitivity for all cloud states is around  $.1 \frac{kg}{m^2}$ . The curve of the sensitivity and the behavior of thicker clouds is not well captured using only 3 LWP bins. The use of 7 cloud states, on the other hand, reproduces the behavior of thicker clouds and guarantees a large number of samples within each cloud state appropriate for a linear regression, especially when later partitioning by additional influences.

### **A.4.3 Sensitivity within Environmental Regimes**

Even when separated into cloud states, aerosol impacts on warm clouds can be strongly modulated by the local environment. To account for the local meteorology, warm

clouds are separated into 100 environmental regimes defined according to the local stability and free tropospheric humidity at the time they were observed (Figure A.9). This approach is similar to that employed by Chen et al. (2014). Within each EIS and  $RH_{700}$  regime, CERES shortwave CRE is linearly regressed against  $\ln(AI)$ . The processes and resulting response are modified by the local meteorology, indicated by the change in sensitivity for different environmental regimes. Unstable environments exhibit almost no variation in sensitivity, varying by only  $\sim 1 \frac{W m^{-2}}{\ln(AI)}$ , while stable regimes can vary by  $\sim 10 \left( \frac{W m^{-2}}{\ln(AI)} \right)$ . The moisture content of free atmosphere influences the sensitivities in stable regimes more than unstable regimes with a clear divide at  $EIS = 1$  K. The highest sensitivity is observed in stable regimes ( $EIS > 5.0K$ ) with a moderately dry free atmosphere (Figure A.9). The most sensitive warm clouds reside in environments with a moderately dry relative humidity of around 27% for an extended range of stabilities from 5 to 10 K. Warming effects (positive sensitivities) are observed in unstable, dry environments. A warming, or reverse Twomey, effect has been noted to occur by others investigating the AIE (Chen et al., 2012, 2014). Consistent with these results, Christensen and Stephens (2011) found that up to 1/3 of ship-tracks, occurring in primarily unstable regions, are darker than their surroundings owing to their thermodynamic feedbacks. The weighted global sensitivity calculated using Equation (A.7) is  $-11 \frac{W m^{-2}}{\ln(AI)}$  when the influence of the environment is accounted for (Figure A.9).

The number of partitions must be narrow enough to separate the various degrees of

buffering by the local meteorology and yet allow an ample number of observations per environmental regime when calculating the constrained sensitivities. To determine an optimal resolution for this dataset, the distribution of observations and sensitivity are separated into 5, 10, and 15 EIS and RH<sub>700</sub> partitions representing 25, 100, and 225 environmental states respectively (Figures A.13, A.17). The distribution of observations among environmental regimes varies smoothly with resolution (Figure A.17). The minimum number of samples decreases from 35,532 to 2,707 to 757 when the resolution increases from 25 regimes to 100 regimes to 225 regimes, respectively. The mirror pattern is likely the result of the EIS in part having a slight dependence on RH<sub>700</sub>, as the RH<sub>700</sub> can alter the height of the 700 mb level needed to calculate EIS. This does not impact results as this dependence is accounted for by environmental regimes. The moistest, most unstable and the driest, stablest environmental regimes always have the largest number of observations. Moist, unstable regimes are likely comprised of trade cumulus or other pre-convective cloud types in regions like the ITCZ. Dry, stable regimes are likely comprised of marine stratocumulus cloud decks off the west coast of continents.

The total sensitivity decreases as the resolution increases, from -11.29 to -11.04 to  $-10.99 \frac{Wm^{-2}}{\ln(AI)}$  (Figure A.13). The 5 by 5 framework degrades the smoothness in  $\lambda_{ENV}$  with respect to the different environmental states. The difference between the 10 by 10 and 15 by 15 estimates of sensitivity indicate that an increase in resolution after 10 partitions will lead to very little change in the overall sensitivity. However,

an increased resolution decreases the number of clouds in all environmental regimes, which will be vital when the environmental regimes are further distributed among cloud states. The use of 100 regimes in analysis is appropriate to ensure proper distribution among all cloud states.

#### **A.4.4 Accounting for Cloud and Environmental States**

The preceding sections clearly demonstrate the importance of controlling for meteorological and cloud state dependencies when evaluating the sensitivity of cloud radiative effects to aerosol, however it is time to revise our framework to include both sets of constraints. Here we define three-dimensional regimes that hold LWP approximately constant while also constraining the local meteorology (Figure A.18). The sensitivities estimated for each of the 700 resulting regimes are shown in Figure A.18. The lowest LWP cloud states show a comparatively damped maximum sensitivity than the thicker cloud states. Higher LWP clouds exhibit an increasing maximum  $\lambda_{BOTH}$ . The variation in magnitude between cloud states within the same environmental regimes confirms that LWP exerts a strong control in modulating the magnitude of the response and must be held constant when estimating the AIE. Mixing different cloud states in Figure A.9 likely conflates differing signals, inaccurately representing the sensitivity in the most populous environmental regimes.

Again, the constrained sensitivities show distinct evidence of a darkening effect where thin clouds in the driest, most unstable environments exhibit a warming, or darkening,

response to aerosol loading. Within the environmental regimes that exhibit a darkening effect, the magnitude is strongly modulated by LWP, suggesting both the expected (cooling) and opposite (warming) responses depend on LWP,  $RH_{700}$ , and EIS. As LWP increases, a warming  $\lambda_{BOTH}$  favors increasingly moist, stable environments.

The summed and weighted sensitivity with constraints on both LWP and meteorology is  $-10.6 \frac{Wm^{-2}}{\ln(AI)}$ . Overall, the largest sensitivity is seen in stable, moderately dry environments (Figure A.18h). These environments are  $\sim 7K$  of stability and  $\sim 30\%$   $RH_{700}$  independent of LWP. Their large sensitivity is due in part to their prominence, as most marine stratocumulus cloud decks occur in stable environments with a dry free troposphere. The weakest sensitivity occurs in unstable, dry regimes and stable, moist regimes. While these environmental conditions and cloud states are less common, discerning global warming signal with stringent constraints is significant.

These results also suggest that AIE is overestimated in approaches that do not hold the LWP approximately constant. When summed and weighted by frequency of occurrence, over almost all environmental regimes, constraining LWP damps the sensitivity (Figure A.18). The difference between the LWP constrained and only environmentally constrained sensitivities reveals the strong dependence of cloud response on stability,  $RH_{700}$ , and LWP. In very few unstable environments, LWP constraints act to amplify the response. This effect is only observed in the the most moist and unstable or dry, stable states that have a high density of observations. LWP constrains in these regimes pulls out otherwise obstructed or buffered signals.

To assess the effect of the resolution used to define environmental states when LWP constraints are added Figure A.18h is replicated using 25, 100, and 225 environmental states (Figure A.22). Sensitivity estimates are less varied (relative to Figure A.9) when both the local meteorology and LWP are constrained, indicating that holding LWP fixed is essential regardless of the number of partitions of EIS and RH<sub>700</sub>. The inclusion of LWP, however, places increasingly restrictive demands on sampling volumes since each environmental regime must be sufficiently populated enough to allow robust sensitivities to be derived within a majority of cloud state partitions.

#### A.4.5 Sensitivity on Regional Scales

None of the results presented thus far have considered regional scale variability. To account for local processes and systematic differences in aerosol (e.g. composition, size, source) not captured by the bulk, global metrics above, the cloud state and environmental regime framework is applied to 15° grid boxes from 60°S to 60°N. Regional variations in cloud sensitivity with a varying number of constraints on local meteorology and cloud state are shown in Figures A.26 and A.27. In the absence of constraints (Figure A.26 top), the sensitivity exhibits larger variations in magnitude and sign than when cloud, environmental, or cloud and environmental constraints are in place (panels b and c and Figure A.27). The unconstrained map (Figure A.26 a) varies from  $-.53$  to  $.77 \frac{\text{W m}^{-2}}{\ln(\text{AI})}$  compared the most constrained map where the sensitivity of warm cloud CRE to aerosol varies only from  $-.11$  to  $.46 \frac{\text{W m}^{-2}}{\ln(\text{AI})}$ . In fact, without controlling for covarying influences of stability, entrainment, and cloud morphology,

vast regions of predominantly trade cumulus clouds exhibit a darkening that reduce the globally integrated warm cloud AIE.

With constraints on only cloud state, the sensitivity shows greater variation in magnitude and sign than any other case (A.26 b). The tropics show an extreme darkening signal, much greater than the unconstrained case. The darkening likely occurs in the lowest, thinnest cloud state regimes and may be due to evaporation. The maximum cooling sensitivity occurs in the southern oceans at a much larger magnitude than the unconstrained case. These signals are likely inflated since covarying meteorological factors are not fully constrained. While limiting the effects of cloud morphology on buffering and covariance is necessary, it is not sufficient for accurately resolving global AIE.

When constrained by local meteorological conditions alone (Figure A.26 c), the sensitivity is damped in all regions. The southern ocean no longer dominates the global AIE, instead the maximum effect is seen in the north Atlantic. The warming sensitivities, or darkening, that were prevalent in the equatorial region are significantly decreased, replaced by large regions of no sensitivity. Clouds can be distributed among different LWP regimes, with differing sensitivities, that cumulatively cancel each other out even in similar environmental conditions. The environmental framework only controls for meteorological covariability, but cloud state plays a large role in modulating the sign and magnitude of effect.

The inclusion of cloud state through LWP into the regime framework is vital to adhere to the original theories of Twomey (1977) and Albrecht (1989). Both assumed the LWP to be held constant, however this cannot be true of observation based estimates of the AIE unless the LWP is explicitly limited to be approximately constant. As seen in Figure A.26b, limits on LWP alone are not stringent enough to elucidate the true AIE and tend to artificially enhance sensitivities. The buffering effects of the environment and local modulating factors must also be accounted for.

Including both cloud and environmental regimes limits the co-variance between aerosol, stability, cloud state, and entrainment on cloud radiative properties (Figure A.27). This likely captures the true regional variation in the response of CRE to aerosol more accurately than any of the other regional estimates. The areas of strongest and weakest sensitivities exhibit coherent patterns that tends to align with distinct cloud and aerosol types. The largest sensitivities are observed in the southern subtropical oceans. Warm clouds off the coast of California exhibit a larger sensitivity with minimal constraints, i.e. with only cloud state or environmental constraints. The equatorial region shows a slight warming to no effect. This is likely the region contributing to the darkening seen in the global regime framework for unstable, dry regions (Figure A.18 h). The resulting global weighted mean sensitivity derived from Eqn (A.11) is likely representative of the complete spectrum of global shortwave warm cloud responses to aerosol.

## A.5 Discussion

The sample regressions show in Figures A.1, A.5, and A.9 illustrate the ability of constraints to reduce the variance of the observations. These constraints translate into a range of global sensitivity estimates. As constraints are applied, the sensitivity decreases from -12.81 to -10.6 to  $-10.13 \frac{W_m^{-2}}{\ln(AI)}$ . The decrease in total sensitivity reveals the need to constrain LWP. Holding only cloud state constant can exacerbate the signal due to mixed meteorologies, but the first order dependence of CRE on LWP requires it to be held constant. When these are applied regionally, local signals are preserved allowing the closest to truth estimate of  $-10.13 \frac{W_m^{-2}}{\ln(AI)}$ . This estimate is only possible through the power of sampling provided by 1.8 million satellite observations partitioned among 700 regimes, or 15,200 when further partitioned on a regional basis to represent local scale processes.

In theory, partial derivatives, such as  $\frac{\partial CRE}{\partial \ln(AI)}$ , assumes other variables are held constant. The folly in treating warm clouds as only a function of aerosol is evident in Figure A.26, where regionally the sensitivity of the warm cloud CRE to aerosol changes with the constraints in place, even "homogeneous" marine stratocumulus cloud deck regions. Vast areas of darkening effects are substantially moderated when the local meteorology and LWP are explicitly considered (Chen et al., 2012). These regional reversals of sensitivity to aerosols demonstrate regime-specific responses on a regional basis. LWP in particular may play a large role in determining if a cloud brightens or darkens as a result of aerosol loading.

Partitioning by regime identifies environments and cloud states that buffer, amplify, or diminish cooling. Buffering can involve any number of meteorological processes that lead to an altered response (?). For example, the local meteorology, especially  $\text{RH}_{700}$ , can work to inhibit or invigorate the cloud's response to aerosol (Ackerman et al., 2004, Lu and Seinfeld, 2005). Instilling limits on  $\text{RH}_{700}$  should decrease any co-variance between the lifetime effect and  $\text{RH}_{700}$  that could arise due to entrainment's role in cloud breakup (Kubar et al., 2015). Entrainment of drier air will force evaporation, decreasing particle size, while entrainment of moister air could have no effect or a reverse effect, increasing the number of CCN within the cloud.

Unstable regimes may act as a buffer to cloud brightening, evident when global observations are partitioned by EIS and  $\text{RH}_{700}$  (Figure A.18h). Unstable regimes contain pre-convective clouds (Nishant and Sherwood, 2017). Shallow cumuli, a common pre-convective cloud type found in the equatorial trade regions, are not likely to undergo the same reaction to aerosol loading as stable warm clouds like marine stratocumulus. Unstable conditions lead to strong vertical mixing and a reduced aerosol sensitivity, as activation favors strong vertical mixing in a stable environment (Cheng et al., 2017). Turbulence and vertical velocity can alter the structure of a cloud, which is especially crucial in extremely thin clouds where a redistribution of liquid water may potentially increase the likelihood of evaporation. Instability may alter the evaporation-entrainment feedback of the cloud, resulting in little to no brightening of the cloud and a severely reduced sensitivity, the result of forced evaporation reducing particle

size. A reduced particle size would affect the lifetime of the cloud as well as the cloud albedo, reducing the sensitivity of the warm cloud radiative effect to aerosol loading as seen in our results for some unstable, dry regions (Jiang et al., 2006). The most unstable regimes in both Figures (A.13) and (A.18h) display the smallest sensitivities, which may be due to in-cloud turbulence decreasing the activation efficiency of the aerosol.

Without controls on the local meteorology, signals like those seen off the coast of South America, a large negative effect dominating the tropical region, may be due in part to the instability of the region and not truly reflect cloud sensitivity to aerosol loading (Figure A.26). In the equatorial Atlantic off the coast of Africa, the strong decrease in CRE with respect to aerosol may not be the result of aerosol loading but that of surface winds decreasing cloud cover (Tubul et al., 2015). Surface winds were not included in analysis because the dependence of the warm cloud radiative response to aerosols depends most on LWP,  $RH_{700}$ , and stability, with only some regions showing a dependence on surface winds in our initial analysis. In the tropics, the warming sensitivity may be meteorologically-driven by increased frequency of trade cumuli and pre-convective clouds as stability decreases. These positive, unconstrained sensitivities are damped with environmental regime constraints (Figure A.26b and A.26c), however, darkening regions still appear in the fully constrained map (Figure A.27), demonstrating that a substantial population of warm clouds display a true, aerosol driven darkening effect.

The role of cloud state constraints is to hold LWP approximately constant. The sensitivity to aerosol depends strongly on LWP, consistent with Wood (2012) and Ackerman et al. (2004). This relationship between LWP and aerosol-cloud-radiation interactions must be parameterized in models in order to constrain covarying effects and models must accurately simulate LWP in order to faithfully represent the cloud response (Quaas et al., 2009, Wang et al., 2011). Model parameterizations have improved the representation of warm cloud moisture fluxes, which strongly control low cloud variance, but confidence in any AIE estimates depend on cloud parameterizations continuing to improve (Guo et al., 2014).

The environmental and cloud state regimes work to limit the co-varying effects on sensitivity estimates. On both global and regional scales, the environmental constraints reveal regime-specific responses (Figures A.9, A.26) that allow the separation of conditions that lead to a buffered response that is especially evident in the tropical regions which undergo a sign change when meteorological constraints are in place (Figure A.26) (Mülmenstädt and Feingold, 2018). In the equatorial regions, controlling for the local meteorology (Figure A.26c) reduces both the sensitivity and reverse Twomey effect compared to both the unconstrained (Figure A.26a) and cloud state constrained (Figure A.26b) estimates. In regions that exhibit strong cloud darkening effects, a deepening boundary layer, with decreasing stability, decouple warm clouds like marine stratocumulus from the surface, fostering cloud break up, and in turn,

decreasing the cloud fraction and associated CRE of the scene. The negative sensitivities seen in the unconstrained top panel of Figure A.26 are likely a result of this process, which happens simultaneously with a reduced stability, and epitomize how a single linear regression of warm cloud CRE against  $\ln(\text{AI})$  can capture meteorological effects when unconstrained (?).

Although not explicitly controlled for, partitioning by LWP should also somewhat limit the effects of precipitation. Clouds with less than  $.15 \frac{\text{kg}}{\text{m}^2}$  rarely precipitate, therefore enforcing a LWP limit at  $.15 \frac{\text{kg}}{\text{m}^2}$  delineates possibly precipitating from non-precipitating clouds (L'Ecuyer et al., 2009). If precipitation does modulate aerosol-cloud interactions, the influence would only be observed in the highest LWP cloud state regimes. This is not to say precipitation is not important to aerosol-cloud interactions. In principle the regime framework presented here must be adapted to subset scenes according to the presence of precipitation, but that is not the focus of our study.

## A.6 Conclusions

Explicitly sorting satellite data by liquid water path, stability, and entrainment places increasingly stronger constraints on the partial derivative of CRE against  $\ln(\text{AI})$ . This is shown to limit covariance between aerosol-cloud-radiation interactions and the environment and cloud state. In the absence of such constraints, buffering or modulation of the response by local meteorology obfuscates estimates of the AIE

(Stevens, 2007). By filtering abundant satellite observations according to the stability and relative humidity of the free atmosphere and cloud liquid water path, the local meteorology and cloud morphology are held approximately constant minimizing the chance of misinterpreting covarying of meteorology and cloud morphology as aerosol effects when regressing CRE against AI (?). These environmental drivers are known to influence cloud extent and radiative effect, and with constraints through the use of regimes, we can better attribute changes in the CRE to aerosol (?). Our results suggest that without constraints, the global mean AIE can be over-estimated by as much as 40% and regional variations can be artificially enhanced by as much as a factor of 2.

With environmental and cloud state constraints in place on a regional basis (Figure A.27), strong, regionally specific cloud responses are identified and confidently attributed to aerosols. Clouds in the southern subtropical oceans, such as marine stratocumulus, exhibit the largest sensitivity to aerosol. Trade cumuli in the equatorial region show a much smaller, almost negligible signal comparatively. In the northern oceans, warm cloud decks from mid-latitude cyclones through the north Atlantic interact with North American and European emissions, leading to a cooling effect.

Interestingly even after cloud state and meteorology are controlled, the analysis still reveals coherent regions of aerosol forced cloud darkening effect (Figures A.18h, A.27). This aggregate dimming, or reverse Twomey, effect occurs in 15% of the regions

studied and appears to be a robust characteristic of low LWP clouds in unstable, dry environments. This is similar to other observation based studies which found the same dimming effect in  $\sim 20\%$  of warm clouds (Chen et al., 2012). Our study suggests such clouds are sufficiently abundant to consistently yield a net warming sensitivity over a substantial, coherent, region of the globe. Models must be able to recreate warm cloud responses, including the a dimming effect, if they are to accurately simulate global aerosol indirect effects.

Both on a regional and global scale, constraints reduce co-variance of sensitivity estimates (Gryspeerd and Stier, 2012). With constraints, the sensitivity can range from .46 to  $-.11 \frac{Wm^{-2}}{\ln(AI)}$  on a regional scale (Figure A.27), while without constraints the range increases from .77 to  $-.52 \frac{Wm^{-2}}{\ln(AI)}$  (Figure A.26a), signaling covarying influences and buffering by the cloud distort the signal on even a regional scale. Future regime classifications should prescribe precipitation limits to further separate the effects of aerosol-cloud-precipitation interactions, which are especially important to the cloud lifetime effect, where precipitation suppression leads to a larger cloud extent and lifetime.

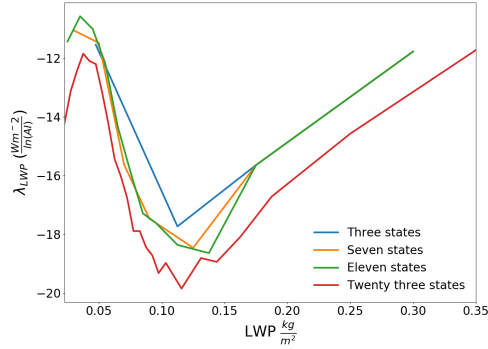


FIGURE A.2

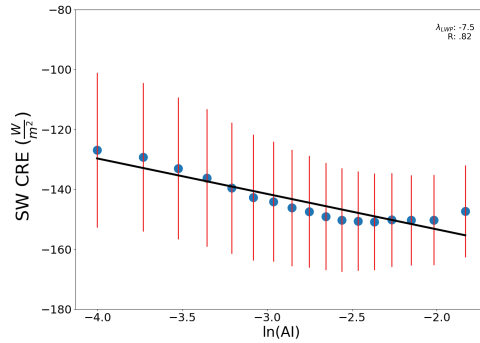


FIGURE A.3

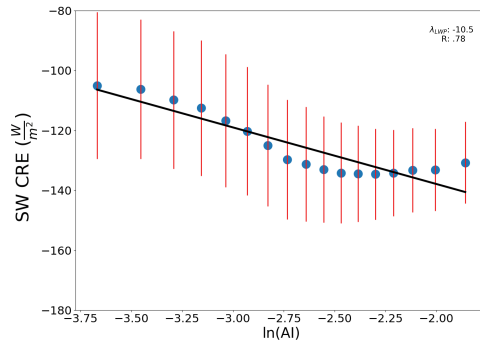


FIGURE A.4

FIGURE A.5: Values of the sensitivity of CRE to aerosol ( $\lambda_{LWP}$  from equation (A.5)) for different resolutions of cloud state regimes. The weighted, summed  $\lambda_{LWP}$  is  $-13.12 \frac{Wm^{-2}}{\ln(AI)}$  with 8 partitions. Plots of warm cloud shortwave CRE against  $\ln(AI)$  are shown below for (b) thin ( $.04$  to  $.06 \frac{kg}{m^2}$ ) and (c) thick ( $.1$  to  $.15 \frac{kg}{m^2}$ ) cloud states. The red lines represent the standard deviation within each  $\ln(AI)$  bin and the blue dots represent the mean SW CRE for each  $\ln(AI)$  bin in plots (b) and (c).

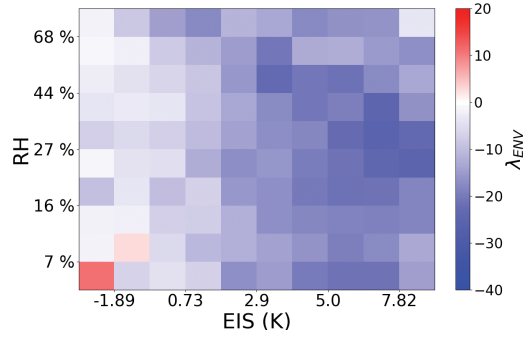


FIGURE A.6

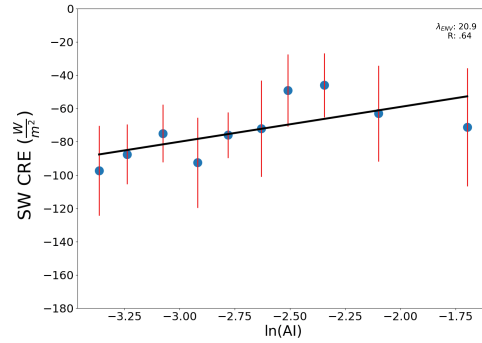


FIGURE A.7

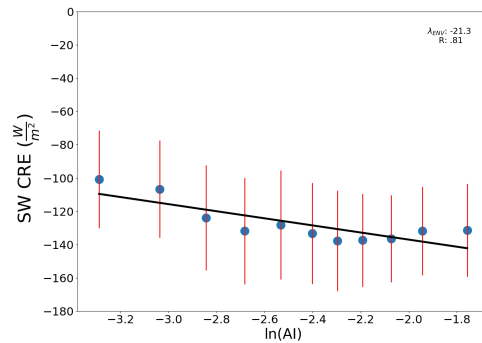


FIGURE A.8

FIGURE A.9: The sensitivity of CRE to aerosol ( $\lambda_{ENV}$ ) from equation (A.7) evaluated with constraints on the environment. When weighted and summed following equation (A.7),  $\lambda_{ENV}$  is  $-11.0 \frac{Wm^{-2}}{\ln(AI)}$ . Plots of the individual regimes from an unstable ( $\sim 1K$ ), dry environment ( $\leq 10\%$  RH<sub>700</sub>) (b) and stable ( $\sim 6K$ ), moist environment ( $\geq 30\%$  RH<sub>700</sub>) (c) where the red lines represent the standard deviation of the SW CRE within each  $\ln(AI)$  bin and the blue dots represent the mean SW CRE for each  $\ln(AI)$  bin.

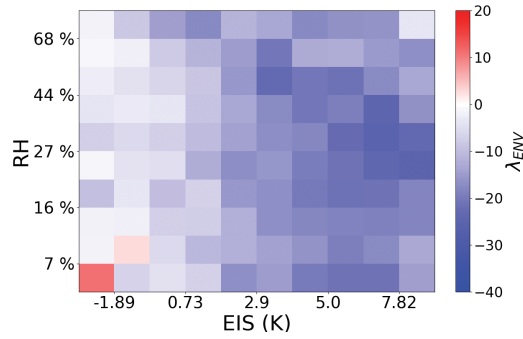


FIGURE A.10

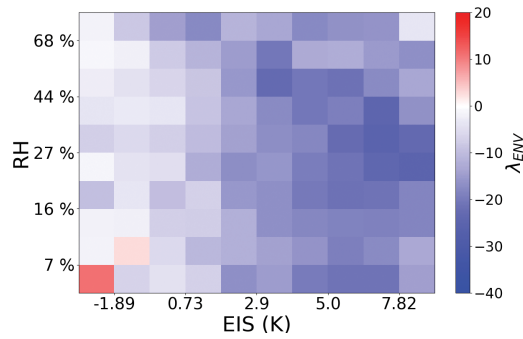


FIGURE A.11

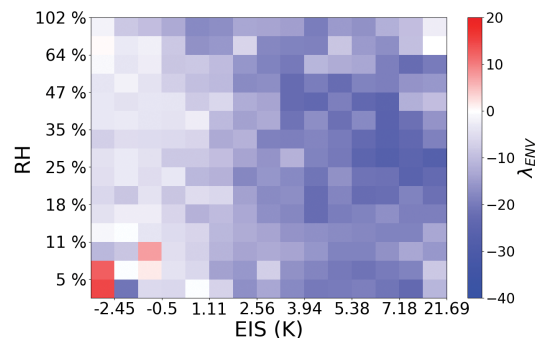


FIGURE A.12

FIGURE A.13: The sensitivity of the warm cloud CRE to aerosol ( $\lambda_{ENV}$ ) found using equation A.7 for environmental frameworks of a) 25 ( $-11.29 \frac{Wm^{-2}}{\ln(AI)}$ ), b) 100 ( $-11. \frac{Wm^{-2}}{\ln(AI)}$ ) and c) 225 ( $-10.99 \frac{Wm^{-2}}{\ln(AI)}$ ) regimes of EIS and  $RH_{700}$ .

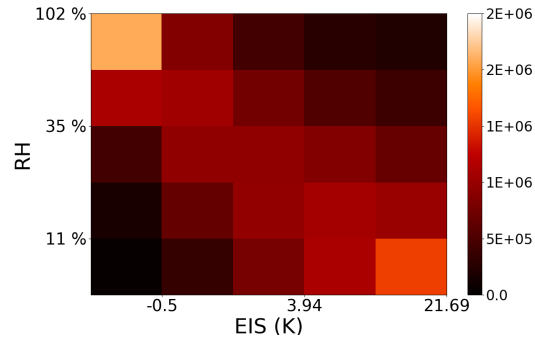


FIGURE A.14

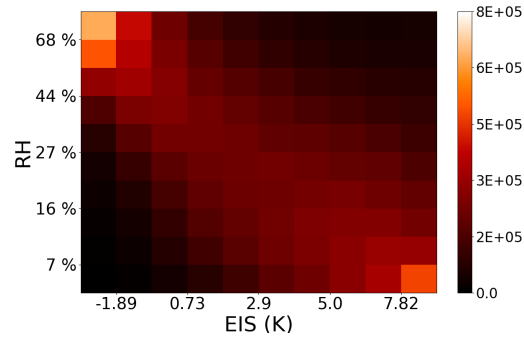


FIGURE A.15

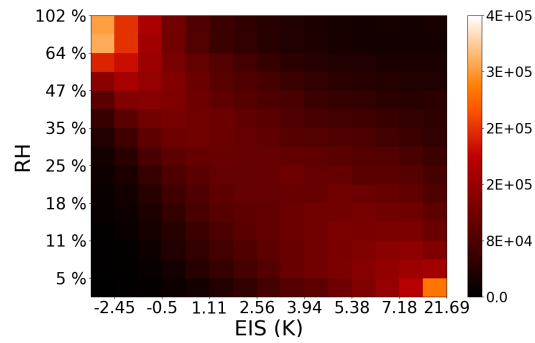


FIGURE A.16

FIGURE A.17: Frequency of clouds partitioned into of a) 25, b) 100, and c) 225 environmental regimes of EIS and RH<sub>700</sub>.

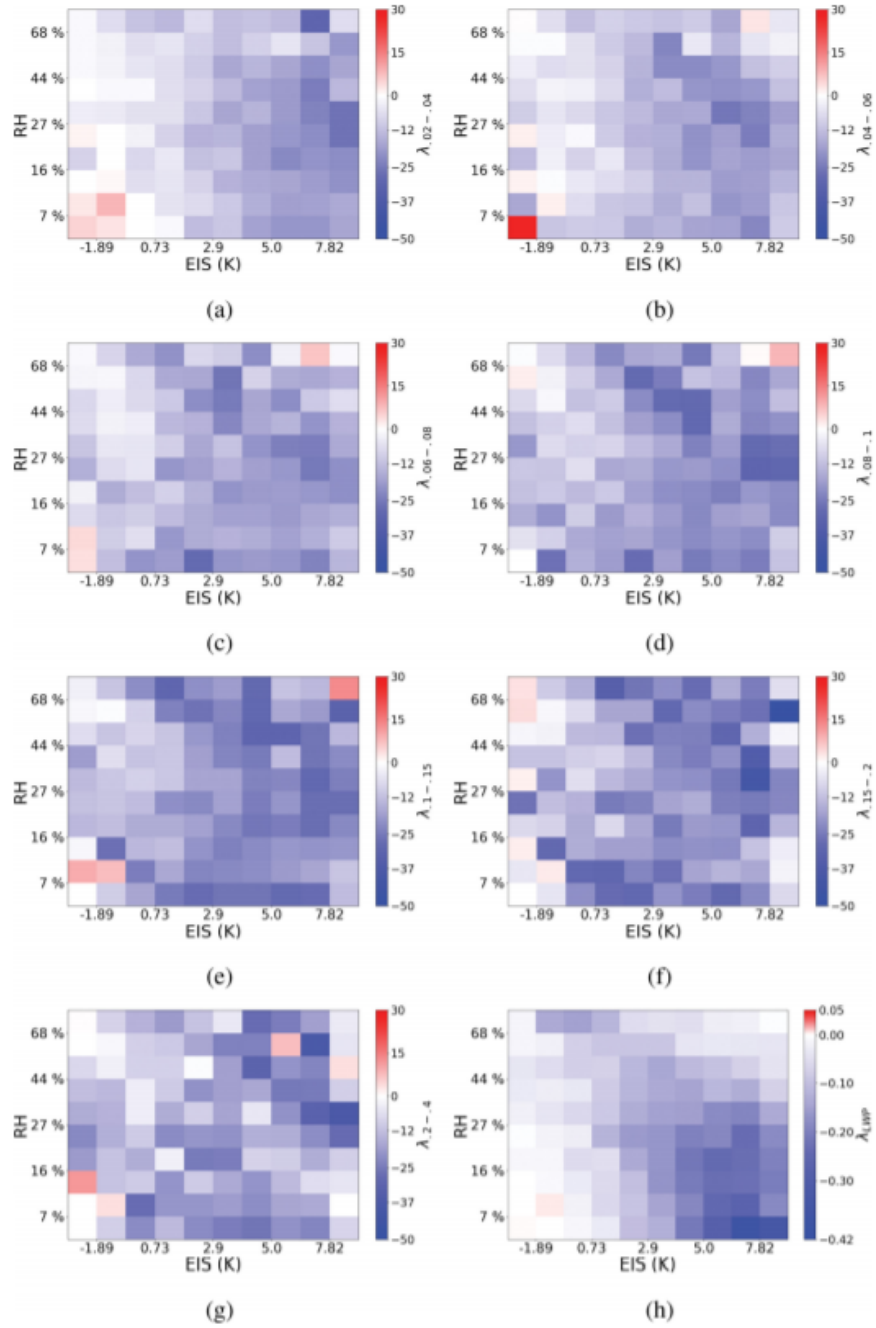


FIGURE A.18: The sensitivity of CRE to aerosol ( $\lambda_{BOTH}$ ) found with constraints on stability,  $RH_{700}$  and cloud state limits of  $??$  .02 to .04  $\frac{kg}{m^2}$  ( $-3.7 \frac{Wm^{-2}}{\ln(AI)}$ ),  $??$  .04 to .06  $\frac{kg}{m^2}$  ( $-2.2 \frac{Wm^{-2}}{\ln(AI)}$ ),  $??$  .06 to .08  $\frac{kg}{m^2}$  ( $-1.4 \frac{Wm^{-2}}{\ln(AI)}$ ),  $??$  .08 to .1  $\frac{kg}{m^2}$  ( $-1. \frac{Wm^{-2}}{\ln(AI)}$ ),  $??$  .1 to .15  $\frac{kg}{m^2}$  ( $-1.5 \frac{Wm^{-2}}{\ln(AI)}$ ),  $??$  .15 to .2  $\frac{kg}{m^2}$  ( $-.5 \frac{Wm^{-2}}{\ln(AI)}$ ), and  $??$  .2 to .4  $\frac{kg}{m^2}$  ( $-.4 \frac{Wm^{-2}}{\ln(AI)}$ ). Panel (h) is the summed, weighted sensitivity  $\lambda_{BOTH}$  within each environmental regime. The weighted, summed sensitivity is  $-10.6 \frac{Wm^{-2}}{\ln(AI)}$  (sum of panel (h)). Note the colorbar for panel (h) is adjusted due to weighting.

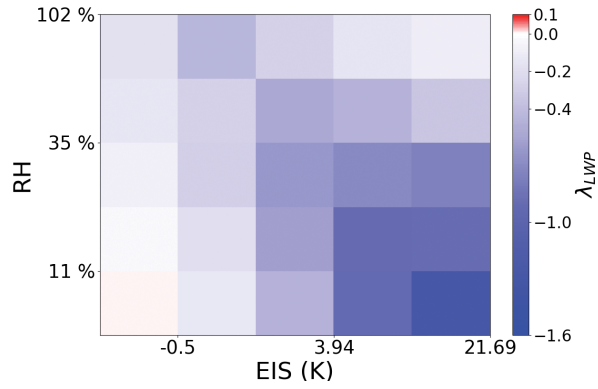


FIGURE A.19

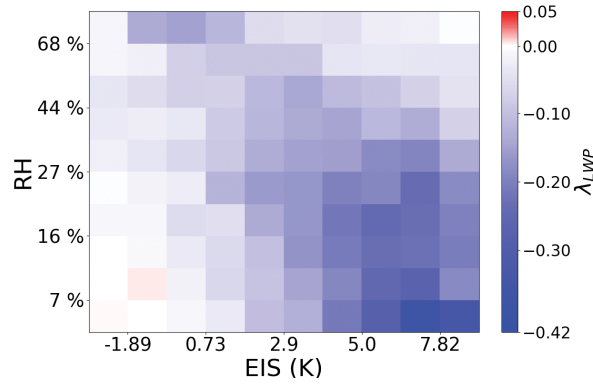


FIGURE A.20

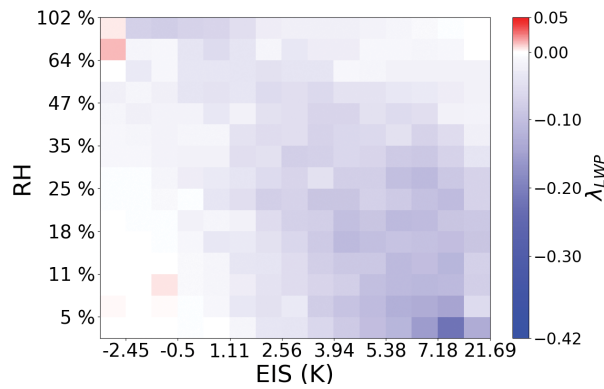


FIGURE A.21

FIGURE A.22: The sensitivities of CRE to aerosol from equation (A.9) within environmental regime resolutions of a) 5 by 5 ( $-10.8 \frac{\text{Wm}^{-2}}{\ln(\text{AI})}$ ), b) 10 by 10 ( $-10.6 \frac{\text{Wm}^{-2}}{\ln(\text{AI})}$ ), and c) 15 by 15 ( $-10.6 \frac{\text{Wm}^{-2}}{\ln(\text{AI})}$ ) summed over all cloud states. Unlike all previous sensitivity estimates, these are weighted by occurrence.

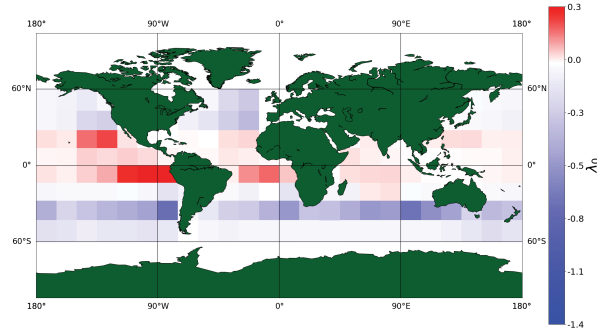


FIGURE A.23

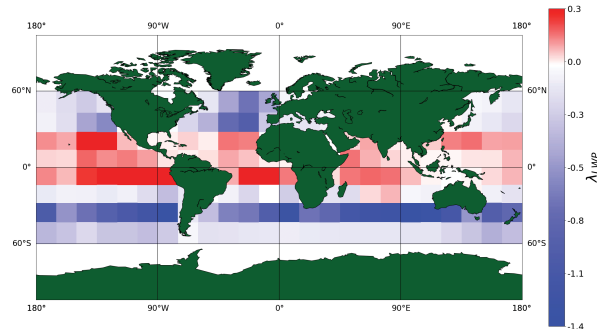


FIGURE A.24

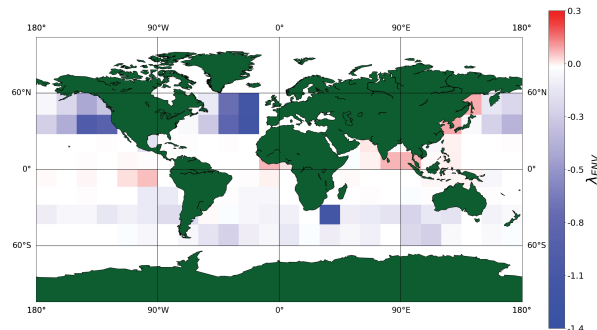


FIGURE A.25

FIGURE A.26: The sensitivity of CRE to aerosol evaluated regionally with (a) no regimes constraints, (b) only cloud state constraints, and (c) only environmental constraints for each  $15^\circ$  by  $15^\circ$  region. Total sensitivities are (a) -11.8, (b) -28.5, and (c) -13.8 when weighted by occurrence.  $\frac{\text{Wm}^{-2}}{\ln(\text{AI})}$ .

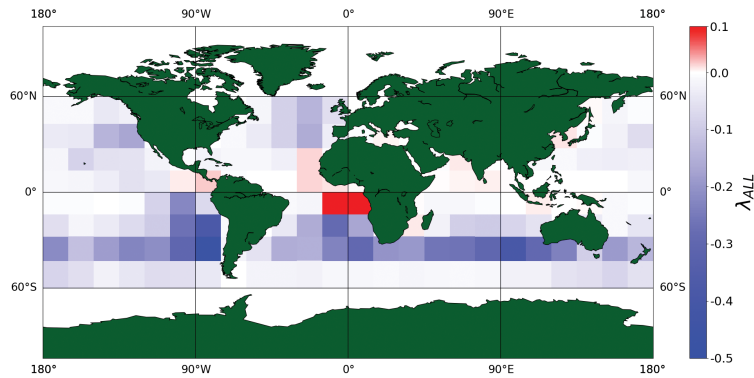


FIGURE A.27: The sensitivity of CRE to aerosol ( $\lambda_{ALL}$ ) found on a regional basis with cloud state and environmental regime constraints. The total regime weighted, global warm cloud sensitivity to aerosol perturbations is  $-10.13 \frac{\text{Wm}^{-2}}{\ln(\text{AI})}$ .

## Bibliography

- Ackerman, A. S., M. P. Kirkpatrick, D. E. Stevens, and O. B. Toon, 2004: The impact of humidity above stratiform clouds on indirect aerosol climate forcing. *Nature*, **432**, 1014.
- Albrecht, B. A., 1989: Aerosols, cloud microphysics, and fractional cloudiness. *Science*, **245**, 1227–1230.
- Altaratz, O., I. Koren, L. Remer, and E. Hirsch, 2014: Cloud invigoration by aerosols—coupling between microphysics and dynamics. *Atmospheric Research*, **140**, 38–60.
- Ångström, A., 1929: On the atmospheric transmission of sun radiation and on dust in the air. *Geografiska Annaler*, **11**, 156–166.
- 1964: The parameters of atmospheric turbidity. *Tellus*, **16**, 64–75.
- Berg, W., T. L'Ecuyer, and C. Kummerow, 2006: Rainfall climate regimes: The relationship of regional trmm rainfall biases to the environment. *Journal of Applied Meteorology and Climatology*, **45**, 434–454.

- Berg, W., T. L'Ecuyer, and S. van den Heever, 2008: Evidence for the impact of aerosols on the onset and microphysical properties of rainfall from a combination of satellite observations and cloud-resolving model simulations. *Journal of Geophysical Research: Atmospheres*, **113**.
- Beydoun, H. and C. Hoose, 2019: Aerosol-cloud-precipitation interactions in the context of convective self-aggregation. *Journal of advances in modeling earth systems*, **11**, 1066–1087.
- Bony, S. and J.-L. Dufresne, 2005: Marine boundary layer clouds at the heart of tropical cloud feedback uncertainties in climate models. *Geophysical Research Letters*, **32**.
- Bony, S., B. Stevens, D. M. Frierson, C. Jakob, M. Kageyama, R. Pincus, T. G. Shepherd, S. C. Sherwood, A. P. Siebesma, A. H. Sobel, et al., 2015: Clouds, circulation and climate sensitivity. *Nature Geoscience*, **8**, 261–268.
- Boucher, O., D. Randall, P. Artaxo, C. Bretherton, G. Feingold, P. Forster, V.-M. Kerminen, Y. Kondo, H. Liao, U. Lohmann, et al., 2013: Clouds and aerosols. *Climate change 2013: the physical science basis. Contribution of Working Group I to the Fifth Assessment Report of the Intergovernmental Panel on Climate Change*, Cambridge University Press, 571–657.
- Bréon, F.-M., D. Tanré, and S. Generoso, 2002: Aerosol effect on cloud droplet size monitored from satellite. *Science*, **295**, 834–838.

- Bretherton, C., P. N. Blossey, and J. Uchida, 2007: Cloud droplet sedimentation, entrainment efficiency, and subtropical stratocumulus albedo. *Geophysical research letters*, **34**.
- Brient, F. and S. Bony, 2012: How may low-cloud radiative properties simulated in the current climate influence low-cloud feedbacks under global warming? *Geophysical Research Letters*, **39**.
- Brient, F., T. Schneider, Z. Tan, S. Bony, X. Qu, and A. Hall, 2016: Shallowness of tropical low clouds as a predictor of climate models' response to warming. *Climate Dynamics*, **47**, 433–449.
- Carrier, M. and J. Lenhard, 2019: Climate models: How to assess their reliability. *International Studies in the Philosophy of Science*, 1–20.
- Carslaw, K., L. Lee, C. Reddington, K. Pringle, A. Rap, P. Forster, G. Mann, D. Spracklen, M. Woodhouse, L. Regayre, et al., 2013: Large contribution of natural aerosols to uncertainty in indirect forcing. *Nature*, **503**, 67.
- Carslaw, K. S., H. Gordon, D. S. Hamilton, J. S. Johnson, L. A. Regayre, M. Yoshioka, and K. J. Pringle, 2017: Aerosols in the pre-industrial atmosphere. *Current Climate Change Reports*, **3**, 1–15, doi:10.1007/s40641-017-0061-2.  
URL <https://doi.org/10.1007/s40641-017-0061-2>

- Chen, Q., I. Koren, O. Altaratz, R. H. Heiblum, G. Dagan, and L. Pinto, 2017: How do changes in warm-phase microphysics affect deep convective clouds? *Atmospheric Chemistry and Physics*, **17**.
- Chen, Y. and J. E. Penner, 2005: Uncertainty analysis for estimates of the first indirect aerosol effect. *Atmospheric Chemistry and Physics*, **5**, 2935–2948.
- Chen, Y.-C., M. Christensen, L. Xue, A. Sorooshian, G. Stephens, R. Rasmussen, and J. Seinfeld, 2012: Occurrence of lower cloud albedo in ship tracks. *Atmospheric Chemistry & Physics*, **12**.
- Chen, Y.-C., M. W. Christensen, D. J. Diner, and M. J. Garay, 2015: Aerosol-cloud interactions in ship tracks using terra modis/misr. *Journal of Geophysical Research: Atmospheres*, **120**, 2819–2833.
- Chen, Y.-C., M. W. Christensen, G. L. Stephens, and J. H. Seinfeld, 2014: Satellite-based estimate of global aerosol–cloud radiative forcing by marine warm clouds. *Nature Geoscience*, **7**, 643–646.
- Chen, Y.-C., L. Xue, Z. Lebo, H. Wang, R. Rasmussen, and J. Seinfeld, 2011: A comprehensive numerical study of aerosol-cloud-precipitation interactions in marine stratocumulus. *Atmospheric Chemistry and Physics*, **11**, 9749–9769.
- Cheng, F., J. Zhang, J. He, Y. Zha, Q. Li, and Y. Li, 2017: Analysis of aerosol-cloud-precipitation interactions based on modis data. *Advances in Space Research*, **59**, 63–73.

- Christensen, M., K. Suzuki, B. Zambri, and G. Stephens, 2014: Ship track observations of a reduced shortwave aerosol indirect effect in mixed-phase clouds. *Geophysical Research Letters*, **41**, 6970–6977.
- Christensen, M. W., Y.-C. Chen, and G. L. Stephens, 2016: Aerosol indirect effect dictated by liquid clouds. *Journal of Geophysical Research: Atmospheres*, **121**, 14–636.
- Christensen, M. W., D. Neubauer, C. A. Poulsen, G. E. Thomas, G. R. McGarraugh, A. C. Povey, S. R. Proud, and R. G. Grainger, 2017: Unveiling aerosol–cloud interactions—part 1: Cloud contamination in satellite products enhances the aerosol indirect forcing estimate. *Atmospheric Chemistry and Physics*, **17**.
- Christensen, M. W. and G. L. Stephens, 2011: Microphysical and macrophysical responses of marine stratocumulus polluted by underlying ships: Evidence of cloud deepening. *Journal of Geophysical Research: Atmospheres*, **116**.
- Cochrane, S. P., K. S. Schmidt, H. Chen, P. Pilewskie, S. Kittelman, J. Redemann, S. LeBlanc, K. Pistone, M. Kacenelenbogen, M. S. Rozenhaimer, et al., 2019: Above-cloud aerosol radiative effects based on oracles 2016 and oracles 2017 aircraft experiments. *Atmospheric Measurement Techniques*, **12**, 6505–6528.
- Coppin, D. and S. Bony, 2015: Physical mechanisms controlling the initiation of convective self-aggregation in a general circulation model. *Journal of Advances in Modeling Earth Systems*, **7**, 2060–2078.

- Dagan, G., I. Koren, and O. Altaratz, 2018a: Quantifying the effect of aerosol on vertical velocity and effective terminal velocity in warm convective clouds. *Atmospheric Chemistry and Physics*, **18**.
- Dagan, G., I. Koren, O. Altaratz, and R. H. Heiblum, 2016: Aerosol effect on the evolution of the thermodynamic properties of warm convective cloud fields. *Scientific reports*, **6**, 38769.
- 2017: Time-dependent, non-monotonic response of warm convective cloud fields to changes in aerosol loading. *Atmospheric Chemistry and Physics*, **17**.
- Dagan, G., I. Koren, O. Altaratz, and Y. Lehahn, 2018b: Shallow convective cloud field lifetime as a key factor for evaluating aerosol effects. *iScience*, **10**, 192–202.
- De Roode, S. R., A. P. Siebesma, S. Dal Gesso, H. J. Jonker, J. Schalkwijk, and J. Sival, 2014: A mixed-layer model study of the stratocumulus response to changes in large-scale conditions. *Journal of Advances in Modeling Earth Systems*, **6**, 1256–1270.
- Dey, S., K. Sengupta, G. Basil, S. Das, N. Nidhi, S. Dash, A. Sarkar, P. Srivastava, A. Singh, and P. Agarwal, 2012: Satellite-based 3d structure of cloud and aerosols over the indian monsoon region: implications for aerosol-cloud interaction. *Remote sensing and modeling of the atmosphere, oceans, and interactions iv*, International Society for Optics and Photonics, volume 8529, 852907.

- Douglas, A. and T. L'Ecuyer, 2019a: Quantifying variations in shortwave aerosol–cloud–radiation interactions using local meteorology and cloud state constraints. *Atmospheric Chemistry and Physics*, **19**, 6251–6268.
- 2019b: Quantifying variations in shortwave aerosol–cloud–radiation interactions using local meteorology and cloud state constraints. *Atmospheric Chemistry and Physics*, **19**, 6251–6268, doi:10.5194/acp-19-6251-2019.  
URL <https://www.atmos-chem-phys.net/19/6251/2019/>
- Douglas, A. R., 2017: *Understanding Warm Cloud Aerosol-cloud Interactions*. Ph.D. thesis, University of Wisconsin–Madison.
- Fan, J., Y. Wang, D. Rosenfeld, and X. Liu, 2016: Review of aerosol–cloud interactions: Mechanisms, significance, and challenges. *Journal of the Atmospheric Sciences*, **73**, 4221–4252.
- Feingold, G., 2003: Modeling of the first indirect effect: Analysis of measurement requirements. *Geophysical research letters*, **30**.
- Feingold, G., A. McComiskey, T. Yamaguchi, J. S. Johnson, K. S. Carslaw, and K. S. Schmidt, 2016: New approaches to quantifying aerosol influence on the cloud radiative effect. *Proceedings of the National Academy of Sciences*, **113**, 5812–5819.
- Fiedler, S., B. Stevens, M. Gidden, S. Smith, K. Riahi, and D. van Vuuren, 2019: First forcing estimates from the future cmip6 scenarios of anthropogenic aerosol optical properties and an associated twomey effect. *Geoscientific Model Development*.

- Gelaro, R., W. McCarty, M. J. Suárez, R. Todling, A. Molod, L. Takacs, C. A. Randles, A. Darmenov, M. G. Bosilovich, R. Reichle, et al., 2017: The modern-era retrospective analysis for research and applications, version 2 (merra-2). *Journal of Climate*, **30**, 5419–5454.
- Gettelman, A. and S. Sherwood, 2016: Processes responsible for cloud feedback. *Current Climate Change Reports*, **2**, 179–189.
- Ghan, S., M. Wang, S. Zhang, S. Ferrachat, A. Gettelman, J. Griesfeller, Z. Kipling, U. Lohmann, H. Morrison, D. Neubauer, et al., 2016: Challenges in constraining anthropogenic aerosol effects on cloud radiative forcing using present-day spatiotemporal variability. *Proceedings of the National Academy of Sciences*, **113**, 5804–5811.
- Goren, T. and D. Rosenfeld, 2014: Decomposing aerosol cloud radiative effects into cloud cover, liquid water path and twomey components in marine stratocumulus. *Atmospheric research*, **138**, 378–393.
- Grandey, B. and P. Stier, 2010: A critical look at spatial scale choices in satellite-based aerosol indirect effect studies. *Atmospheric Chemistry and Physics Discussions*, **10**.
- Gryspeerdt, E., T. Goren, O. Sourdeval, J. Quaas, J. Mülmenstädt, S. Dipu, C. Unglaub, A. Gettelman, and M. Christensen, 2019a: Constraining the aerosol influence on cloud liquid water path. *Atmospheric Chemistry and Physics*, **19**, 5331–5347.

- 2019b: Constraining the aerosol influence on cloud liquid water path. *Atmospheric Chemistry and Physics*, **19**, 5331–5347.
- Gryspeerdt, E., J. Quaas, and N. Bellouin, 2016: Constraining the aerosol influence on cloud fraction. *Journal of Geophysical Research: Atmospheres*, **121**, 3566–3583.
- Gryspeerdt, E., J. Quaas, S. Ferrachat, A. Gettelman, S. Ghan, U. Lohmann, H. Morrison, D. Neubauer, D. G. Partridge, P. Stier, et al., 2017: Constraining the instantaneous aerosol influence on cloud albedo. *Proceedings of the National Academy of Sciences*, **114**, 4899–4904.
- Gryspeerdt, E. and P. Stier, 2012: Regime-based analysis of aerosol-cloud interactions. *Geophysical research letters*, **39**.
- Gryspeerdt, E., P. Stier, and D. Partridge, 2013: Satellite observations of cloud regime development: the role of aerosol processes. *Atmospheric Chemistry and Physics Discussions*, **13**.
- Gryspeerdt, E., P. Stier, B. White, and Z. Kipling, 2015: Wet scavenging limits the detection of aerosol effects on precipitation. *Atmospheric Chemistry and Physics*, **15**, 7557–7570.
- Guo, Z., M. Wang, Y. Qian, V. E. Larson, S. Ghan, M. Ovchinnikov, P. A. Bogenschutz, C. Zhao, G. Lin, and T. Zhou, 2014: A sensitivity analysis of cloud properties to clubb parameters in the single-column community atmosphere model (scam5). *Journal of Advances in Modeling Earth Systems*, **6**, 829–858.

- Hahn, C. and S. Warren, 2007a: A gridded climatology of clouds over land (1971-96) and ocean (1954-97 from surface observations worldwide. Technical report, Office of Biological and Environmental Research.
- 2007b: A gridded climatology of clouds over land (1971-96) and ocean (1954-97 from surface observations worldwide. Technical report, Office of Biological and Environmental Research.
- Hamilton, D. S., L. A. Lee, K. J. Pringle, C. L. Reddington, D. V. Spracklen, and K. S. Carslaw, 2014: Occurrence of pristine aerosol environments on a polluted planet. *Proceedings of the National Academy of Sciences*, **111**, 18466–18471.
- Hasekamp, O. P., E. Gryspeerdt, and J. Quaas, 2019: Analysis of polarimetric satellite measurements suggests stronger cooling due to aerosol-cloud interactions. *Nature communications*, **10**, 1–7.
- Haynes, J. M., T. S. L'Ecuyer, G. L. Stephens, S. D. Miller, C. Mitrescu, N. B. Wood, and S. Tanelli, 2009: Rainfall retrieval over the ocean with spaceborne w-band radar. *Journal of Geophysical Research: Atmospheres*, **114**.
- Heiblum, R. H., L. Pinto, O. Altaratz, G. Dagan, and I. Koren, 2019: Core and margin in warm convective clouds—part 2: Aerosol effects on core properties. *Atmospheric Chemistry and Physics*, **19**.

- Henderson, D. S., T. L'Ecuyer, G. Stephens, P. Partain, and M. Sekiguchi, 2013: A multisensor perspective on the radiative impacts of clouds and aerosols. *Journal of Applied Meteorology and Climatology*, **52**, 853–871.
- Holloway, C. E., A. A. Wing, S. Bony, C. Muller, H. Masunaga, T. S. L'Ecuyer, D. D. Turner, and P. Zuidema, 2017: Observing convective aggregation. *Surveys in Geophysics*, **38**, 1199–1236.
- Igel, M. R., A. J. Drager, and S. C. Van Den Heever, 2014: A cloudsat cloud object partitioning technique and assessment and integration of deep convective anvil sensitivities to sea surface temperature. *Journal of Geophysical Research: Atmospheres*, **119**, 10515–10535.
- Jiang, H., G. Feingold, and I. Koren, 2009: Effect of aerosol on trade cumulus cloud morphology. *Journal of Geophysical Research: Atmospheres*, **114**.
- Jiang, H., H. Xue, A. Teller, G. Feingold, and Z. Levin, 2006: Aerosol effects on the lifetime of shallow cumulus. *Geophysical Research Letters*, **33**.
- Johnson, B., K. Shine, and P. Forster, 2004: The semi-direct aerosol effect: Impact of absorbing aerosols on marine stratocumulus. *Quarterly Journal of the Royal Meteorological Society*, **130**, 1407–1422.
- Juárez, T., B. Kahn, E. Fetzer, et al., 2009: Cloud-type dependencies of modis and amsr-e liquid water path differences. *Atmospheric Chemistry and Physics Discussions*, **9**, 3367–3399.

- Koren, I., O. Altaratz, and G. Dagan, 2015: Aerosol effect on the mobility of cloud droplets. *Environmental Research Letters*, **10**, 104011.
- Koren, I., G. Dagan, and O. Altaratz, 2014: From aerosol-limited to invigoration of warm convective clouds. *science*, **344**, 1143–1146.
- Kubar, T. L., D. L. Hartmann, and R. Wood, 2009: Understanding the importance of microphysics and macrophysics for warm rain in marine low clouds. part i: Satellite observations. *Journal of the atmospheric sciences*, **66**, 2953–2972.
- Kubar, T. L., G. L. Stephens, M. Lebsock, V. E. Larson, and P. A. Bogenschutz, 2015: Regional assessments of low clouds against large-scale stability in cam5 and cam-clubb using modis and era-interim reanalysis data. *Journal of Climate*, **28**, 1685–1706.
- Lebsock, M. and H. Su, 2014: Application of active spaceborne remote sensing for understanding biases between passive cloud water path retrievals. *Journal of Geophysical Research: Atmospheres*, **119**, 8962–8979.
- Lebsock, M. D., G. L. Stephens, and C. Kummerow, 2008: Multisensor satellite observations of aerosol effects on warm clouds. *Journal of Geophysical Research: Atmospheres*, **113**.
- L’Ecuyer, T. S., W. Berg, J. Haynes, M. Lebsock, and T. Takemura, 2009: Global observations of aerosol impacts on precipitation occurrence in warm maritime clouds. *Journal of Geophysical Research: Atmospheres*, **114**.

- L'Ecuyer, T. S. and J. H. Jiang, 2011: Touring the atmosphere aboard the a-train. *AIP Conference Proceedings*, American Institute of Physics, volume 1401, 245–256.
- L'Ecuyer, T. S. and G. L. Stephens, 2002: An estimation-based precipitation retrieval algorithm for attenuating radars. *Journal of applied meteorology*, **41**, 272–285.
- Lee, S.-S., G. Feingold, and P. Y. Chuang, 2012: Effect of aerosol on cloud–environment interactions in trade cumulus. *Journal of the Atmospheric Sciences*, **69**, 3607–3632.
- Levy, R., L. Remer, R. Kleidman, S. Mattoo, C. Ichoku, R. Kahn, and T. Eck, 2010: Global evaluation of the collection 5 modis dark-target aerosol products over land. *Atmospheric Chemistry and Physics*, **10**, 10399–10420.
- Liu, J., Z. Li, and M. Cribb, 2016: Response of marine boundary layer cloud properties to aerosol perturbations associated with meteorological conditions from the 19-month amf-azores campaign. *Journal of the Atmospheric Sciences*, **73**, 4253–4268.
- Loeb, N. G. and S. Kato, 2002: Top-of-atmosphere direct radiative effect of aerosols over the tropical oceans from the clouds and the earth's radiant energy system (ceres) satellite instrument. *Journal of Climate*, **15**, 1474–1484.
- Lu, M.-L. and J. H. Seinfeld, 2005: Study of the aerosol indirect effect by large-eddy simulation of marine stratocumulus. *Journal of the atmospheric sciences*, **62**, 3909–3932.

- Lubin, D. and A. M. Vogelmann, 2006: A climatologically significant aerosol longwave indirect effect in the arctic. *Nature*, **439**, 453–456.
- L’Ecuyer, T., N. Wood, T. Haladay, G. Stephens, and P. Stackhouse Jr, 2008: The impact of clouds on the atmospheric radiation budget in the r04 cloudsat fluxes and heating rates data set. *J. Geophys. Res.*
- Ma, P.-L., P. J. Rasch, H. Chepfer, D. M. Winker, and S. J. Ghan, 2018: Observational constraint on cloud susceptibility weakened by aerosol retrieval limitations. *Nature communications*, **9**, 1–10.
- McCoy, D., F.-M. Bender, J. Mohrmann, D. Hartmann, R. Wood, and D. Grosvenor, 2017: The global aerosol-cloud first indirect effect estimated using modis, merra, and aerocom. *Journal of Geophysical Research: Atmospheres*, **122**, 1779–1796.
- Michibata, T., K. Suzuki, Y. Sato, and T. Takemura, 2016: The source of discrepancies in aerosol–cloud–precipitation interactions between gcm and a-train retrievals. *Atmospheric Chemistry and Physics*, **16**, 15413–15424.
- Morrison, H., 2017: An analytic description of the structure and evolution of growing deep cumulus updrafts. *Journal of the Atmospheric Sciences*, **74**, 809–834.
- Mülmenstädt, J. and G. Feingold, 2018: The radiative forcing of aerosol–cloud interactions in liquid clouds: wrestling and embracing uncertainty. *Current Climate Change Reports*, **4**, 23–40.

- Mülmenstädt, J., E. Gryspeerdt, M. Salzmann, P.-L. Ma, S. Dipu, and J. Quaas, 2019: Separating radiative forcing by aerosol–cloud interactions and rapid cloud adjustments in the echam–hammoz aerosol–climate model using the method of partial radiative perturbations. *Atmospheric Chemistry and Physics (Online)*, **19**.
- Myhre, G., D. Shindell, and J. Pongratz, 2014: Anthropogenic and natural radiative forcing.
- Nam, C., S. Bony, J.-L. Dufresne, and H. Chepfer, 2012: The ‘too few, too bright’ tropical low-cloud problem in cmip5 models. *Geophysical Research Letters*, **39**.
- Nelson, E. L. and T. S. L’Ecuyer, 2018: Global character of latent heat release in oceanic warm rain systems. *Journal of Geophysical Research: Atmospheres*, **123**, 4797–4817.
- Nelson, E. L., T. S. L’Ecuyer, S. M. Saleeby, W. Berg, S. R. Herbener, and S. C. Van Den Heever, 2016: Toward an algorithm for estimating latent heat release in warm rain systems. *Journal of Atmospheric and Oceanic Technology*, **33**, 1309–1329.
- Neubauer, D., S. Ferrachat, S.-L. Drian, P. Stier, D. G. Partridge, I. Tegen, I. Bey, T. Stanelle, H. Kokkola, U. Lohmann, et al., 2019: The global aerosol-climate model echam6. 3-ham2. 3-part 2: Cloud evaluation, aerosol radiative forcing, and climate sensitivity. *Geoscientific Model Development*, **12**, 3609–3639.

- Nishant, N. and S. Sherwood, 2017: A cloud-resolving model study of aerosol-cloud correlation in a pristine maritime environment. *Geophysical Research Letters*.
- Oreopoulos, L., N. Cho, D. Lee, and S. Kato, 2016: Radiative effects of global modis cloud regimes. *Journal of Geophysical Research: Atmospheres*, **121**, 2299–2317.
- Parkinson, C. L., 2003: Aqua: An earth-observing satellite mission to examine water and other climate variables. *IEEE Transactions on Geoscience and Remote Sensing*, **41**, 173–183.
- Penner, J. E., M. Andreae, H. Annegarn, L. Barrie, J. Feichter, D. Hegg, A. Jayaraman, R. Leitch, D. Murphy, J. Nganga, et al., 2001: Aerosols, their direct and indirect effects. *Climate Change 2001: The Scientific Basis. Contribution of Working Group I to the Third Assessment Report of the Intergovernmental Panel on Climate Change*, Cambridge University Press, 289–348.
- Penner, J. E., L. Xu, and M. Wang, 2011: Satellite methods underestimate indirect climate forcing by aerosols. *Proceedings of the National Academy of Sciences*, **108**, 13404–13408.
- Pincus, R. and M. Baker, 1994: Precipitation, solar absorption, and albedo susceptibility in marine boundary layer clouds. *Nature*, **372**, 250–252.
- Platnick, S. and S. Twomey, 1994: Determining the susceptibility of cloud albedo to changes in droplet concentration with the advanced very high resolution radiometer. *Journal of Applied Meteorology*, **33**, 334–347.

- Quaas, J., Y. Ming, S. Menon, T. Takemura, M. Wang, J. E. Penner, A. Gettelman, U. Lohmann, N. Bellouin, O. Boucher, et al., 2009: Aerosol indirect effects—general circulation model intercomparison and evaluation with satellite data. *Atmospheric Chemistry and Physics*, **9**, 8697–8717.
- Ramanathan, V., P. Crutzen, J. Kiehl, and D. Rosenfeld, 2001: Aerosols, climate, and the hydrological cycle. *science*, **294**, 2119–2124.
- Randall, D., M. Khairoutdinov, A. Arakawa, and W. Grabowski, 2003: Breaking the cloud parameterization deadlock. *Bulletin of the American Meteorological Society*, **84**, 1547–1564.
- Rockström, J., W. Steffen, K. Noone, Å. Persson, F. S. Chapin, E. F. Lambin, T. M. Lenton, M. Scheffer, C. Folke, H. J. Schellnhuber, et al., 2009: A safe operating space for humanity. *nature*, **461**, 472–475.
- Rosenfeld, D., 2006: Aerosol-cloud interactions control of earth radiation and latent heat release budgets. *Solar Variability and Planetary Climates*, Springer, 149–157.
- Rosenfeld, D., U. Lohmann, G. B. Raga, C. D. O’Dowd, M. Kulmala, S. Fuzzi, A. Reissell, and M. O. Andreae, 2008: Flood or drought: how do aerosols affect precipitation? *science*, **321**, 1309–1313.
- Rosenfeld, D., Y. Zhu, M. Wang, Y. Zheng, T. Goren, and S. Yu, 2019: Aerosol-driven droplet concentrations dominate coverage and water of oceanic low-level clouds. *Science*, **363**, eaav0566.

- Sandu, I. and B. Stevens, 2011: On the factors modulating the stratocumulus to cumulus transitions. *Journal of the Atmospheric Sciences*, **68**, 1865–1881.
- Sassen, K., Z. Wang, and D. Liu, 2008: Global distribution of cirrus clouds from cloudsat/cloud-aerosol lidar and infrared pathfinder satellite observations (calipso) measurements. *Journal of Geophysical Research: Atmospheres*, **113**.
- Schneider, T., C. M. Kaul, and K. G. Pressel, 2019: Possible climate transitions from breakup of stratocumulus decks under greenhouse warming. *Nature Geoscience*, **12**, 163.
- Seinfeld, J. H., C. Bretherton, K. S. Carslaw, H. Coe, P. J. DeMott, E. J. Dunlea, G. Feingold, S. Ghan, A. B. Guenther, R. Kahn, et al., 2016: Improving our fundamental understanding of the role of aerosol- cloud interactions in the climate system. *Proceedings of the National Academy of Sciences*, **113**, 5781–5790.
- Slingo, A., 1990: Sensitivity of the earth’s radiation budget to changes in low clouds. *Nature*, **343**, 49–51.
- Small, J. D., P. Y. Chuang, G. Feingold, and H. Jiang, 2009: Can aerosol decrease cloud lifetime? *Geophysical Research Letters*, **36**.
- Smith, C., R. Kramer, G. Myhre, K. Alterskjær, W. Collins, A. Sima, O. Boucher, J.-L. Dufresne, P. Nabat, M. Michou, S. Yukimoto, J. Cole, D. Paynter, H. Shiogama, F. O’Connor, E. Robertson, A. Wiltshire, T. Andrews, C. Hannay, and P. Forster, 2020: Effective radiative forcing and adjustments in cmip6

- models. doi:10.5194/acp-2019-1212.
- Sorooshian, A., G. Feingold, M. D. Lebsock, H. Jiang, and G. L. Stephens, 2009: On the precipitation susceptibility of clouds to aerosol perturbations. *Geophysical Research Letters*, **36**.
- Stechmann, S. N. and S. Hottovy, 2016: Cloud regimes as phase transitions. *Geophysical Research Letters*, **43**, 6579–6587.
- Stephens, G., D. Winker, J. Pelon, C. Trepte, D. Vane, C. Yuhas, T. L'ecuyer, and M. Lebsock, 2018: Cloudsat and calipso within the a-train: Ten years of actively observing the earth system. *Bulletin of the American Meteorological Society*, **99**, 569–581.
- Stephens, G. L., 2005: Cloud feedbacks in the climate system: A critical review. *Journal of climate*, **18**, 237–273.
- Stephens, G. L. and C. D. Kummerow, 2007: The remote sensing of clouds and precipitation from space: A review. *Journal of the Atmospheric Sciences*, **64**, 3742–3765.
- Stephens, G. L. and N. B. Wood, 2007: Properties of tropical convection observed by millimeter-wave radar systems. *Monthly weather review*, **135**, 821–842.
- Stevens, B., 2007: On the growth of layers of nonprecipitating cumulus convection. *Journal of the atmospheric sciences*, **64**, 2916–2931.
- 2013: Aerosols: Uncertain then, irrelevant now. *Nature*, **503**, 47.

- Stevens, B. and G. Feingold, 2009a: Untangling aerosol effects on clouds and precipitation in a buffered system. *Nature*, **461**, 607–613.
- 2009b: Untangling aerosol effects on clouds and precipitation in a buffered system. *Nature*, **461**, 607–613.
- Stier, P., 2016: Limitations of passive remote sensing to constrain global cloud condensation nuclei. *Atmospheric Chemistry and Physics*, **16**.
- Su, W., N. G. Loeb, K.-M. Xu, G. L. Schuster, and Z. A. Eitzen, 2010: An estimate of aerosol indirect effect from satellite measurements with concurrent meteorological analysis. *Journal of Geophysical Research: Atmospheres*, **115**.
- Takemura, T., Y. J. Kaufman, L. A. Remer, and T. Nakajima, 2007: Two competing pathways of aerosol effects on cloud and precipitation formation. *Geophysical research letters*, **34**.
- Takemura, T., T. Nozawa, S. Emori, T. Y. Nakajima, and T. Nakajima, 2005: Simulation of climate response to aerosol direct and indirect effects with aerosol transport-radiation model. *Journal of Geophysical Research: Atmospheres*, **110**.
- Takemura, T., H. Okamoto, Y. Maruyama, A. Numaguti, A. Higurashi, and T. Nakajima, 2000: Global three-dimensional simulation of aerosol optical thickness distribution of various origins. *Journal of Geophysical Research: Atmospheres*, **105**, 17853–17873.

- Tanelli, S., S. L. Durden, E. Im, K. S. Pak, D. G. Reinke, P. Partain, J. M. Haynes, and R. T. Marchand, 2008: Cloudsat's cloud profiling radar after two years in orbit: Performance, calibration, and processing. *IEEE Transactions on Geoscience and Remote Sensing*, **46**, 3560–3573.
- Toll, V., M. Christensen, J. Quaas, and N. Bellouin, 2019: Weak average liquid-cloud-water response to anthropogenic aerosols. *Nature*, **572**, 51–55.
- Tsushima, Y., M. A. Ringer, T. Koshiro, H. Kawai, R. Roehrig, J. Cole, M. Watanabe, T. Yokohata, A. Bodas-Salcedo, K. D. Williams, et al., 2016: Robustness, uncertainties, and emergent constraints in the radiative responses of stratocumulus cloud regimes to future warming. *Climate dynamics*, **46**, 3025–3039.
- Tubul, Y., I. Koren, and O. Altaratz, 2015: The tropical atlantic surface wind divergence belt and its effect on clouds. *Earth System Dynamics*, **6**, 781.
- Twohy, C. H., M. D. Petters, J. R. Snider, B. Stevens, W. Tahnk, M. Wetzal, L. Russell, and F. Burnet, 2005: Evaluation of the aerosol indirect effect in marine stratocumulus clouds: Droplet number, size, liquid water path, and radiative impact. *Journal of Geophysical Research: Atmospheres*, **110**.
- Twomey, S., 1977a: The influence of pollution on the shortwave albedo of clouds. *Journal of the atmospheric sciences*, **34**, 1149–1152.
- 1977b: The influence of pollution on the shortwave albedo of clouds. *Journal of the Atmospheric Sciences*, **34**, 1149–1152.

- Van der Dussen, J., S. De Roode, S. D. Gesso, and A. Siebesma, 2015: An les model study of the influence of the free tropospheric thermodynamic conditions on the stratocumulus response to a climate perturbation. *Journal of Advances in Modeling Earth Systems*, **7**, 670–691.
- Van der Dussen, J., S. De Roode, and A. Siebesma, 2014: Factors controlling rapid stratocumulus cloud thinning. *Journal of the Atmospheric Sciences*, **71**, 655–664.
- Wang, M., S. Ghan, X. Liu, T. S. L’Ecuyer, K. Zhang, H. Morrison, M. Ovchinnikov, R. Easter, R. Marchand, D. Chand, et al., 2012: Constraining cloud lifetime effects of aerosols using a-train satellite observations. *Geophysical Research Letters*, **39**.
- Wang, M., S. Ghan, M. Ovchinnikov, X. Liu, R. Easter, E. Kassianov, Y. Qian, and H. Morrison, 2011: Aerosol indirect effects in a multi-scale aerosol-climate model pnnl-mmf. *Atmospheric Chemistry and Physics*, **11**, 5431.
- Watanabe, M., Y. Kamae, H. Shiogama, A. M. DeAngelis, and K. Suzuki, 2018: Low clouds link equilibrium climate sensitivity to hydrological sensitivity. *Nature Climate Change*, **8**, 901–906.
- Wentz, F. and T. Meissner, 2000: Algorithm theoretical basis document (atbd) version 2: Amsr ocean algorithm. *Remote Sensing Systems Tech. Rep. A*, **121599**, 59.
- Wentz, F. J. and T. Meissner, 2007: Supplement 1 algorithm theoretical basis document for amsr-e ocean algorithms. *NASA: Santa Rosa, CA, USA*.

- Williams, K. and M. Webb, 2009: A quantitative performance assessment of cloud regimes in climate models. *Climate dynamics*, **33**, 141–157.
- Williams, K. D. and A. Bodas-Salcedo, 2017: A multi-diagnostic approach to cloud evaluation. *Geoscientific Model Development*, **10**, 2547–2566.
- Wood, R., 2012: Stratocumulus clouds. *Monthly Weather Review*, **140**, 2373–2423.
- Wood, R. and C. S. Bretherton, 2004: Boundary layer depth, entrainment, and decoupling in the cloud-capped subtropical and tropical marine boundary layer. *Journal of climate*, **17**, 3576–3588.
- 2006: On the relationship between stratiform low cloud cover and lower-tropospheric stability. *Journal of climate*, **19**, 6425–6432.
- Wood, R., M. P. Jensen, J. Wang, C. S. Bretherton, S. M. Burrows, A. D. Del Genio, A. M. Fridlind, S. J. Ghan, V. P. Ghatge, P. Kollias, et al., 2016: Planning the next decade of coordinated research to better understand and simulate marine low clouds. *Bulletin of the American Meteorological Society*, **97**, 1699–1702.
- Xue, H. and G. Feingold, 2006: Large-eddy simulations of trade wind cumuli: Investigation of aerosol indirect effects. *Journal of the atmospheric sciences*, **63**, 1605–1622.
- Yuan, T., L. Remer, and H. Yu, 2011: Microphysical, macrophysical and radiative signatures of volcanic aerosols in trade wind cumulus observed by the a-train.

- Zelinka, M. D., T. A. Myers, D. T. McCoy, S. Po-Chedley, P. M. Caldwell, P. Ceppi, S. A. Klein, and K. E. Taylor, 2020a: Causes of higher climate sensitivity in cmip6 models. *Geophysical Research Letters*, **47**, e2019GL085782.
- 2020b: Causes of higher climate sensitivity in cmip6 models. *Geophysical Research Letters*.
- Zuidema, P., D. Painemal, S. De Szoeko, and C. Fairall, 2009: Stratocumulus cloud-top height estimates and their climatic implications. *Journal of Climate*, **22**, 4652–4666.